Physics and Astronomy, School of Physical and Chemical Sciences,
University of Canterbury, Christchurch, New Zealand

Comparing satellite and ground based observations of cloud over the Southern Ocean

Cameron McErlich

A thesis submitted in partial fulfilment of the requirements

for the degree of Master of Science in Physics

at the University of Canterbury

Supervisor: Professor Adrian McDonald

March 2020

Abstract

Clouds are poorly represented in climate models. This has been attributed to factors that include simulating too little cloud cover and under-representing the amount of supercooled liquid water in clouds. This leads to biases the cloud radiative effect, which in turn causes a positive shortwave radiation bias over the Southern Ocean, where too much sunlight is hitting the surface of the ocean. This thesis presents an analysis of the 2BCL5 and DARDAR satellite datasets, as well as comparison with the ground based AWARE dataset. This work was undertaken with the aim of collecting and comparing satellite and ground based observations of cloud to develop a representation of the vertical structure of clouds and their phase over the Southern Ocean.

Comparisons between 2BCL5 and DARDAR found that the two display differences in the amount of cloud observed. 2BCL5 detects more clouds than DARDAR, except below 1 km where DARDAR shows a greater amount of cloud. The two also show differences in their partitioning between the ice, mixed and liquid cloud phases. 2BCL5 always detects more mixed phase cloud while DARDAR mostly classifies as either ice or liquid phase. This was found to be due to differences in the way the datasets classify cloud; 2BCL5 will generalise a whole cloud layer as mixed phase cloud if it detects both ice and supercooled liquid water while DARDAR will classify the parts of cloud that are ice, liquid, and mixed phase separately.

Comparisons between 2BCL5/DARDAR and AWARE find that 2BCL5 matches better with AWARE than DARDAR does. Between 1.5 km and 4.5 km 2BCL5 agrees with AWARE while DARDAR shows a greater spread. These differences were found to be statistically significant. Below 1.5 km neither satellite dataset matches better with AWARE, even though DARDAR sees more cloud below 1km than 2BCL5. DARDAR seeing more cloud can likely be attributed to a greater amount of false positives where DARDAR is classifying noise in the radar signal incorrectly as cloud. Above 7 km neither 2BCL5 or DARDAR does a good job matching with AWARE, which highlights the limitations of AWARE at high altitudes rather than the satellites seeing the same amount of cloud.

Acknowledgements

I would like to thank and acknowledge my supervisor Professor Adrian McDonald for his guidance and wisdom as I undertook this thesis, without you this would have not been possible. Thanks to the input from those in the Atmospheric Physics group, namely Peter for his help with installing and operating code needed for my analysis. Special thanks goes to Israel Silber at Pennsylvania State University for providing me with access to the AWARE dataset, as well the CloudSat Data Processing Center and ICARE Data and Services Center for allowing me to use the 2B-CLDCLASS-LIDAR R05 and DARDAR products respectively. Final thanks and appreciation go to my friends and family who have supported me outside of my studies.

Contents

List of Figures

List of Tables

Chapter 1

Introduction

1.1 Clouds and their role in the climate

When it comes to the Earth's climate, clouds play a critical role. They can act to cool the climate by reflecting incoming solar radiation back into space. Clouds also absorb outgoing infrared radiation and re-radiate it back towards the surface, trapping heat and causing the surface climate to warm. Clouds are formed when air rises and water vapor condenses into cloud droplets. Eventually enough cloud droplets are created to form a visible cloud. The atmosphere is in hydrostatic balance, where the downward force of gravity balances the upward force of the vertical pressure gradient (Marshall & Plumb, 2008; Cook, 2013). The pressure gradient is given by the total mass of the atmosphere above a height. Clouds form because as air rises the pressure decreases, due to there being less weight from the atmosphere above. This decrease in pressure causes the air to expand and as it expands its temperature decreases. The rate temperature changes as air rises and falls in the atmosphere is known as the lapse rate, and for dry air moving adiabatically (no loss or gain of heat) the value is approximately 10 K km^{-1} and called the adiabatic lapse rate. For moist air where the condensation of water vapor occurs, there is a release of latent heat that offsets the cooling. This causes the adiabatic lapse rate to decreases to 3 K km^{-1} in the lower tropical troposphere. This is called the moist adiabatic lapse rate which rises to become close to that of dry air in the upper troposphere as there is a lesser release of latent heat (Smith, 1986; Marshall & Plumb, 2008). As air rises it can hold less water vapor, so once a critical threshold is reached the excess water vapor condenses into clouds. Water vapor needs a surface to condense, such as dust, pollen, and other aerosols called cloud condensation nuclei (Boucher et al., 2013).

The effect clouds have on Earth's global mean energy budget can be seen in Figure 1.1, taken from a study by Kiehl and Trenberth (1997). It shows 77 Wm^{-2} (~22%) of all incoming shortwave radiation being reflected primarily by clouds, with some reflection due to aerosols and the atmosphere (Barry & Carleton, 2001). Incoming shortwave radiation consists of wavelengths between 0.1 μm and 3 μm (Visconti, 2016). This is comprised of visible and ultraviolet light, as well as the near infrared part of the electromagnetic spectrum. A large amount of outgoing longwave radiation is emitted by the Earth's surface, although most of this is absorbed by clouds and atmosphere, then reradiated in many directions. Much of this is redirected back towards the surface. Longwave radiation consists of wavelengths between 4 μm and 100 μm in the thermal infrared part of the electromagnetic spectrum (Marshall & Plumb, 2008). Different types of cloud have different properties that affect how they interact with radiation. High level clouds consisting mainly of ice tend

to transmit the incoming radiation while trapping outgoing longwave radiation, having a warming effect. Low level clouds generally have a higher albedo and are composed of more liquid water, tending to reflect the incoming solar radiation and have a cooling effect at the surface (Quante, 2004; Vergara-Temprado et al., 2018). Thus, details about cloud distribution and changes to that distribution can have a significant impact on the Earth's surface climate. Overall research suggests that clouds provide a net cooling, with a cloud radiative effect (the difference in the radiative effects between cloudy and clear sky conditions) of approximately 20 Wm^{-2} (Wielicki et al., 1995; Kiehl & Trenberth, 1997; Boucher et al., 2013).

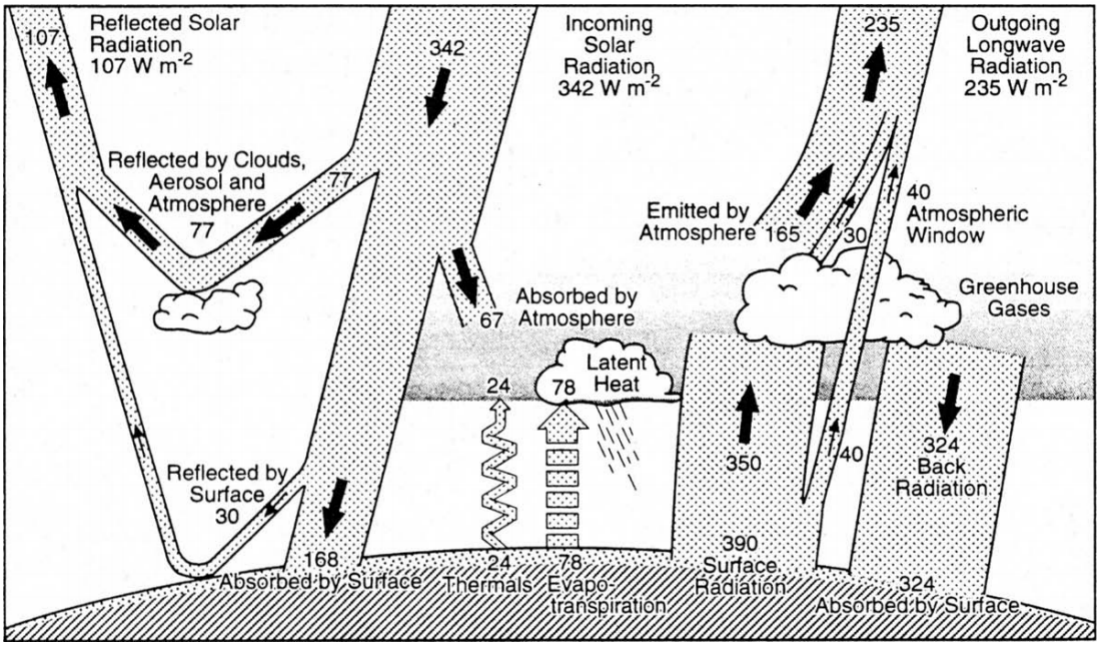

Figure 1.1: Global mean energy balance of the Earth showing the incoming and outgoing radiation. All units are in Wm^{-2} (Kiehl & Trenberth, 1997).

As well as the reflection and absorption of radiation, clouds also play an important part in the global transfer of energy. While incoming solar radiation will be essentially parallel, the amount of energy per unit surface area at the equator will be greater than at the poles because of the spherical geometry of the Earth. Due to the tilt of Earth's axis by 23.5 degrees, during summer each pole will be titled towards the sun and receive solar radiation. During the winter season each pole will be tilted away from the sun and receive no solar radiation (Marshall & Plumb, 2008). It is a combination of these two effects that determine Earth's annual energy balance between net shortwave and longwave radiation as shown in Figure 1.2 (Pidwirny, 2006), which is dependent on latitude.

As expected, the blue curve shows the that shortwave radiation has a maximum over the tropics and a minimum at the poles. Conversely the red curve showing the longwave radiation displays a maximum over the poles and a minimum over the tropics. This difference causes a surplus of energy at the tropics and a deficit of energy at the poles. This implies

that there must be a transport of energy from low to high latitudes because the balance of incoming/outgoing energy must be satisfied. This meridional transfer of heat energy is carried out by the atmosphere and oceans, driven by the temperature difference between the equator and the poles.

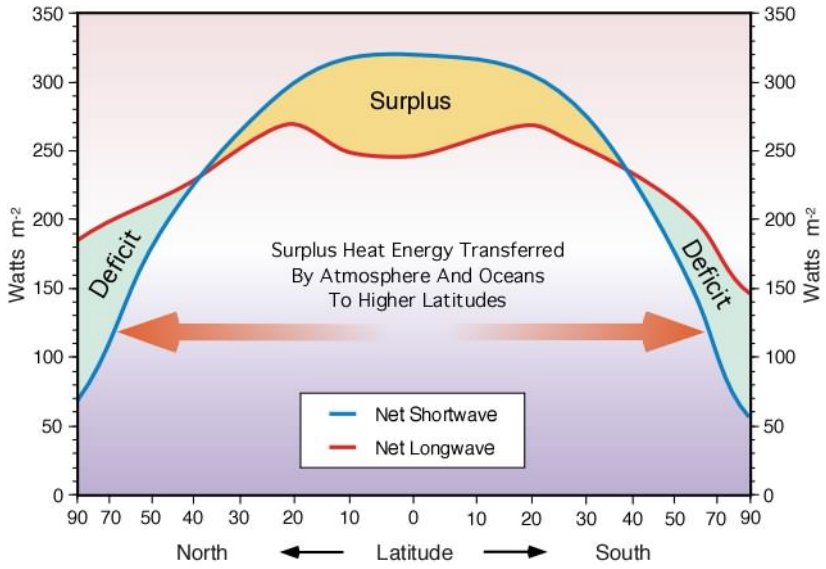

Figure 1.2: Balance between average net shortwave and longwave radiation from 90° North to 90° South. It shows a surplus of energy at the equator and a deficit at the poles, suggesting that surplus heat must be transferred to higher latitudes by the atmosphere and ocean (Pidwirny, 2006).

The majority of the atmospheric meridional heat transport is achieved by the Hadley circulation in the tropics, whereas at mid to high latitudes heat transport is achieved by eddies generated through a process known as baroclinic instability. The Hadley circulation causes an upwelling of warm, moist air at the equator. Once it rises, more upwelling air from below pushes the air outwards towards higher latitudes. As it then cools, the air releases moisture and sinks at the subtropics as it warms adiabatically during its descent. This warm, dry air then flows back towards the equator where it gains moisture and once again rises again, completing the cycle of Hadley circulation. Baroclinic instability arises from Earth's rotation and is associated with small perturbations from the mean flow of air circulation. These perturbations grow by converting available potential energy from the temperature gradient between the equator and poles into kinetic energy (Holton, 2004; Vallis, 2006). It is these eddies that stir the atmosphere, carrying warm air poleward and cool air towards the equator.

Most of the oceanic meridional heat transport is achieved by either the deep-oceanic Thermohaline or the surface wind-driven circulation. The Thermohaline circulation, controlled both by temperature and salinity variations, causes cold, salty water located at the polar regions to sink. This water is then transported deep in the ocean towards the tropics where it then rises. The cold, polar water is replaced by warmer water that flows from the tropics

towards the poles by surface currents. Once it reaches the polar regions the water cools, as the formation of sea ice acts to reject salt; This makes the underlying water saltier. This cold, salty water will once again sink, continuing this transport of energy poleward (Bigg et al., 2003).

Clouds play a role in the atmospheric component of meridional heat transport. In the tropics where Hadley Circulation transports heat towards the poles, cumulonimbus clouds are the primary mechanism for vertical heat transport (Marshall & Plumb, 2008). High cumulonimbus clouds over the equator transport water vapour, and therefore latent heat, up into the atmosphere. This is then transported horizontally to higher latitudes, where it condenses and releases its latent heat as precipitation (Quante, 2004). For eddies generated by baroclinic instability, a sizable portion of energy transfer is associated with cloud and the transport of latent heat. This can be seen in Figure 1.3 (NASA, 2013) which shows the cloud coverage on July 11, 2005, based largely on observations from the Moderate Resolution Imaging Spectroradiometer (MODIS; NASA 2013). Eddies can be seen in the cloud structure at mid latitudes in both hemispheres. This shows a coupling between cloud and the meridional transport of heat. Eddies produced through baroclinic instability produce cloud perturbations that aid in transporting warmer air towards the poles and cooler air towards the equator.

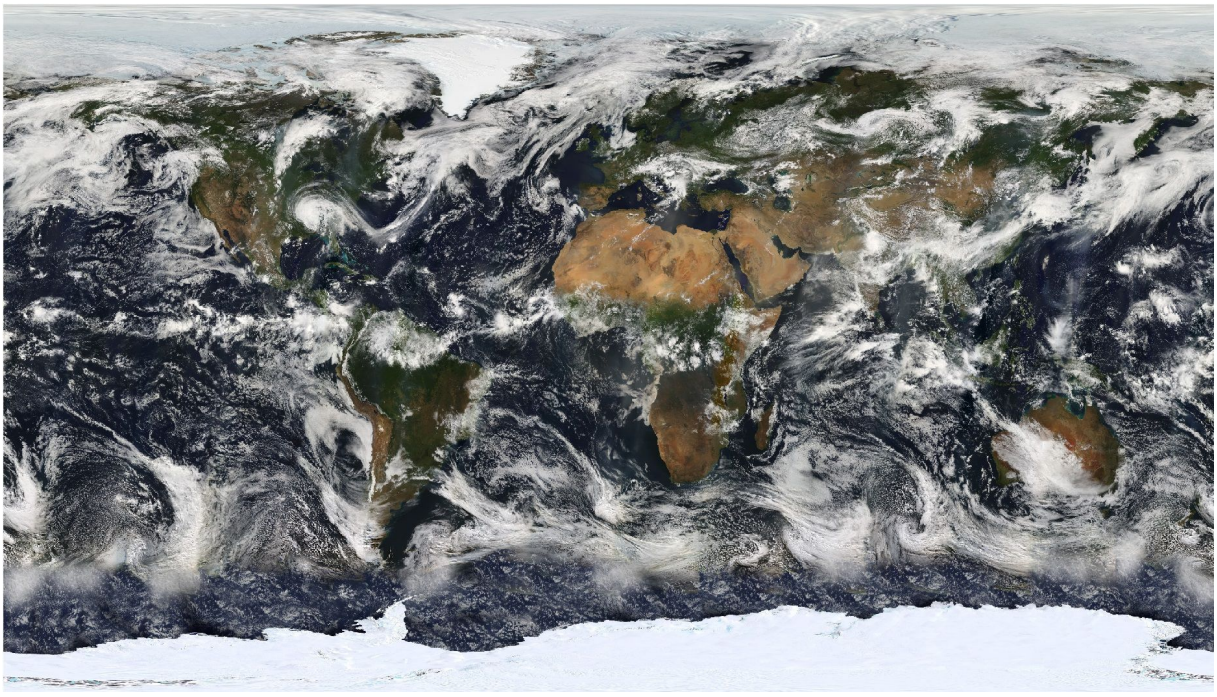

Figure 1.3: Global cloud coverage on 11th July, 2005 based on MODIS observations (NASA, 2013).

1.2 Climate Processes

While clouds are important in the global energy balance and meridional energy transport, they are but a part of the many components and processes that determine the state of the climate. The IPCC Third Assessment Report (IPCC, 2001) defines the climate system as consisting of five important components: the atmosphere, cryosphere, hydrosphere, biosphere and the land surface.

The atmosphere consists of the mass of air and other gases that surround Earth. Greenhouse gases such as methane (CH_4) and carbon dioxide (CO_2) absorb the outgoing radiation and re-radiate it back towards the surface to cause a warming effect, similarly to clouds. While this is similar to clouds, greenhouse gases lack the reflectivity of clouds that can also generate a cooling effect. Some gases, such as ozone (O_3), behave as a greenhouse gas in the troposphere where it absorbs longwave radiation. However at higher levels in the stratosphere it absorbs incoming shortwave radiation, which has a significant effect on the amount of energy that reaches the surface (Cook, 2013). The atmosphere also consists of clouds and aerosols. As discussed earlier in the chapter, clouds have a net cooling effect of 20 Wm^{-2}. The effects of aerosols, like clouds, can also act to both warm and cool. While aerosols can act to scatter the incoming sunlight and produce cooling, some have a strong absorbing effect that produces warming (Myhre et al., 2013a).

Figure 1.4 shows the impact different anthropogenic sources have on the amount of energy absorbed by the Earth and reflected back to place, also called the radiative forcing (Myhre et al., 2013b). The figure also includes a concept of effective radiative forcing, that allows for variables such as aerosols and cloud cover to respond to the forcing agents like greenhouse gases. A positive radiative forcing here means that they absorb more than they reflect and provide a net warming. It shows that greenhouse gases such as CO_2 produce most of the positive radiative forcing, but are offset by negative forcing such as aerosol-cloud interactions. They find the best estimate of total anthropogenic radiative forcing to be 2.29 Wm^{-2}. Aerosols also play an important role in the formation of clouds serving as cloud condensation nuclei and ice nucleating particles upon which cloud droplets and ice crystals can form (Boucher et al., 2013). This means the amount of aerosol also affects the amount of cloud which in turn changes the climate system. As discussed earlier in the chapter, the atmosphere is also important for the energy transfer towards the poles from the tropics.

The hydrosphere consists of all liquid water on the surface of the Earth. This includes freshwater sources such as lakes and rivers, or saltwater sources such as the oceans. The oceans in particular, which cover approximately 70% of the Earth's surface, play an important role in the storage and transport of heat. Thermohaline circulation, as discussed earlier, causes cold, salty water located at the polar regions to be transported deep in the ocean towards

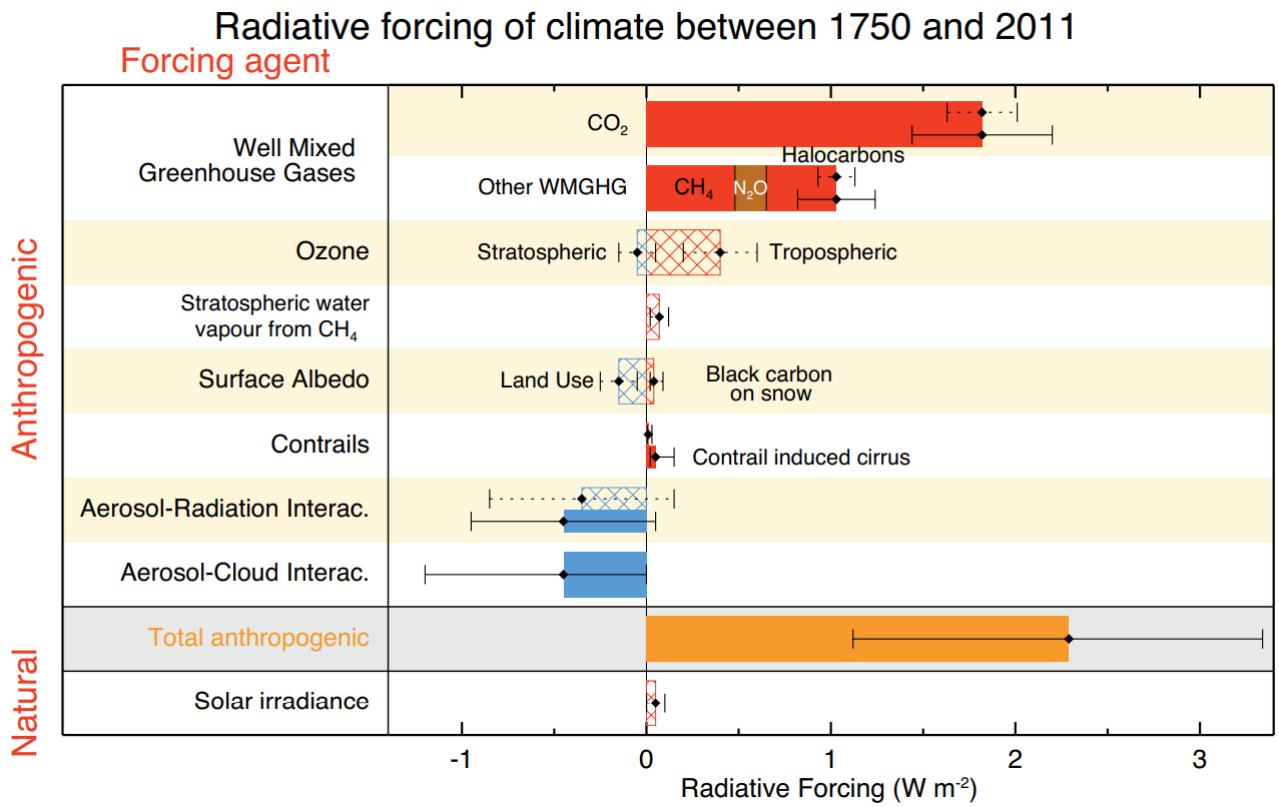

Figure 1.4: Radiative forcing (hatched) and effective radiative forcing (solid) for the period between 1750 and 2011. Uncertainties (5 to 95% confidence range) are given for radiative forcing (dotted lines) and effective radiative forcing (solid lines; Mhyre et al., 2013b).

the tropics, where it then rises (Bigg et al., 2003). The ocean also stores large amounts of CO2 that have been released into the atmosphere. A recent study by Gruber et al. (2019), investigated the amount of CO2 stored in the ocean between 1994 and 2007. They found that 34 ± 4 petagrams of carbon had been stored, equivalent to 31 ± 4% of the global anthropogenic CO2 emissions over this period.

The cryosphere consists of surface ice, such as glaciers, snow, sea ice, and the Antarctic and Greenland ice sheets. Due to the high albedo of ice the cryosphere is important for the reflection incoming solar radiation.

The biosphere is the part of Earth consisting of living organisms, both marine and terrestrial. The biosphere influences the intake and release of greenhouse gases such as methane and nitrous oxide (Boucher et al., 2013), with vast amounts of carbon from carbon dioxide being stored in plants. The land surface represents the topography and coverage of the terrestrial surface of the Earth. Different types of vegetation and soil change the surface albedo and influence how absorbed solar energy from the sun is returned to the atmosphere. Plants can also act to draw moisture from the soil and transfer it into the atmosphere (Viterbo, 2002).

All parts of the climate system are linked together and interact with each other in many processes. This is shown in Figure 1.5, a schematic of the interactions between the five components of the climate system (IPCC, 2001). The ocean and atmosphere are coupled together. For example, atmospheric winds drive ocean circulation and sea surface temperatures. In turn sea surface temperatures affect the atmospheric winds and circulation (Fedorov, 2008). Sea surface temperatures also affect the exchanges of heat and moisture between the atmosphere and ocean. High sea surface temperatures means more moisture which condenses into low level clouds in the marine boundary layer. These clouds reflect incoming solar radiation and cool the surface in a negative feedback (Leahy et al., 2013; Fallmann et al., 2017). The exchange of aerosols and particles between the ocean and atmosphere are also important. Much carbon dioxide is stored in the oceans, entering from the atmosphere in cold polar water. It then sinks into the deep ocean and is released back into the atmosphere in warm upwelling water near the equator (IPCC, 2001). Exchanges of water between the atmosphere, land and ocean form the basis of the water cycle which acts to cool the oceans through evaporation due to latent heat. This latent heat is then released into the atmosphere during precipitation (Trenberth & Stepaniak, 2006). The atmosphere is linked to the land surface by its roughness and topography, which influences the winds in the lower part of the atmosphere and affects circulation. The cryosphere sea ice inhibits the exchange of energy between the ocean and atmosphere, but also has influences on the ocean circulation (Boucher et al., 2013). These are just a few examples of the numerous linked processes impacting the climate.

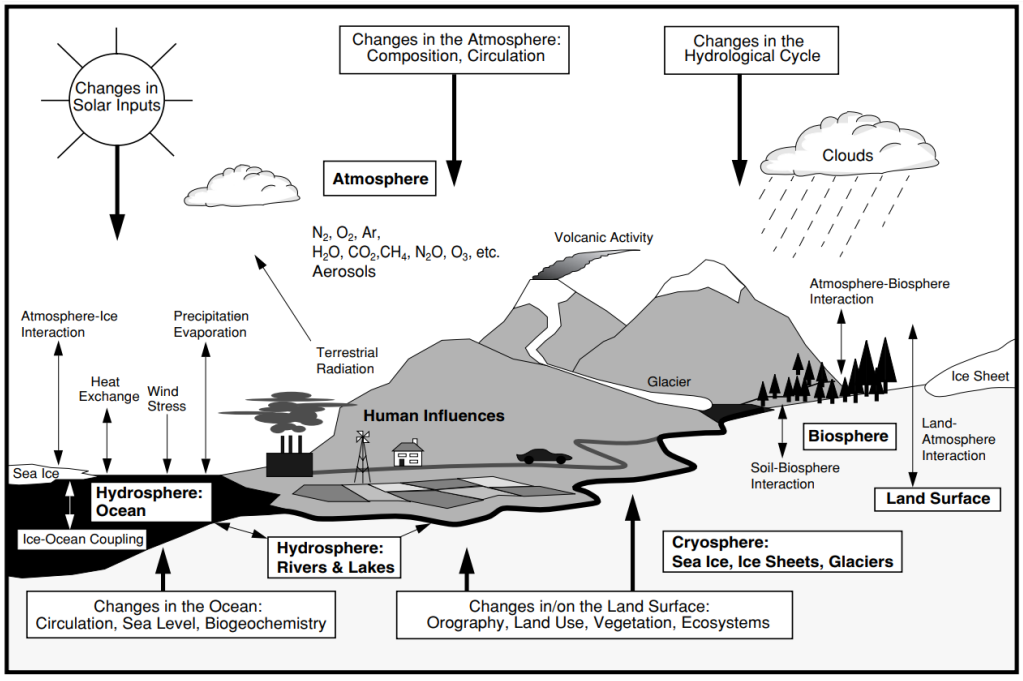

Figure 1.5: The components of the global climate system (bold), their processes and interactions (thin arrows), and some of the aspects that may change (bold arrows) as the climate system changes (IPCC, 2001).

1.3 Climate Models

1.3.1 General Circulation Models

General Circulation Models (GCMs) have been developed to model the climate system using a set of governing equations. These equations are used to mathematically simulate the transfer and interaction of both energy and matter throughout the atmosphere, land and oceans. Typically GCMs come in the form of an Atmospheric General Circulation Model (AGCM), Oceanic General Circulation Model (OCGM), or an Atmosphere-Ocean General Circulation Model (AOGCM) that couples both atmosphere and ocean together. GCMs also often include Land Surface Models (LSMs) which represent the exchange of energy and water between land surfaces and atmosphere/ocean and models to represent the formation and interactions of sea ice. LSMs also determine the surface coverage with snow, ice, glaciers, natural vegetation, managed vegetation, and urban environments able to be simulated (Cook, 2013).

GCMs break the surface of the Earth up into a three dimensional grid made up of a number of cells with a specified size This separates the Earth into horizontal and vertical layers, as can be seen in Figure 1.6 (Schneider et al., 2017). The spatial resolution of GCMs varies between models, but for AGCMs a horizontal resolution of between 100 - 200 km and vertical resolutions of less than a kilometer is typical, which OGCMs tend to have a greater resolution (Cook, 2013). The IPCC Fifth Assessment Report evaluated a number of AOGCMs involved in the Coupled Model Intercomparison Project Phase 5 (Flato et al., 2013). They found that the typical horizontal resolution for AOGCMs is roughly 1 to 2 degrees for the atmospheric component and around 1 degree for the oceanic component. The typical number of vertical layers in the models are around 30 to 40 for the atmosphere and around 30 to 60 for the ocean. Another model, HADGEM3, has horizontal resolutions that vary between 2.5 degrees of latitude by 3.75 degrees of longitude and 0.556 degrees of latitude by 0.833 degrees of longitude for the atmospheric part of the model and 2.0, 1.0 or 0.25 degree horizontal resolutions for the oceanic part of the model. It has vertical resolutions between 38 - 85 vertical levels for the atmospheric part and 42 - 75 levels for the oceanic part (MetOffice, 2019).

Because GCMs have such large resolutions on their grid cells, many processes occurring on scales much smaller than the model grid must be represented by parameterisations. Parameterisations link unresolved processes to variables contained within the model (Barry & Carleton, 2001; McGuffie & Henderson-Sellers, 2014). To run the models, the equations that govern it are then solved at each grid cell following a set of initial conditions to represent the climate forcing. These equations are then solved repeatedly as the GCM evolves with time, creating a simulation of the climate where the energy and matter transfer of each cell is influenced by neighbouring cells.

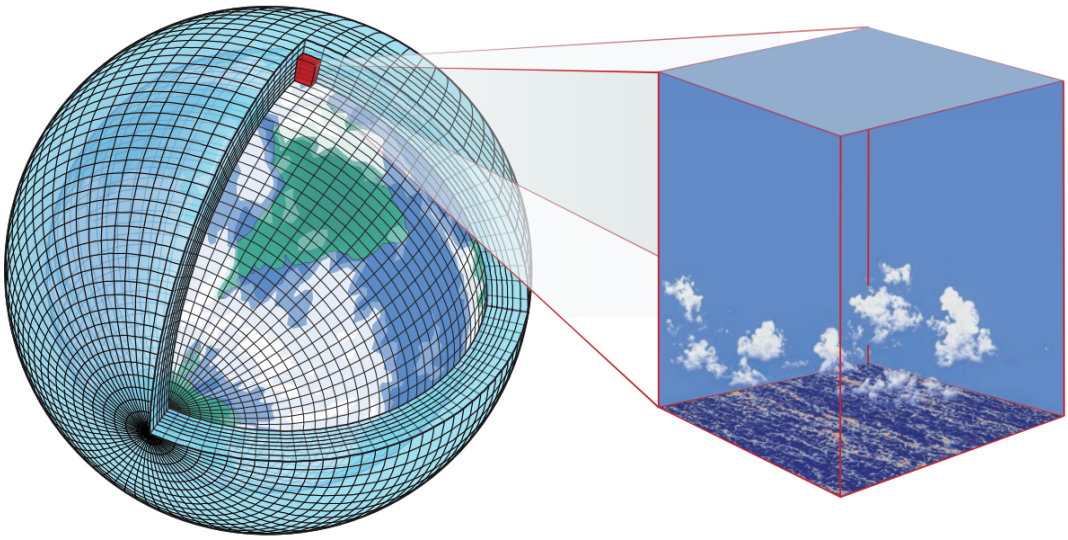

Figure 1.6: Schematic of the Earth being broken up into a number of different grid cells for use in climate modelling (Schneider et al., 2017).

While it is difficult to assess how well GCMs predict the future climate, they are tested to check if they can reproduce historical climate and weather conditions. A critical component of model evaluation is the use of observations to provide a reference point. If the observations are poor it will be difficult to assess the quality of the models with any certainty. Given the importance of clouds in the climate system, they are something that needs high quality measurements for reference purposes. Flato et al. (2013) found, as part of the IPCC Fifth Assessment Report, that AOGCMs simulate general features of the global-scale annual mean surface temperature increase over the past 150 years. This includes the rapid warming observed in the second half of the 20th century as well as the cooling that followed large volcanic eruptions. One would expect that if the models can predict historical records then their future predictions would also be reliable.

1.3.2 Earth System Models

While GCMs provide a representation of Earth's physical processes in both the atmosphere and oceans, they do not take all factors that influence climate into account. Earth System Models (ESMs) take climate modelling a step further and simulate not only the physical processes of atmospheric and oceanic circulation, but also chemical and biological processes that are not modelled by GCMs. These biochemical processes include representations of the carbon cycle, ozone, methane cycle, dynamic global vegetation coverage (which in turn impacts CO_2 uptake), and atmospheric chemistry interactions (Flato et al., 2013; Heavens et al., 2013).

While ESMs are able to provide the best predictions of future climate, they still have problems with estimating feedback processes that change with the climate. Variations in water vapour, the change in atmospheric temperature with altitude (the lapse rate) and feedback due to clouds, are all places where the models have fundamental issues (Dessler & Wong, 2009; Ingram, 2012; Flato et al., 2013). Out of these issues, clouds are considered as the largest source of uncertainty in estimating global climate sensitivity in models such as ESMs (Boucher et al., 2013; Bony et al., 2015). The evaluation of climate models in the IPCC Fifth Assessment Report (Flato et al., 2013) found that models had a spread in their equilibrium climate sensitivity ranging from 2.7°C to 4.4°C. Equilibrium climate sensitivity is the equilibrium change in global and annual mean surface air temperature after doubling the atmospheric concentration of CO2 relative to pre-industrial levels. They also ascribed a very high confidence this spread was primarily due to cloud feedback, with most models reporting a positive or near neutral feedback. With the critical role that clouds play in the climate, it is important that climate models accurately represent clouds in order to predict what might happen in the future.

1.4 Cloud Feedbacks

Although clouds have many processes that influence the state of the climate, there are also climate processes that in turn affect clouds. Changes in the climate will change the global and seasonal distribution of clouds as well as their composition, affecting the way they interact with radiation and transport energy. This results in a number of cloud-climate feedback processes which can be either positive where changes in cloud/climate will continue to reinforce each other or negative, where changes in cloud/climate will oppose each other.

Cloud feedback processes are complex. Clouds are affected by both large scale processes such as air circulation, humidity and global temperature gradients, but also microphysical processes such as cloud phase and aerosols (Gettelman & Sherwood, 2016). Different types of cloud and their position over the planet also change which feedbacks are important.

For example, both observations (Bender et al., 2011; Norris et al., 2016) and climate simulations (Grise & Polvani, 2016) suggest that mid-latitude and subtropical storm tracks (the paths by which storms such as cyclones travel) are shifting towards the poles. This arises as a result of increasing temperatures generating a larger pole to equator temperature gradient, as well as increased baroclinic instability (Chen & Held, 2007). The movement of the storm tracks shift the cloud to higher latitudes where less incoming solar radiation reduces the net radiative cooling effect that have. This would be a positive feedback where increases in temperature would reduce the cooling effects of cloud and further increase the temperature.

However, Gettelman and Sherwood (2016) remark that determining the result of the feedback is more complex than this. Changes to the storm tracks and the subsequent shifting of cloud may alter the properties of the cloud which alters its radiative balance. Changes to the structure of cyclones that form along the storm tracks may be driven by different processes and also change the cloud cover and radiative properties.

The biggest region of cloud feedback is over the subtropical oceans from 20°to 40° in both hemispheres. These regions have low-level clouds that are not convective, such as stratocumulus clouds. Bretherton (2015), reviewed four processes that are responsible for this marine boundary layer cloud feedback, which were summarised in the review by Gettelman and Sherwood (2016) and shall be restated here.

The first of these is the strength of the marine layer inversion, where a layer of warm air over cold air suppresses the upward motions of the clouds and traps the moisture in the boundary layer. In a warmer climate, this inversion strengthens and its entrainment decreases (cloud has less mixing with air), which promotes thicker cloud. An increased amount of low level cloud produces a cooling effect in a negative feedback. However, this negative feedback is opposed by a second process where changes in the moisture gradient between the boundary layer and troposphere increase with a stronger inversion. This means that the same amount of entrainment from above the inversion layers will have a greater drying effect on the cloud, causing it to be thinner. This a positive feedback opposing the inversion strengthening.

The third process is that as temperature increases, radiative cooling decreases. This is because increased water vapor in the atmosphere inhibits longwave radiative cooling from the cloud tops. This decreases turbulent motions at the cloud top, which in turn decreases the entrainment of the cloud. This means the cloud top will be lower, and it will be thinner causing a positive feedback. But subsidence (the rate at which cool air descends), which slows in a warmer climate, is reduced. Cloud would then thicken and cloud layer would be raised. This is a positive feedback that opposes the radiative cooling decrease from increased water vapor. These processes are summarised in Figure 1.7 (Gettelman & Sherwood, 2016).

The overall net feedback as a result of these processes will depend on their relative magnitudes. Studies show that the feedback from these clouds is positive (Andrews et al., 2012; Vial, 2013). A study by Qu et al. (2015) used sea surface temperatures to constrain the marine low level cloud feedback in climate models. They also found that this feedback is positive.

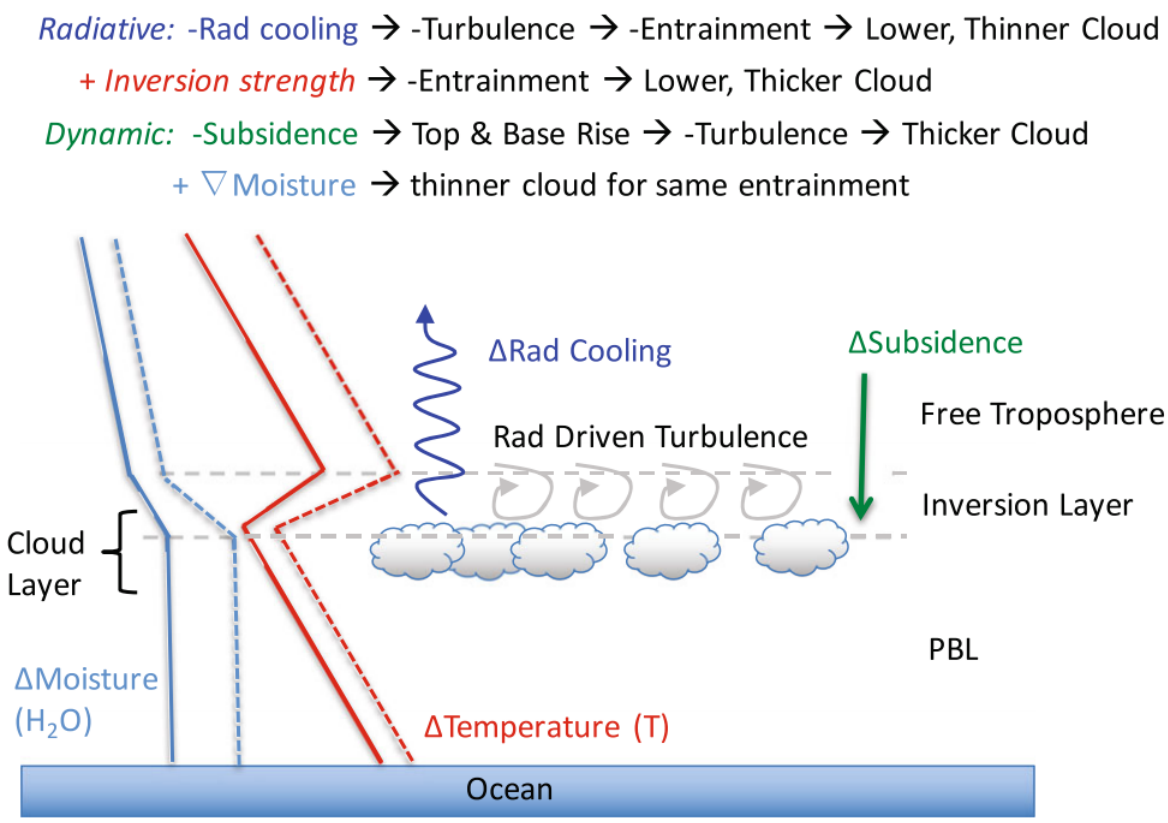

Figure 1.7: Marine boundary-layer stratocumulus cloud feedback mechanisms. PBL stands for planetary boundary layer (Gettelman & Sherwood, 2016).

1.5 Radiation biases in Climate Models

One of the results of the poor representation of clouds and their feedback processes in the models are biases in the cloud radiative effect, the difference between the radiative effects between cloudy and clear sky conditions. Biases occur in both the longwave and the shortwave. A comprehensive study was carried out by Trenberth and Fasullo (2010) using observational information on the global energy budget to evaluate climate models. Figure 1.8 shows an example from their study that illustrates biases in the Japanese 25-year Reanalysis (JRA-25; Trenberth & Fasullo, 2010) compared to observations.

It shows biases for the absorbed solar radiation (ASR) and the outgoing longwave radiation (OLR). These two components are used to examine the top of the atmosphere net radiation (R_T = ASR - OLR).

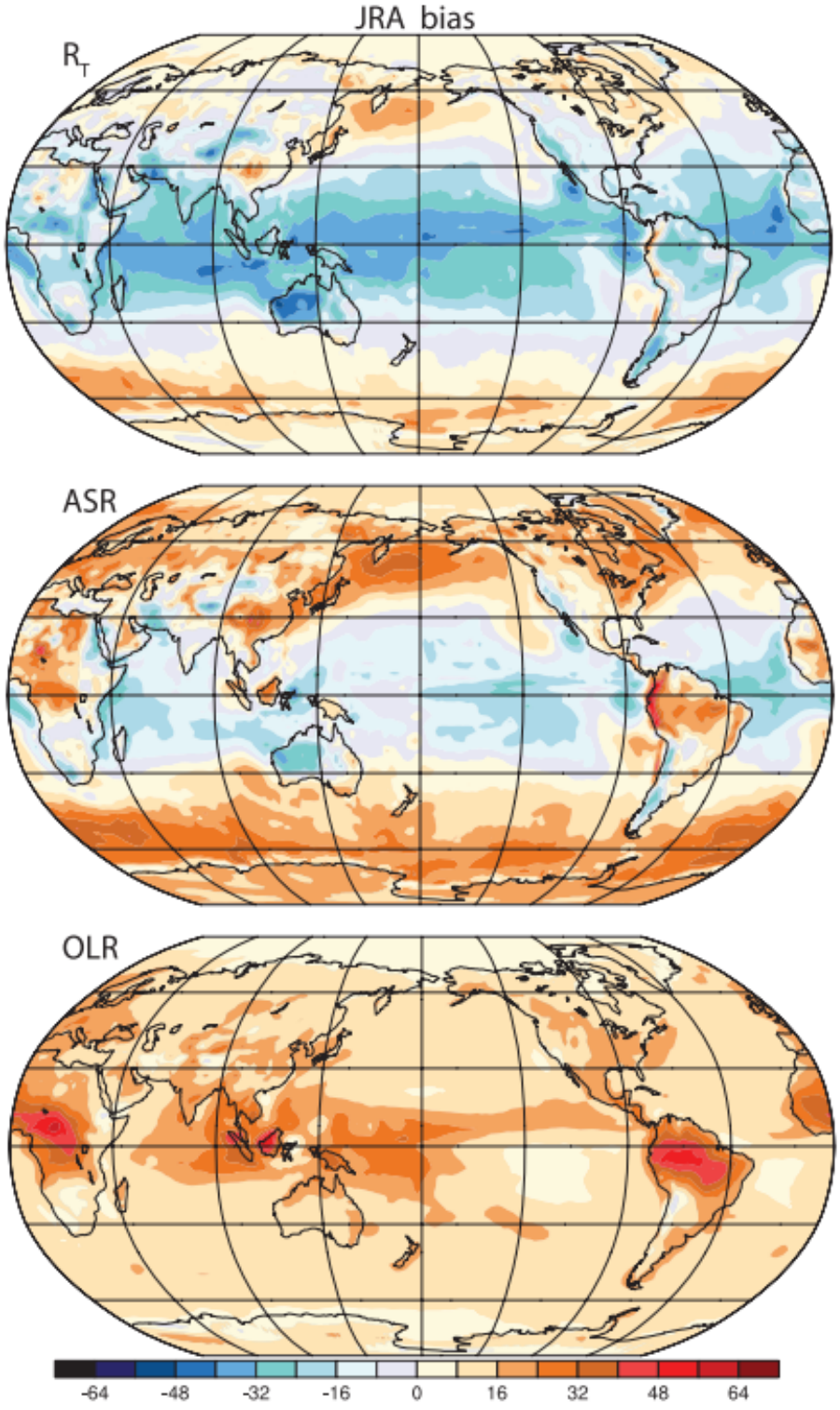

Figure 1.8: Radiation biases (in Wm^{-2}) from JRA-25 compared to observations. The absorbed solar radiation (ASR; 2nd panel) and the outgoing longwave radiation (OLR; 3rd panel) are combined to examine the top of the atmosphere net radiation (R_T = ASR - OLR; 1st panel). Overall a substantial negative bias is observed. This is offset by a large positive bias over the Southern Ocean in particular (Trenberth & Fasullo, 2010).

The second panel shows the ASR bias is negative in the tropics, especially over the ocean. This is likely to be due to an excess of shortwave cloud forcing (Trenberth & Smith, 2008). At higher latitudes ASR biases become positive where there is not enough shortwave cloud forcing. This ASR pattern is dampened/heightened at high/low latitudes in the first panel of R_T, due to the constant positive biases in the third pane for OLR. These are pronounced over low-latitude land areas, where not enough clouds are simulated, as well as over warm tropical oceans.

Together they show that R_T is deficient across the tropics, particularly over the oceans, where the models are simulating too much OLR and not enough ALR. At higher latitudes, R_T is excessive where there the biases in ALR and OLR are both positive. This is most prominent over the Southern Ocean. On a global basis R_T biases are dominated by low latitudes, with significant contributions from both ASR and OLR causing a negative bias in the global mean.

Although all clouds have an effect on the climate, it can be seen in Figure 1.8 that clouds over the oceans are especially important for determining the radiation budget. Due to the low background albedo of the sea surface compared to that of land the radiation budget of this region is very sensitive to these clouds (Cess, 1990). In particular, the Southern Ocean is a key component of the global climate system and radiation due to an almost constant presence of cloud. With an annual mean cloud coverage of around 80% – 90% (Kay et al., 2012; McCoy et al., 2014; Matus & L'ecuyer, 2017) the Southern Ocean is the cloudiest place on Earth. Figure 1.8 indicates significant shortwave radiation biases over the Southern Ocean of up to 30 Wm^{-2}. This shortwave bias induces a warm sea surface temperature bias (Hyder et al., 2018). This is believed to limit the accuracy of models and is a key factor in modelling the climate, particularly the Southern Hemisphere.

Hyder et al. (2018) recently identified that 70% of the sea surface temperature bias in CMIP5 climate models relative to observations can be attributed to the models not representing clouds and their properties correctly. Other work has shown that problems with the models include simulating too little cloud cover (Bodas-Salcedo et al., 2012; Schuddeboom et al., 2018; Kuma et al., 2019), excessive sunlight absorbed by the ocean surface (Trenberth & Fasullo, 2010; Hyder et al., 2018), a lack of clouds in the cold sectors of cyclones (Bodas-Salcedo et al., 2014), and a lack of reflective supercooled liquid water clouds (Bodas-Salcedo et al., 2016; Kuma et al., 2019).

Supercooled liquid water clouds occur where liquid water droplets exist inside the cloud below 0°C (Alexandrov et al., 2016). This requires the water to be pure and free of nucleation sites that can initiate freezing (Rosenfeld & Woodley, 2000). As explained earlier in the chapter, determining the cloud phase is important as ice crystals and water droplets have differing radiative properties and therefore reflect and absorb different levels of incoming

shortwave radiation (Haynes et al., 2011; Scott & Lubin, 2014).

Work has identified the prevalence of supercooled liquid water clouds above the Southern Ocean (Chubb et al., 2013; Jolly et al., 2018; Listowski et al., 2018; Morrison et al., 2011) and their potential importance in contributing to known model biases (Bodas-Salcedo et al., 2016; Kay et al., 2016; Kuma et al., 2019). In particular, Bodas-Salcedo et al. (2016) identified that clouds with supercooled liquid tops contribute between 27% and 38% to the total reflected solar radiation over the Southern Ocean, with climate models being found to simulate these clouds poorly. The New Zealand Earth System Model (NZESM) produces more ice cloud and less supercooled liquid cloud compared to MERRA-2 reanalysis data, which shows a smaller shortwave radiation bias (Schuddeboom et al., 2018; Kuma et al., 2019). Models that overestimate the amount of ice cloud produce a positive shortwave radiation bias in their output, as the ice crystals in the cloud reflect less incoming solar radiation than supercooled liquid water clouds.

This can be seen in Figure 1.9 which shows differences between the radiative properties of supercooled liquid and ice phase clouds (Vergara-Temprado et al., 2018). It also shows the effect of ice nucleating particles on mixed phase clouds. The introduction of ice nucleating particles, which act as a surface for ice crystals to form upon, deplete the cloud of its liquid as it freezes into ice.

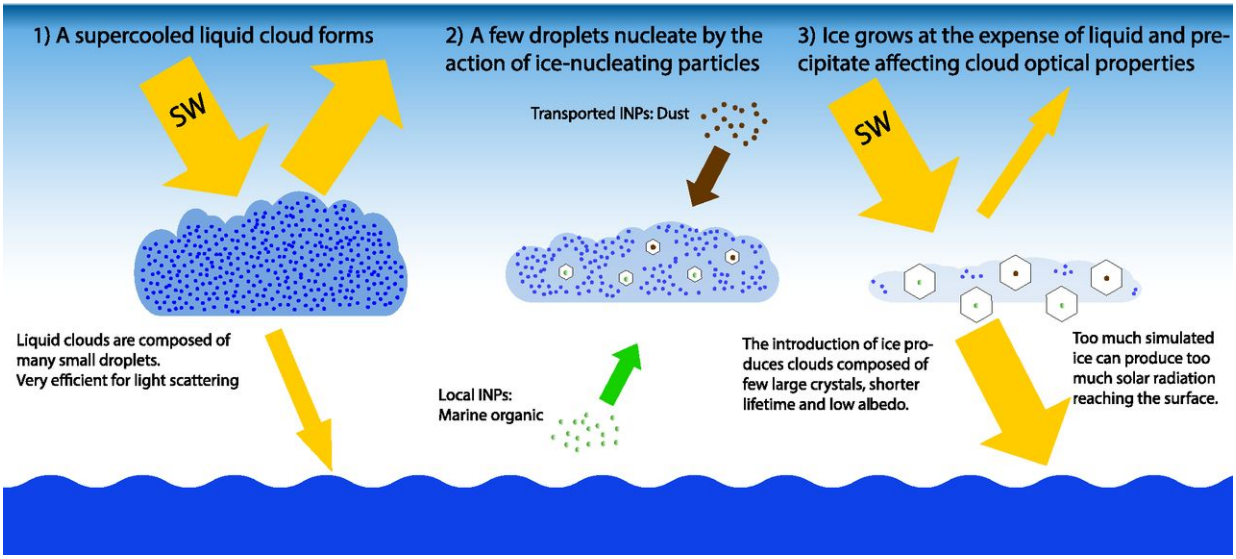

Figure 1.9: Schematic representation of differences between the radiative properties of ice and supercooled liquid water cloud. Supercooled liquid water clouds are effective at scattering light whereas ice clouds transmit more incoming solar radiation. It also shows how ice nucleating particles can act to deplete mixed phase clouds of their supercooled liquid (Vergara-Temprado et al., 2018).

The shortwave bias has also been linked to a number of problems in models that increase the uncertainty on climate predictions, such as the double-Intertropical Convergence Zone (Hwang & Frierson, 2013), errors in the meridional energy transport (Mason et al., 2015), the position of the Southern Hemisphere storm track (Ceppi, Hwang, Frierson, & Hartmann, 2012) and also the intensity of the Southern Hemisphere jet (Kay et al., 2016), which is critical to understanding the climate at Southern hemisphere mid-latitudes.

1.6 Motivation of Thesis

This thesis is related to work being undertaken in the Deep South National Science Challenge. Deep South seeks to understand the role of Antarctica and the Southern Ocean in determining the climate and future environment of New Zealand, through development of the New Zealand Earth System Model (NZESM). The NZESM is a climate model being developed in partnership with the Unified Model Consortium, led by the UK Met Office, which is derived from and feeds back into the UK Earth System Model (UKESM). Part of the Deep South National Science Challenge focuses on clouds and aerosols using measurements over the Southern Ocean to develop observational constraints that will improve their representation in the NZESM.

Previous work in the clouds and aerosols project focused on collecting and analysing atmospheric measurements to better understand the causes of the misrepresentations of clouds and aerosols in NZESM. They identified systematic biases in the intercalibration between some satellite data sets over the Southern Ocean which strengthens the need for ground based datasets being used to validate satellite observations. Machine learning methods were applied to CFMIP Observation Simulator Package (COSP; Bodas-Salcedo et al. (2011)) output to evaluate the NZESM (Williams et al., 2016) against satellite observations (Schuddeboom et al., 2018, 2019). Shipborne observational datasets of cloud properties (Klekociuk et al., 2019; Kuma et al., 2019) as well as aerosols and their composition were collected, providing a valuable resource to evaluate NZESM and constrain its performance over the Southern Ocean. Furthermore, a ground based lidar simulator was implemented in the COSP model (Bodas-Salcedo et al., 2011) to compare measurements from the research voyages against NZESM output (Kuma et al., 2019). These studies confirmed that the atmospheric model in NZESM forms too few low level clouds over the Southern Ocean compared to observations. They also confirmed that the NZESM produces more ice cloud and less supercooled liquid cloud compared to MERRA-2 reanalysis data, which shows a smaller shortwave radiation bias than simulated by NZESM.

Work in this thesis is aligned with one of the Deep South clouds and aerosols project's goals which seeks to quantify the proportions of liquid, ice and mixed phase cloud above the

Southern Ocean in an effort to improve parameterizations of cloud phase in the NZESM. Mixed phase clouds consist of a combination of ice crystals and supercooled liquid water droplets (water droplets that are significantly below the freezing point of water). The aim of this work is to collect and compare satellite and ground based cloud observations to develop a representation of the vertical structure of clouds and cloud phase over the Southern Ocean.

To do this a combination of space and ground based observations of cloud and their properties were used. The second chapter of this thesis covers the satellite and ground based data products used in the analysis and how they were processed. Chapter three covers further processing of the satellite products to produce a global climatology of cloud and its phases. It also covers a comparison between two satellite observational datasets and evaluation about which may be more representative of cloud. Chapter four covers the processing of the ground based dataset and a comparison between the ground and satellite observations of cloud, with the aim of determine which satellite dataset is more representative. The final chapters discuss the significance of the results in relation to previous studies as well as a final summary of presented work in this thesis and possible future work.

Chapter 2

Datasets

2.1 Satellite Based Datasets

2.1.1 CloudSat and CALIPSO

All of the satellite datasets used in this research are joint products of the CloudSat (Stephens et al., 2008) and CALIPSO (Winker et al., 2009) satellites. Launched together in April 2006, they investigate the vertical distribution and properties of cloud. CloudSat and CALIPSO are designed to work together and follow each other closely in orbit to take observations only seconds apart. For the majority of their operating life, they were part of a collection of satellites occupying a low Earth orbit called the A-Train. (Stephens et al., 2002). A partial equipment failure in 2017 meant that CloudSat was shifted into a lower orbit to preserve the longevity of the instrument. CALIPSO was then moved into this lower orbit so that the two could continue to combine their measurements. In addition, CloudSat has operated in daylight-only mode since 2011 due to a battery anomaly which has reduced the quality of collected data.

The main instrument aboard CALIPSO is the Cloud-Aerosol Lidar with Orthogonal Polarization, or CALIOP (Winker et al., 2007). Lidar, which stands for light detection and ranging, uses a similar process to radar to take measurements. Pulses of laser light in the ultraviolet to near infrared are emitted from the lidar, which are reflected off the clouds in the atmosphere. A component of this reflection bounces back towards the lidar itself, which collects the backscatter. CALIOP sends out two signals to measure backscatter and depolarisation data at wavelengths of 1064 nm and 532 nm simultaneously. The backscatter is used to derive vertical profiles of clouds and aerosols, the ratio of backscatter for the two wavelength is used discriminate between clouds and aerosols as well as determine the composition of cloud (Winker et al., 2009; Z. Liu, 2009). The lidar depolarisation ratio of the backscatter can be used to estimate the phase of the cloud as either ice or liquid water (Hu et al., 2009). CALIOP has fundamental sampling resolutions of 30 m in the vertical and 333 m horizontal, although this decreases at higher levels where signals tend to be weaker as the atmosphere begins to appear more uniform (Winker et al., 2007).

CloudSat carries the Cloud Profiling Radar (CPR) which operates at a frequency of 94 GHz, has a horizontal footprint of 1.4 km x 1.8 km, and vertical resolution of 485 m up to a height of 25km (Stephens et al., 2008). Similarly to CALIPSO, CloudSat uses the strength of the signal reflected off the clouds to determine vertical structure.

The main difference between radar and lidar are the wavelengths at which they operate; radar operates at a millimeter wavelength while lidar operates at optical wavelengths. This results in different sensitivities between the two when detecting cloud particles in the atmosphere. Radars can penetrate through optically thick clouds which gives them an advantage in detecting multiple cloud layers. However, radars are limited due to their long wavelength in the detection of mid-level ice clouds, or supercooled water clouds with relatively small water droplets. Lidar is sensitive enough to detect these mid level clouds, but is limited by its short wavelength which results in strong attenuation through optically thick clouds and therefore struggles to detect anything beyond optical depths more than around three (Alexander & Protat., 2018). This means that space based lidar instruments, such as CALIOP, are suited to measure high and mid-level clouds due to their lower optical thicknesses. Space based radar instruments, such as the CPR are suited to penetrate through optically thick cloud layers and measure low level cloud. While the CPR signal can penetrate through optically thick clouds, CloudSat has difficulties observing boundary layer clouds below 1.2 km due to ground clutter, although detection can be improved by subtracting an estimate of the surface clutter from the radar measurements (Marchand et al., 2008; Tanelli et al., 2008).

2.1.2 2BCL5

Analysis was carried out on the 2B-CLDCLASS-LIDAR R05 (2BCL5) dataset generated by combining measurements from CloudSat/CALIPSO to determine the vertical distribution of cloud and cloud phase and cloud type (Sassen et al., 2008; Wang, 2019). Because of the different horizontal and vertical resolution of the two instruments, which change depending on the altitude, data from several CALIOP footprints are matched to the larger CPR footprints. Due to their greater resolution, CALIOP footprints are able to provide finer information on the cloud structure in high signal to noise ratio cases.

CALIOP output provides lidar linear depolarization ratios of clouds, which can be used for cloud phase discrimination in principle (Sassen, 1991). While the CALIOP lidar linear depolarization ratio can classify measurements as liquid or ice phases, due to the limited penetration of lidar for thick clouds and the lidar depolarization measurements being scattered, there are limitations for identifying the mixed phase cloud correctly. Instead an approach based on the microphysical and optical properties of ice particles and water droplets is considered. Differences between the number concentration, vertical distribution and radiative properties of ice particles and water droplets generate a temperature dependent radar reflectivity (Z_e) threshold (D. Zhang et al., 2010). This is then used alongside the integrated attenuated backscattering coefficient and cloud base/top temperatures to distinguish between the ice, liquid and mixed phases in places where the cloud temperature cannot determine the phase alone (Wang, 2019). 2BCL5 uses temperature data from another CloudSat product, ECMWF-AUX, that contains ECMWF (European Centre for Medium-Range Weather

Forecasts) variables such as temperature and specific humidity.

For cloud base temperatures below -38.5 °C, only ice is permitted. For cloud base temperatures above 1 °C, the cloud is classified as liquid when the cloud top temperature is above a threshold of -3 °C, liquid or mixed when the cloud top temperature is between -38.5 °C and -3 °C, or mixed for cloud top temperature below -38.5 °C. For cloud base temperatures between -38.5 °C and 1 °C, all phases are permitted (liquid, ice and mixed), and are determined based on a set of conditions. If either a liquid layer is detected or the integrated backscatter coefficient (IBC) is greater than 0.015 and cloud base temperature is greater than 1, it indicates the presence of liquid water. If the radar reflectivity is above the threshold Z_e, or the cloud top temperature is less than -30 °C then it indicates the presence of ice. If both of these conditions are met then it indicates mixed phase cloud. This can be seen in Figure 2.1, which shows the flow diagram for phase determination of the combined radar and lidar measurements for 2BCL5 (Wang, 2019). Note that the Tice = -7 °C given in the diagram is an incorrect value from 2BCL4, an older version of the 2BCL5 dataset.

Initially an older version of the product, the 2B-CLDCLASS-LIDAR R04 (2BCL4) dataset, was used with data from 2007 to 2010. The 2BCL5 product has data from 2006 to 2017 and improvements over the 2BCL4 product in the algorithms used. The CloudSat 2B-CLDCLASS-LIDAR R05 Product Process Description and Interface Control Document (Wang, 2019) explained improvements between how cloud phase was determined between the 2BCL4 and 2BCL5 products. Firstly, they identified that the T_{ice} threshold was too cold and changed it from -7 °C to -3 °C in light of new evidence indicating the presence of ice particles in clouds where the cloud top temperature is colder than -4 °C. Changing the T_{ice} threshold slightly increased mixed-phase cloud occurrence. Secondly, they identified that 2B-CLDCLASS-LIDAR data uses a cloud fraction estimation algorithm designed for warm boundary layer clouds, which underestimated cloud fractions for polar boundary layer ice clouds due to weaker signals. The algorithm was changed so that the 2B-CLDCLASS-LIDAR algorithm identifies the possible underestimation and avoided its impact on cloud classification. In light of these updates the 2BCL5 product was obtained and used in the analysis. 2BCL5 was obtained from the CloudSat Data Processing Centre[1] for the years 2006 - 2017.

[1] http://www.cloudsat.cira.colostate.edu/data-products/level-2b/2b-cldclass-lidar?term=98

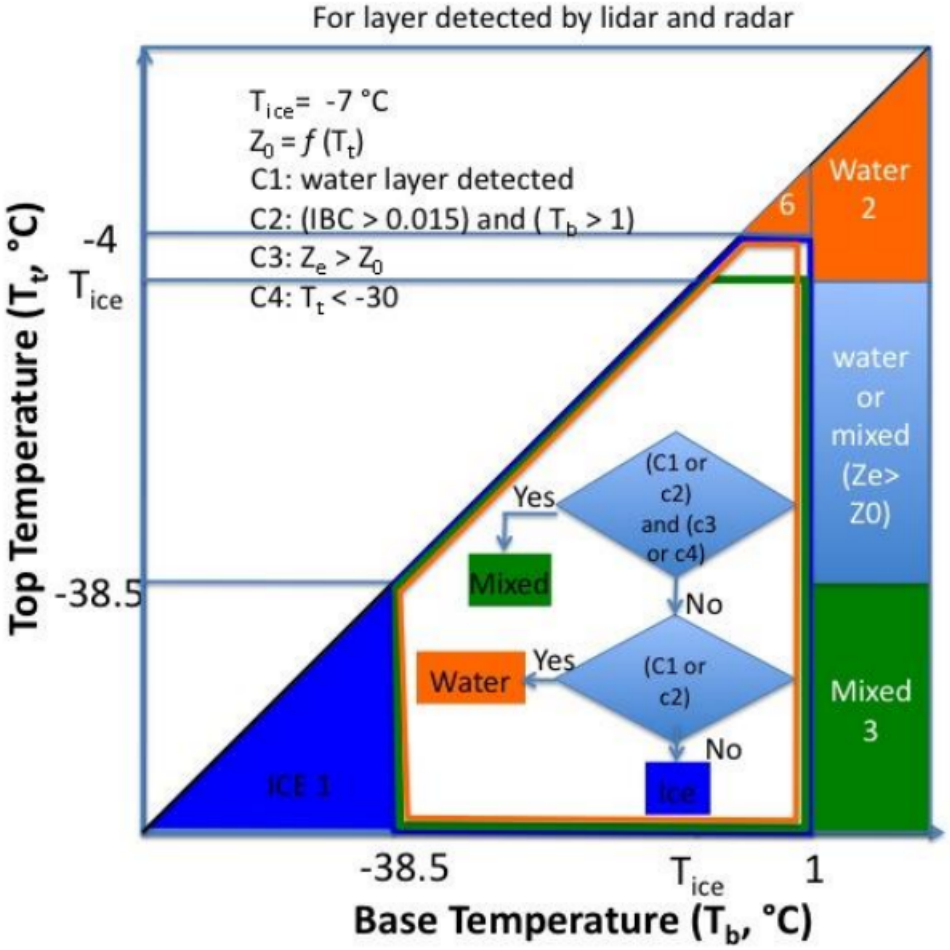

Figure 2.1: Phase determination processes for the 2BCL4 product, an older version of 2BCL5 (Wang, 2019).

2.1.3 DARDAR

Another satellite dataset, the raDAR/liDAR (DARDAR) dataset, was also used. Like 2BCL5, DARDAR also is a joint product of CloudSat and CALIPSO cloud measurements (Delanoë & Hogan, 2010). DARDAR v.2.11 (Ceccaldi et al., 2013) was obtained from the ICARE data and services centre[2] for the year of 2016. 2016 was chosen to coincide DARDAR observations with the ground based measurements also used this study.

DARDAR provides vertically resolved profiles of cloud phase, including ice, mixed and liquid phase clouds. As part of their phase determining algorithms they also include thermodynamic variables such as temperature, pressure and specific humidity. These are given by means of another CloudSat product, ECMWF-AUX, that is also used by 2BCL5. These are interpolated to each CloudSat cloud profiling radar bin. Similarly to 2BCL5, CALIPSO footprints are matched to CloudSat resolution. DARDAR has resolutions of 60 m in the

[2] `http://www.icare.univ-lille1.fr/projects/dardar`

vertical and 1 km in the horizontal.

DARDAR cloud phase classification processes are explained in detail in Delanoë and Hogan (2010) and updated in Ceccaldi et al. (2013) which explains changes due to the release of the DARDAR v2 product. These processes will be explained in brief.

First they defined "cold" pixels within their profiles where the wet-bulb temperature (T_w) was less than 0 °C. The wet bulb temperature is given by the ECMWF-AUX data, calculated from the temperature, pressure and humidity. They assume initially that all of the "cold" cloud pixels assigned to will be ice and the rest liquid water, as the web bulb temperature is above 0 °C in these cases. What they try to do next is to locate any supercooled liquid in the region of -40 °C $< T_w <$ 0 °C and then change the classification from ice to liquid.

Similarly to 2BCL5 they do not use the lidar depolarization ratio to determine cloud phase (Sassen, 1991), as the signal is too noisy to allow identification of supercooled droplets with enough certainty. Instead they use lidar backscatter signal at 532 nm, since to lidar the top of liquid clouds appears as a strong echo that is typically confined over only a few hundred meters (Hogan et al., 2003, 2004).

From there, they locate any attenuating high backscatter layers ($532 > 2.10^{-5}$ m^{-1} sr^{-1}) in the detections and then classify them into five groups: warm liquid water, supercooled liquid water, supercooled liquid water mixed with ice, highly concentrated ice, and the top of updrafts in convective towers.

The decision tree presented in Figure 2.2 shows how they classify these layers based on temperature, horizontal extent of layer, thickness, reflectivity, and altitude (Ceccaldi et al., 2013). If the wet bulb temperature is greater than 0 °C, then the layer is composed of warm liquid water. If a layer is less than 20 km wide and located in a vertically oriented cloud whose reflectivity is greater than 5 dBZ, then it is classified as the top of convective cloud tower. Pixels are classified as ice in high concentration if the layer is more than 300 m thick or if the wet bulb temperature is lower than -40 °C and as supercooled liquid water otherwise. One of the limitation of radar is that it is not able to detect pure supercooled liquid water because its signal is dominated by larger particles (Hogan et al., 2003). So, if the radar detects a signal collocated with supercooled liquid water layers detected by the lidar, they are then classified as supercooled liquid water mixed with ice.

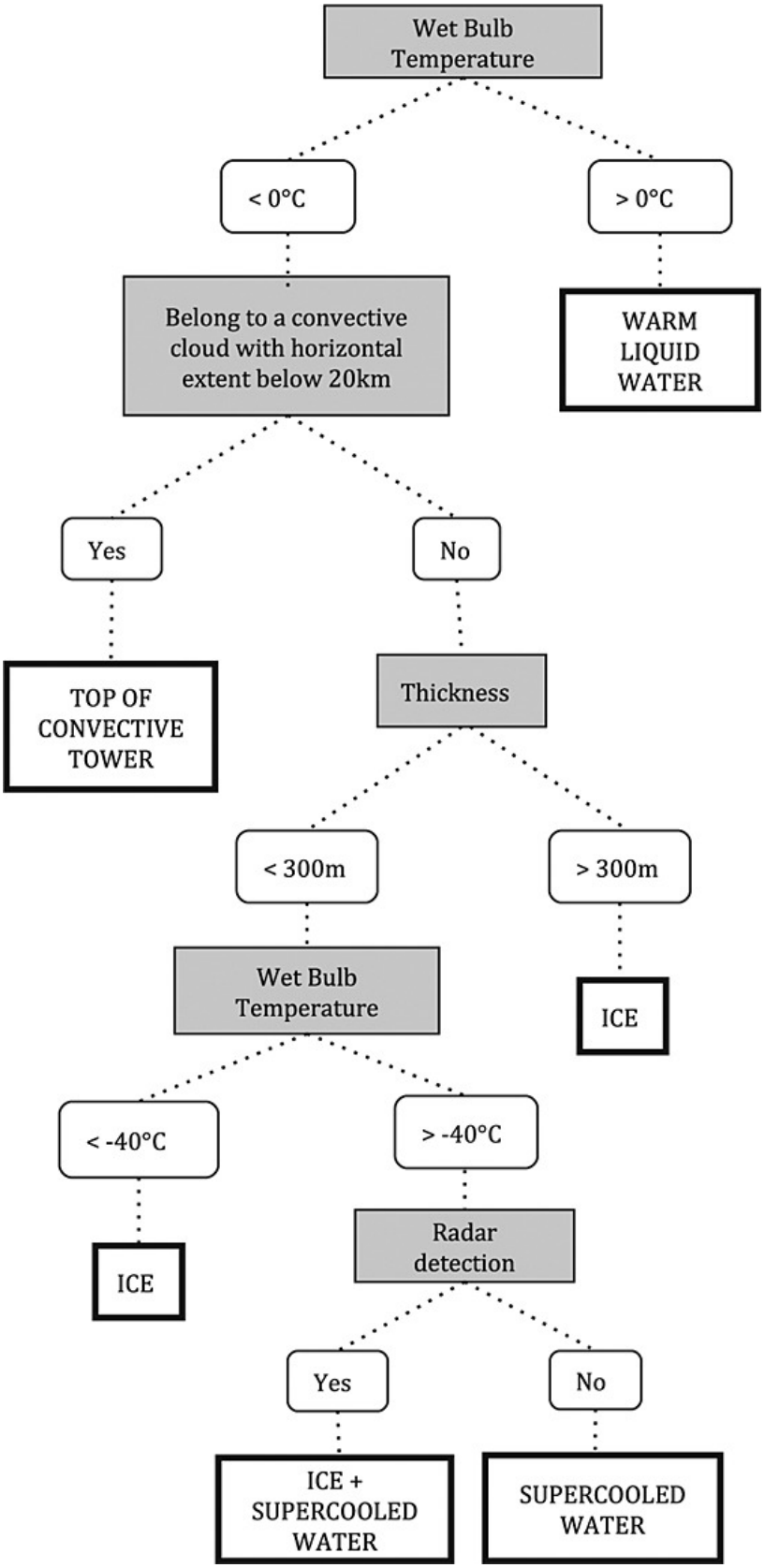

Figure 2.2: Decision tree for DARDAR phase classification, which sorts cloud layers with a strong backscatter signal (Ceccaldi et al., 2013).

2.2 Ground Based Datasets

2.2.1 AWARE

Ground based observations used in this study were obtained during the 2016 Atmospheric Radiation Measurement (ARM) West Antarctic Radiation Experiment (AWARE) field campaign over Antarctica.

The AWARE campaign was supported by the U.S. Department of Energy, started in November 2015 and concluded at the beginning of January 2017 (Witze, 2016). AWARE was the first climate-related field campaign in West Antarctica in more than 40 years and provides a rare surface based dataset for comparison with satellite based observations (Lubin et al., 2015). The AWARE campaign was motivated by the effects a changing climate is having on the West Antarctic Ice Sheet and the need for more field work to be undertaken in West Antarctica (Lubin et al., 2015).

One objective of AWARE was to examine the microphysical properties of cloud to gain an understanding of the warming mechanisms of West Antarctica. This included measurements of the cloud type, cloud fraction, cloud base, as well as altitude dependent measurements of cloud particle size distribution, thermodynamic phase, cloud particle vertical velocity, and precipitation rate and type. Such measurements took place mainly at McMurdo Station (77.85°S, 166.72°E).

The data specifically used in this study were cloud masks gathered by the Ka-Band ARM Zenith Radar (KAZR; Widener et al., 2012) and the High Spectral Resolution Lidar (HSRL; Eloranta, 2005), gathered from 1 January to 31 December 2016 over McMurdo Station. KAZR was operated in alternation between two modes. Moderate sensitivity (MD) mode was used to detect upper-tropospheric clouds and general (GE) mode was used to detect lower-tropospheric clouds. HSRL and KAZR operate using the same principles as discussed earlier in the chapter for the CloudSat and CALIPSO lidar/radar instruments. The methodology detailing how these cloud masks are derived is detailed in Silber et al. (2018) but will be discussed below in brief.

Detection of the HSRL hydrometeors (which includes both cloud and precipitation) were based on histograms of log-scaled particulate backscatter cross-section (βp) against linear depolarization ratio (LDR). These were used to classify the HSRL data into three categories: clear-sky aerosols, hydrometeors, or liquid-cloud (a subgroup of the hydrometeors). Because the histograms showed a seasonal dependence, they were generated on a monthly basis. From the histograms three populations were apparent. HSRL returns characterized by relatively low βp (cresting near 10^{-7} $m^{-1}sr^{-1}$) and low LDR values were attributed to clear-sky

aerosols. HSRL returns characterised by relatively high LDR (> 0.2) and βp varying from low to high values were attributed to ice particles of varying concentration, size, shape, and orientation. Finally a population with high βp and low LDR (< 0.15) was attributed to liquid water. Because the shapes of these populations varied from month to month through the seasons, a classification method which considers the βp and LDR features was developed.

Figure 2.3 shows an example of the classification for the months of March (subplots a and c) and August (subplots b and d) where βp against LDR has been investigated. KAZR signal-to-noise ratio (SNR) data from both the GE and MD modes was gridded separately to the HSRL data grid using two-dimensional linear interpolation. Using each of the two gridded data arrays and by setting a fixed SNR threshold of 16 dB, cloud masks were generated. The HSRL masks were combined with the KAZR (GE and MD modes) masks to form a full single hour cloud ice and liquid hydrometeor mask. From there hourly statistics such as hydrometeor and liquid-cloud base, thickness, and profile occurrence arrays were produced. Total and profile hydrometeor occurrence fractions were normalized relative to the hourly (HSRL and KAZR combined) data availability, assuming the measured period provided acceptable representation of the whole hour. Hours in which the combined data availability was below 25% were omitted from the occurrence fraction analysis to prevent potential low-sampling biases from affecting the statistics.

There were times where HSRL was unable to observe cloud meaning that only a KAZR detection was obtained. These KAZR measurements are classified as an unknown phase. Silber et al. (2018) notes that while liquid phase cloud will make up a part of this category, it is likely to represent ice phase cloud. Reasons for this include that the majority of unknown phase cloud is above 4 km where little liquid phase cloud was detected and much is located at temperatures colder than the verge of the homogeneous freezing regime at - 38 °C (Lamb & Verlinde, 2011).

The AWARE observations also includes soundings of other atmospheric variables such as temperature and pressure. These were gathered twice daily over McMurdo station during 2016 using a radiosonde. Soundings were linearly-gridded to the vertical grid of the hourly cloud masks (Silber et al., 2018).

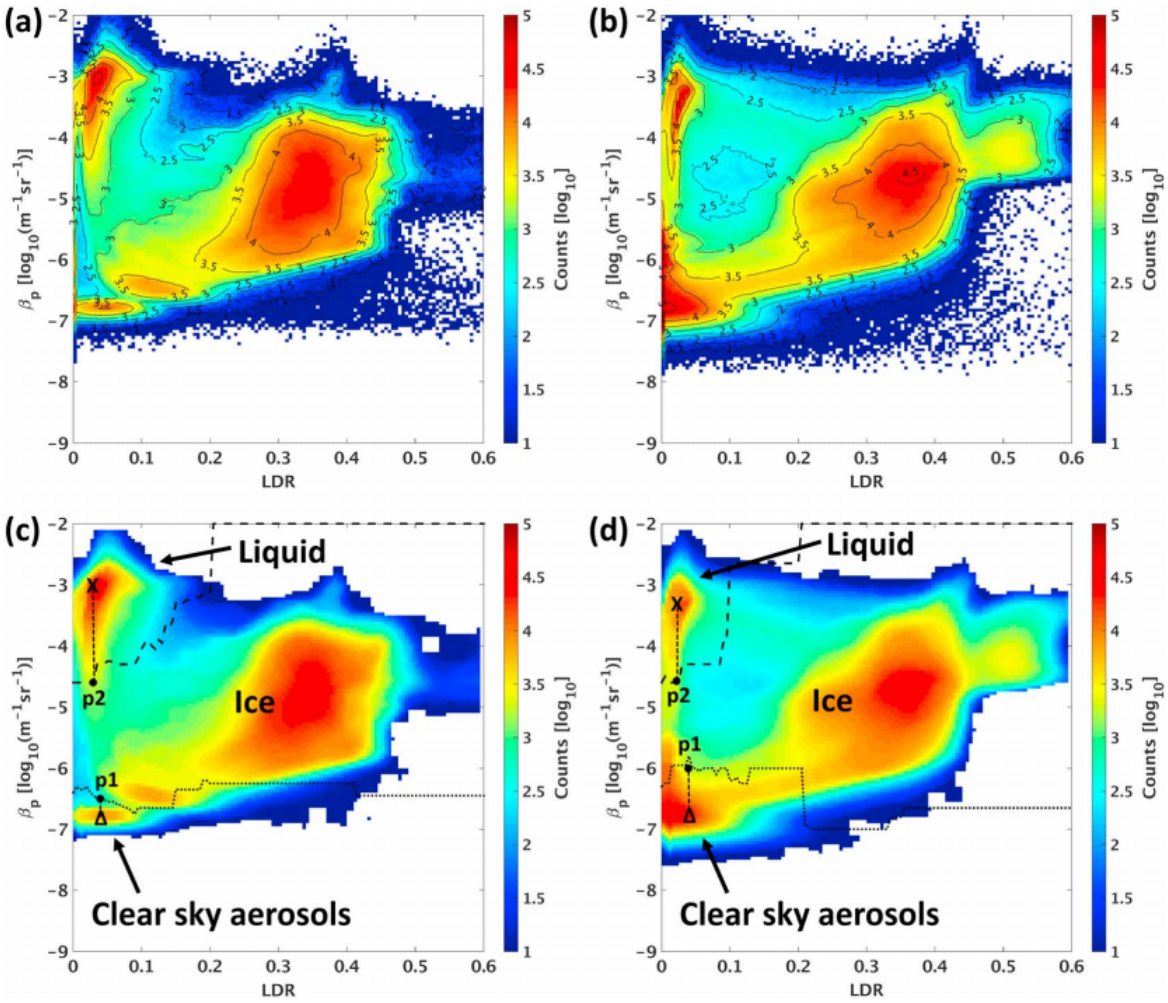

Figure 2.3: HSRL linear depolarization ratio (LDR) versus log-scaled particulate backscatter cross-section (βp) two-dimensional monthly histograms for (a and c) March 2016 and (b and d) August 2016. The bottom panels depict the histograms after the measurements were filtered. They also show the locations of the different populations (liquid, ice and clear sky aerosols) within the histograms, as well as the resolved boundary lines between them (Silber et al., 2018).

2.3 Other Datasets

2.3.1 ERA5 climate reanalysis

Monthly averages of ERA5 temperature profiles between 2006 - 2017 were used in this study, obtained from the Copernicus Climate Change Service (C3S, 2017). ERA5 is a climate reanalysis produced by the European Centre for Medium-Range Weather Forecasts (Hoffmann et al., 2019). Reanalyses combine observational measurements with model output to provide a numerical description of the recent climate. Over 240 variables are available, such as atmospheric and sea surface temperatures, surface pressure, vertical and horizontal wind speeds, and specific and relative humidity (Hoffmann et al., 2019; ECMWF, 2019). Hourly analysis

for ERA5 is available from 1950 - present and is generated with a horizontal resolution of 31 km on with 137 levels, from the surface up a height of around 80 km (Hersbach & Dee, 2016).

2.4 Previous studies comparing ground and satellite based cloud observations

In one of the few studies taking place around the Southern Ocean, Alexander & Protat (2018) used lidar based measurements gathered at Cape Grim (41S) compared with DARDAR satellite data. They found that DARDAR underestimated cloud below 1.5 km by a factor of three. It is noted that due to a lack of a cloud radar at Cape Grim they filtered their dataset to exclude thick clouds that attenuated the lidar. They only included low level single cloud layers where both the ground based lidar and DARDAR mask could detect the cloud top and cloud base.

Other studies also find an underestimation of satellite observations compared to surface based observations (Blanchard et al., 2014; Protat et al., 2014; Liu et al., 2017). An exception to this is Mioche et al. (2015) who compared surface and satellite observations at Ny-Alesund (78N). They found an overestimate of low-level cloud occurrence by satellite when compared with a surface-based lidar. They authors associate this overestimate with different cloud determination algorithms and a dataset with a short duration. CloudSat has difficulties observing boundary layer clouds below 1.2 km due to ground clutter, although detection can be improved by subtracting an estimate of the surface clutter from the radar measurements (Marchand et al., 2008; Tanelli et al., 2008.) From these studies one would expect that both 2BCL5 and DARDAR will underestimate the low level cloud.

These studies comparing ground and satellite based cloud observations are related to results obtained during this study in greater detail during the discussion chapter.

Chapter 3

Processing and analysis of satellite based observations

3.1 2BCL5 Processing

The 2BCL5 data obtained from the CloudSat Data Processing Centre [3] came in the Hierarchical Data Format (HDF), designed to organize and store large amounts of data. Each of the HDF files contains roughly 1 - 2 hours of combined CloudSat and CALIPSO observations with fourteen to fifteen observations in a day. The HDF files contains geolocation data fields related to the spatial and temporal position the satellites are observing, such as latitude, longitude, elevation and time. The files also contain observational data fields that are related to variables measured by the satellites, such as cloud base, cloud top, cloud phase, cloud fraction and cloud type. Cloud base is the detected height of the bottom of the cloud in kilometers and cloud top the height of the top of the cloud. Cloud phase is the given phase of the cloud of either liquid, mixed or ice. Cloud fraction is the percentage of each satellite footprint that is covered in cloud, and cloud type is the given classification of clouds such as cirrus, stratus and cumulus (Wang, 2019).

The cloud variables are organised by the 2BCL5 processing algorithms into layers which separated distinct clouds detected in the vertical column of the satellite footprint. Up to ten layers of clouds in each footprint are determined and each cloud layer has a corresponding value for the cloud top, base, phase, fraction and type. This is not ideal as in order to form a cloud mask that displays the cloud phase and cloud fraction as a function of altitude, cloud layers occurring at the same time need to be treated together in a vertical column. All processing carried out on the 2BCL5 data is carried out with the aim of creating a cloud mask that joins cloud layers together.

Individual 2BCL5 files are grouped by month then further split by sorting into latitude bins of five degrees. This allows analysis of different regions such as over the Southern Ocean, while maintaining a significant amount of measurements in each latitude bin. This processing produces 34 latitude bands with sorted 2BCL5 data, as the CloudSat and CALIPSO satellites do not extend past $\pm$ 82° in their orbits.

[3] http://www.cloudsat.cira.colostate.edu/data-products/level-2b/2b-cldclass-lidar?term=98

Two products are generated to represent the presence of cloud. The first is the cloud occurrence, which is derived as a function of altitude for different cloud phases. This is done using cloud fields in the 2BCL5 dataset. Cloud occurrence indicates the amount of cloud that is present at a particular altitude. A mask is created to remove data where there is no detection by the satellite as well as points without any cloud detected. At each satellite detection, the vertical extent of the cloud is then determined using values for the cloud base and cloud top. The corresponding value for the cloud fraction, which is a single value, is given to each vertical bin between the cloud base and cloud top. This process is repeated for each separate cloud layer in the detection. Further partitioning using information about the three phases of liquid, mixed and ice cloud produces separate cloud masks for each phase, which are combined to equal the total amount of cloud. Cloud occurrence profiles for each phase are then calculated at each altitude by summing the cloud fraction across each vertical bin over the required time period. Profiles are then normalised by dividing by the total number of measurements.

The cloud occurrence profiles with phase information for each year, month and latitude bin are processed separately. The profiles can then be added together using a weighted sum and then normalised using the total number of measurements in each profile. This allows for a finer resolution in the 2BCL5 dataset that can be reduced to larger spatial and temporal resolutions if needed.

The second product is the cloud fraction, which is derived by taking the ratio between the number of observations with at least one detected cloud and the total number of observations made, both cloudy and clear sky. Because the cloud fraction looks at the presence or absence of cloud in each atmospheric column making up a 2BCL5 detection, it is independent of altitude. This differs from the 'cloud fraction' field in 2BCL5 used to generate the cloud occurrence. From here onward cloud fraction is defined as the ratio between the presence or absence of cloud, rather than the data field in the 2BCL5 product.

There is an issue with inconsistencies in the 2BCL5 fields, in which the cloud fields have valid measurements, but there is a value for the cloud phase of 0. This is outside the range of values for the phase in the 2BCL5 measurements where 1 = ice, 2 = mixed and 3 = liquid. This results in errors in how the phase profiles for cloud occurrence are determined, where these points are allocated as liquid phase cloud when processed. This is an incorrect determination as 2BCL5 allocates liquid pixels first in their arrays, followed by mixed and ice phase pixels. These inconsistencies fall at the end of the 2BCL5 arrays so they are instead likely to be ice phase measurements. To fix the problem these points are removed using a secondary mask, as they are not a considerable part of the dataset and will not affect results.

3.2 2BCL5 Analysis

3.2.1 Quality of 2BCL5 observations

One of the first aspects to be analysed with the data is to assess its quality. 2BCL5 data ranges from June 2006 to December 2017, which gives 138 possible months of data. In reality, there are times where the satellites are unable to operate so this is reduced. Examples include December 2009 where a battery anomaly forced the Cloud Profiling Radar aboard CloudSat offline, as well as 17th April 2011 to 15th May 2012 where another battery anomaly caused CloudSat to fall out of formation with the other satellites in the A-Train. After the second battery anomaly the quality of data was further reduced as CloudSat could only operate in daylight-only mode where the sun could power its solar arrays. These interruptions in the operation of the satellites left 122 months of collected data to analyse.

The amount of 2BCL5 observations gathered each month are investigated. Figure 3.1 shows the total number of days in each month where measurements were taken by the satellites. Gaps indicate months with no data, due to the satellite not being in operation. Red bars represent months with measurements for less than half of the days in the month.

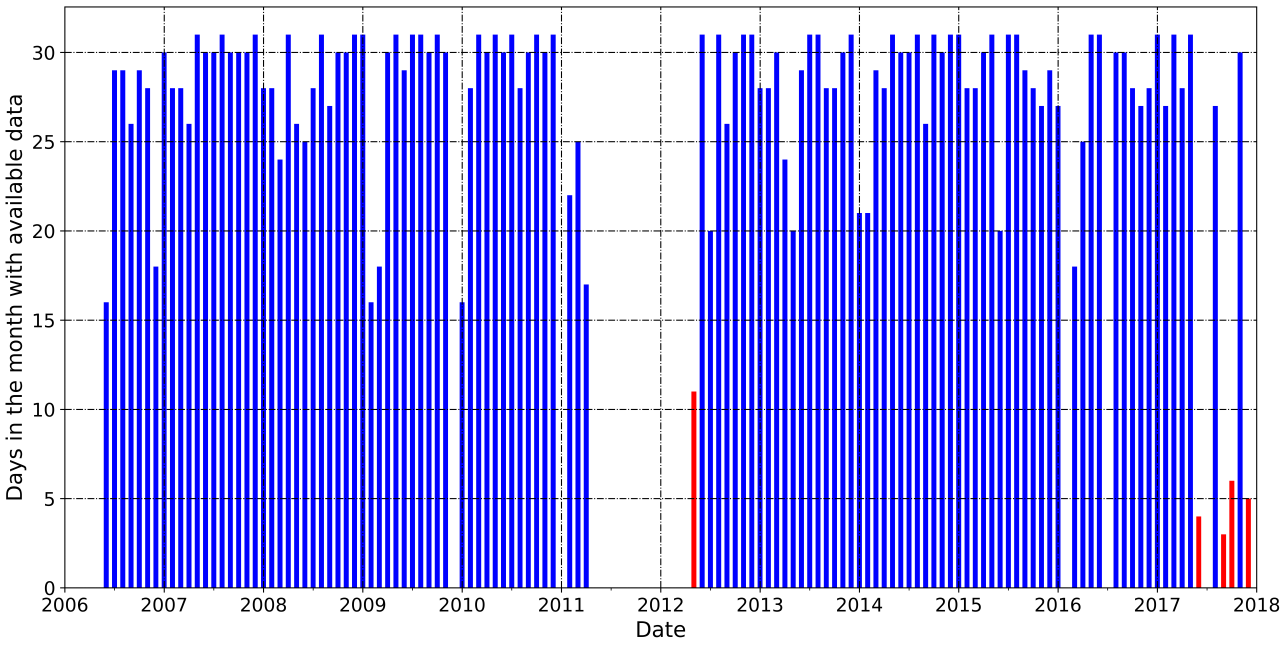

Figure 3.1: Days with available 2BCL5 data for each month between 2006 and 2017. Red bars indicate months with less than half availability. Gaps indicate months with no available 2BCL5 data. The x-axis has ticks at every six months, labelled at the start of each year.

Examination of Figure 3.1 shows there are five months that have little amounts of data. The lack of measurements during three of these can be explained as CloudSat had periods of inoperation. CALIPSO had a brief outage during another months (September 2017) which

caused 10 days without data, although this is not enough to explain that only six days in the month have measurements. It is likely that CloudSat and CALIPSO measurements are lost during the processing of the 2BCL5 product.

These five months with less than half the amount of available data will be considered when doing global analysis on the 2BCL5 dataset as they still provide accurately measured cloud occurrence, cloud fraction and cloud phase information. Due to a low sampling rate they may not be representative of the month as a whole, compared to months with higher data availabilities. Figure 3.2 shows the variability in the 2BCL5 cloud occurrence for the month of December, to compare whether the 2017 average is representative of the other months. The average monthly profiles for 2BCL5 cloud occurrence data are shown on each sub-figure, with the target year highlighted as the filled blue curve.

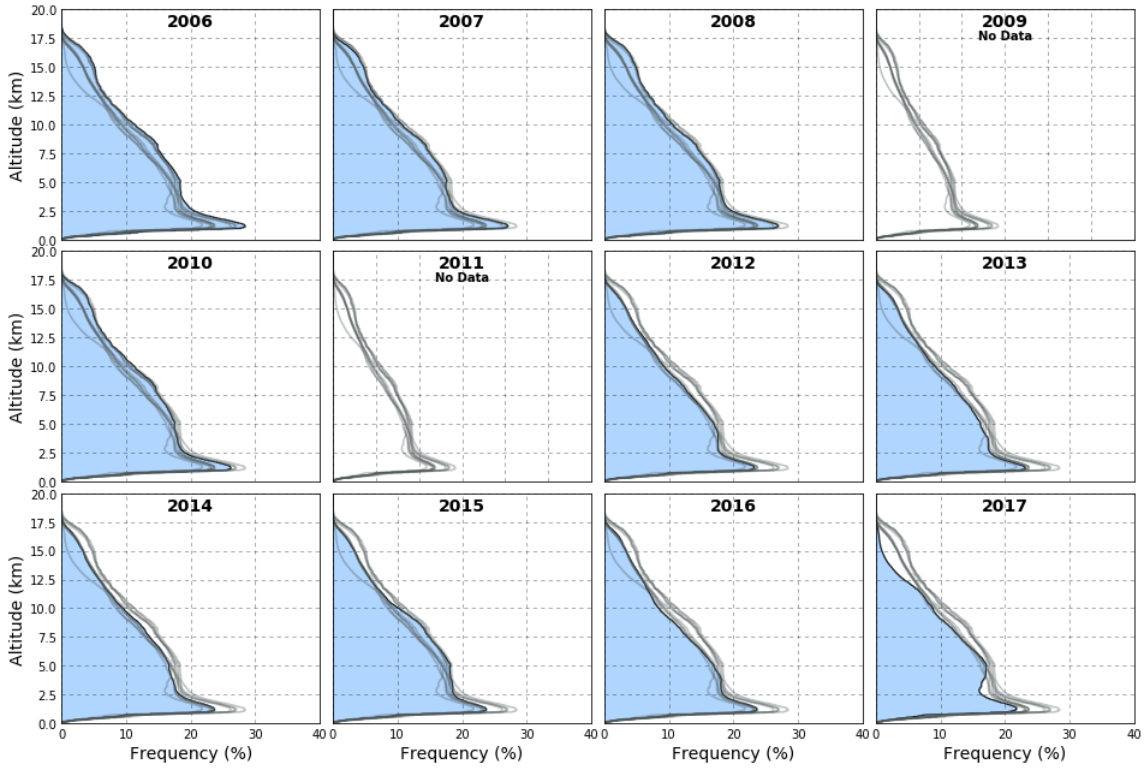

Figure 3.2: Geophysical variability of 2BCL5 cloud occurrence between 2006 and 2017 for the month of December. The target year is indicated by the filled blue curve with the grey lines representing the profiles from the other sub-figures.

While Figure 3.2 shows that the 2017 average of cloud occurrence is different from the other years, within the internannual variation it still represents the December average. Figures for June, September and October can be found in Appendix A and show better matches. It shows that the months with available 2BCL5 measurements for less than half the days in the month are still representative of the average and will be considered when considering each month separately.

The 122 months of 2BCL5 data that was binned into 34 latitude bands gave 4182 distinct spatial and temporal regions in my analysis. From here cloud occurrence profiles are created for 4087 of these, leaving 95 regions where cloud occurrence and cloud phase could not be determined due to poor quality data within the files themselves; The satellites would be operating but failed to get a cloud detection. All regions where cloud phase cannot be determined fall within 2012 - 2017 during April to August, and between latitudes of 60S to 85S. This corresponds to the winter season over the Southern Ocean/Antarctic regions. These missing cloud occurrence profiles are caused by CloudSat not operating due to a lack of sunlight.

3.2.2 Ascending and descending nodes

Due to the removal of data that fell into the dark portion of CloudSat's orbit after 2011, another aspect of data quality that is investigated is whether there are any significant differences between the amount of cloud that is detected during the ascending and descending portions of the satellite's orbits. The ascending node is when the satellite is traveling south to north over the Earth's surface. The descending node is when the satellite is traveling from north to south over the Earth's surface. During 2006 to 2017 when CloudSat and CALIPSO were in sun-synchronous polar orbits as part of the A-Train, they crossed the equator during their ascending node at 1:30 PM local solar time each day. Conversely the crossed the equator during the descending node at 1:30 AM local solar time each day. This caused their ascending node to occur mostly on the sunlight part of the Earth and descending node to occur mostly on the dark part.

The 2BCL5 data could be separated into ascending and descending nodes by using the gradient of the change in latitude. The cloud fraction, varying with latitude and time was then plotted for each of the nodes. Figure 3.3 shows cloud fraction for the ascending node and Figure 3.4 shows the cloud fraction for the descending node.

Figure 3.3 for the ascending node shows clear seasonal patterns in the cloud fraction. Over the Arctic there is a higher amount of cloud during the summer months than the winter months. The Southern Ocean shows a consistently high level of cloud, although there is a small amount of seasonality that varies cloud fraction. The only difference in the spatial availability of 2BCL5 measurements before and after CloudSat's 2011 battery anomaly, is an absence of data between April and August. As explained previously in this chapter, this gap is due to CloudSat not having enough sunlight to power its instruments. Corresponding cloud fraction measurements for months belonging to the Arctic winter are still present even after the 2011 battery anomaly. This occurs for two reasons. One is that CloudSat crosses

the equator during its ascending node at 1:30 PM local solar tine, so the ascending and descending nodes do not completely match with the day/night cycle. The second reason is that it takes 9.5 minutes for the CPR to become fully operational after entering the sunlit portion of its orbit, which occurs over the Antarctic (Nayak, 2012).

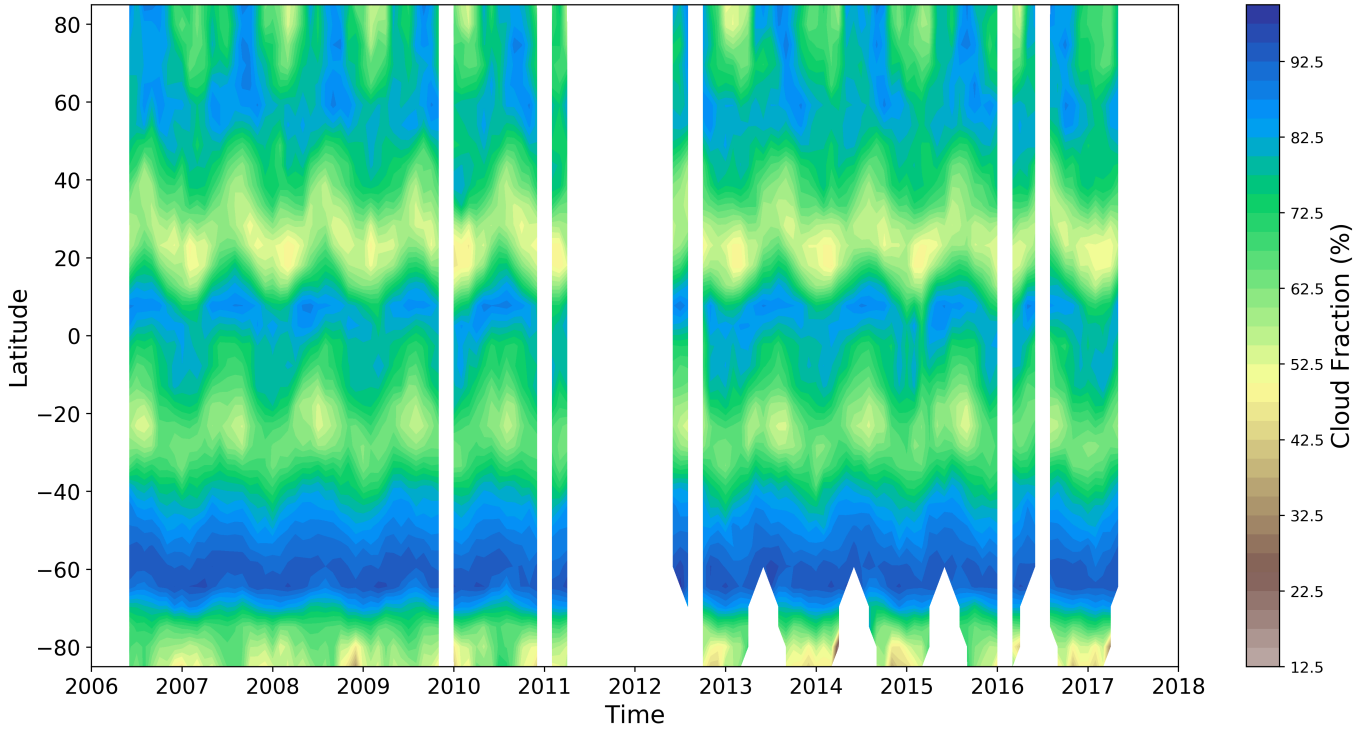

Figure 3.3: Cloud fraction for 2BCL5 during its ascending node between 2006 and 2017. White spaces indicate an absence of data. Tick marks on the x-axis indicate January 1st of a particular year.

For the descending node, Figure 3.4 shows a significant difference after 2011 compared to the ascending node. While both show the same seasonal cycle in cloud fraction, the descending node shows a lack of cloud fraction measurements, except for some at higher latitudes near the poles. For the Antarctic region, cloud fraction measurements are only able to be obtained during the Southern Hemisphere summer, out to a latitude of about 65S during December for the descending orbits. The Arctic region shows a similar picture where measurements are only available during the Northern Hemisphere summer. The only difference is Arctic measurements extend much further towards the equator, reaching a maximum latitude of about 40N during June. This happens due to the ascending/descending nodes not matching with the day/night cycle, and the 9.5 minutes after entering the sunlit portion of its orbit it takes for the CPR to become fully operational (Nayak, 2012).

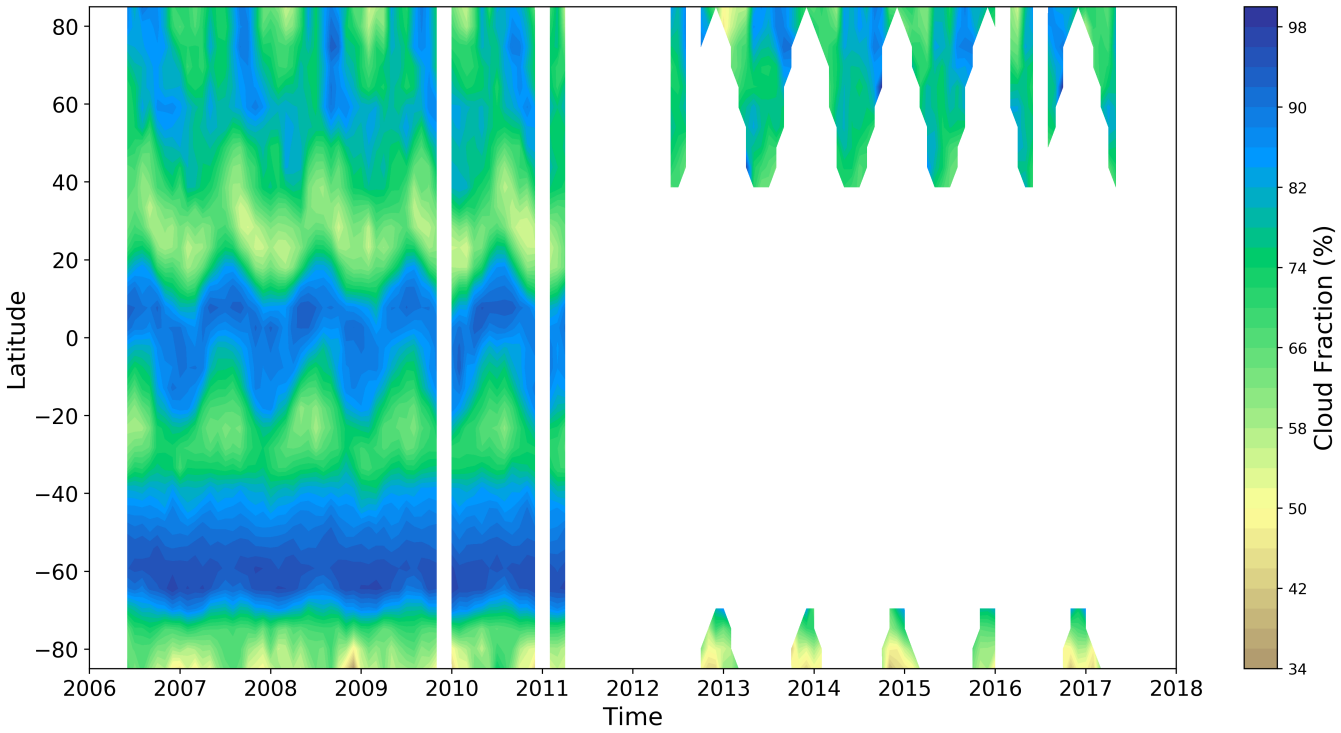

Figure 3.4: Cloud fraction for 2BCL5 during its descending node between 2006 and 2017. White spaces indicate an absence of data. Tick marks on the x-axis indicate January 1st of a particular year.

While the ascending and descending nodes both show similar seasonal patterns, another aspect to consider is whether they detect different amounts of cloud fraction. Any significant differences would mean they need to be treated separately as data after 2011 would be biased without cloud fraction measurements for the descending node. Figure 3.5 shows the differences between the total cloud fraction for the ascending and descending nodes.

Between 90N and 40N the ascending node shows a 5% - 10% greater cloud fraction than the descending node during the Northern Hemisphere summer. The descending node shows a greater cloud fraction during the winter months of up to 5%. This shows a clear seasonal variation here between the two. Below 40S there is also the same seasonal variation that occurs above 40N, but this is much weaker with differences of only a few percent. After 2011 the differences get stronger but this due to a reduction in the amount of available descending mode measurements that introduces a sampling bias and increases the variability.

Between 40N and 50S there is the greatest difference between the nodes. In all cases the descending node shows a greater amount of cloud than the ascending node where the strength of this difference varies with the season up to a maximum of 15%. That the descending node is showing more cloud indicates a diurnal cycle where more cloud is present during the night than the day, as the descending node occurs mostly on the dark side of the Earth.

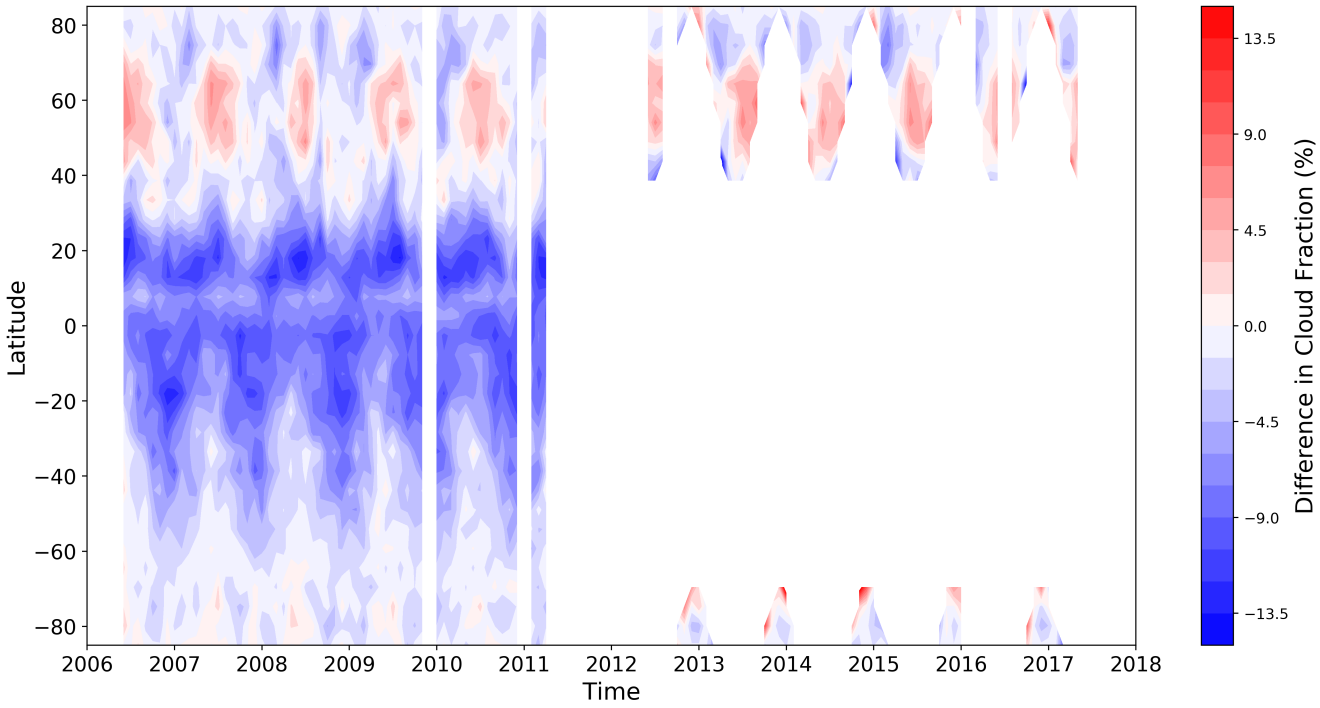

Figure 3.5: Difference in cloud fraction between the ascending and descending nodes. A negative difference, indicated in blue, means that the descending node has a greater cloud fraction. A positive difference, indicated in red, means that the ascending node has a greater cloud fraction. Tick marks on the x-axis indicate January 1st of a particular year.

Previous work on the diurnal cycle of cloud observations show that over land the cloud convection reaches its maximum in the late afternoon or early evening (Dai et al., 1999; Soden, 2000; Yang & Slingo, 2001; Stubenrauch et al., 2006; Y. Zhang & Klein, 2010; Zhao et al., 2017; Noel et al., 2018; Shang et al., 2018), causing the formation of clouds that persist into the night. Over the oceans cloud convection reaches its maximum in the late evening and early morning (Yang & Slingo, 2001; Stubenrauch et al., 2006; Wood, 2012; Noel et al., 2018; Chepfer et al., 2019).

Looking into the diurnal cycle of clouds in the tropics (30N - 30S) where the negative difference between the ascending and descending nodes is the greatest, a recent study by Chepfer et al. (2019) investigated the diurnal variations of cloud and relative humidity in the region. They found that optically thin cloud fraction profiles, dependent on relative humidity, maximize during night-time in the entire troposphere. They also found that over the oceans opaque clouds in the lower atmosphere are at their maximum during the second half of the night. This matches Figure 3.5 where the descending node shows a greater amount of cloud between 30N and 30S.

Noel et al. (2018) investigated the diurnal cycle of cloud profiles over land and ocean between 51S and 51N measured by the Cloud-Aerosol Transport System (CATS) lidar from

the International Space Station. As part of their study they compared CATS profiles to those measured by CALIPSO. Their results suggested that over oceans CALIPSO measurements describe the daily minimum of the cloud fraction profile during their daytime overpass (1:30 PM local solar time) and its daily maximum during their nighttime overpass (1:30 AM local solar time). This further shows a diurnal cycle of cloud over the oceans. Over land CALIPSO is more representative of daily averages as the diurnal cycle is less prominent, except at altitudes above 10 km where they capture part of the diurnal variability.

Since the CloudSat/CALIPSO descending node occurs from early evening to early morning, it makes sense that the descending node has a greater average cloud fraction which when compared to the ascending node shows diurnal variation. While the diurnal cycle is in Figure 3.5, seasonal patterns still show themselves at the dominant factor in the change of cloud coverage. Stubenrauch et al. (2006) also found a similar conclusion that shows the seasonal cycle in cloud coverage dominated the diurnal cycle. Figure 3.5 illustrates that the difference between the ascending and descending nodes is weakest over the Southern Ocean, only a few percent at the most. Figures 3.3 and 3.4 also show the weakest seasonal cycle over the Southern Ocean compared to other regions, due to an almost continuous presence of cloud coverage. Following on from these conclusions, the 2BCL5 dataset was not split into its ascending and descending nodes, but instead treated as a whole.

3.2.3 Latitudinal cross sections of 2BCL5 cloud occurrence

With the quality of the 2BCL5 dataset assessed, the distributions of cloud and cloud phase for 2BCL5 were analysed. Using the 5 degree latitude bands the data had been binned to, vertical profiles of cloud occurrence were partitioned into ice, mixed and liquid phase cloud for each season. The profiles that illustrate the cloud occurrence for the Northern/Southern Hemisphere using 2BCL5 measurements between 2006 and 2017 can be found in Appendix B.

They show a seasonal variability of the different cloud phases makes physical sense. There is more ice and less liquid present during the winter months than summer, which flips between the Northern and Southern Hemisphere as expected. Mixed phase is also greater during the winter where low temperatures allow both ice and supercooled liquid water cloud to coexist. The geographical variation shows that the cloud top height gets greater towards the equator and the frequency of the liquid phase cloud increases as temperature increases. These phases changes are associated with changes in thermodynamic profile of the atmosphere between latitudes and seasons (Donohoe & Battisti, 2013).

The patterns displayed in the cloud occurrence profiles (Figures B.1 and B.2) are better examined by combining each profile to make cross sectional contours of cloud occurrence and phase. This gives a clearer picture of the global distribution of cloud over the Earth as seen from space by the CloudSat and CALIPSO satellites, shown in Figure 3.6.

Also included on the plot are isotherms showing the altitude of 0 °C and -38 °C. These isotherms were produced using monthly ERA5 reanalysis temperature data (See Chapter 2.3.1) across each latitude and altitude. Monthly isotherms were generated between 2006 - 2017, corresponding to the 2BCL5 dataset, and then averaged to form a single isotherm. The 0 °C isotherm indicates the edge of where liquid will begin to freeze into ice phase cloud,at temperatures above this there should only be liquid phase cloud. The -38 °C isotherm indicates the homogeneous freezing regime (Lamb & Verlinde, 2011), below which any liquid in the cloud will rapidly freeze into ice crystals and cloud will only be ice phase. Between the two there will be a combination of ice and supercooled liquid water, so liquid, ice and mixed phase cloud can be present.

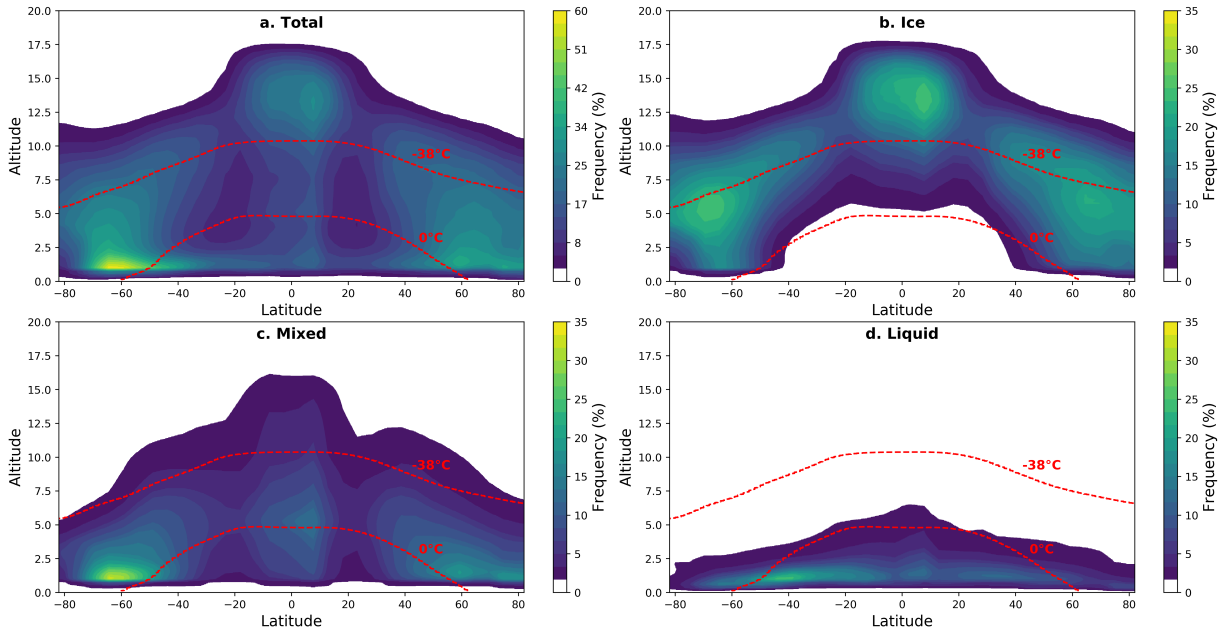

Figure 3.6: Latitudinal distribution of cloud occurrence as a function of altitude for the total cloud (a.) as well as the ice (b.), mixed (c.) and liquid (d.) phase clouds for 2BCL5 observations. The red dashed lines indicate isotherms of constant temperature.

Figure 3.6a shows the global distribution of cloud occurrence across each latitude and altitude for all phases combined. Large cloud occurrences are observed in the polar regions and the tropics. The maximum cloud is located at approximately 60S, and is dominated by low level cloud below 2 km. This makes sense as it corresponds to the Southern Ocean which has a higher cloud occurrence than land (Eastman et al., 2011). Similarly 60N also shows a high amount of low level cloud, while the tropics are dominated by high level cloud as a result

of the convective processes that occur there. The minima in cloud occurrence are observed at 20N/S either side of the equator, which correspond with subtropical regions where the Hadley cell circulation causes a downwelling of cool, dry, cloudless air. The structure of cloud occurrence also shows cloud is distributed to higher altitudes at the equator compared to the poles. This is because the height of the tropopause is greater due to the deep convection that takes place in the tropics (Marshall & Plumb, 2008). For Figure 3.6a, little can be said about how the cloud matches with the 0 °C and -38 °C isotherms.

Figure 3.6b-d shows the latitudinal distributions of cloud occurrence for ice, mixed and liquid phase cloud as seen by 2BCL5 at different altitudes. These contours are plotted using the same scale to compare the relative values between their cloud occurrences.

Figure 3.6b shows that the ice phase cloud has three distinct maxima. Two of these occur at 65N/S at an altitude of 5 km and are similar in their shape. The other occurs over the tropics at a height of 13 km. The minimum in the ice phase occurs between 40N and 40S where almost no ice cloud is detected below an altitude of 5 km. The ice phase cloud has a maximum cloud occurrence of 27% over the Southern Ocean and tropics. Over the Arctic the highest level of cloud occurrence is a few percent lower at 23%. Ice phase cloud has an absence at tropical and subtropical regions below 5 km. This matches well with the position of the 0 °C isotherm, although there are regions above/below the isotherm where ice cloud is absent/present. This initially suggests that 2BCL5 is incorrectly classifying ice phase cloud, but is instead can be explained by variations in the position of the isotherms. Isotherms are produced by taking an average across all years without accounting for factors like seasonal cycles in the temperature. During warmer/colder months the positions of the isotherms will be raised/lowered.

Figure 3.6c shows that mixed phase cloud is present across all latitudes up to a height of 5 km near the poles and 15 km in the tropics. 60S shows a 35% maximum of low level mixed phase cloud over the Southern Ocean. This is matched by a weaker 20% maximum at 60N. Mixed phase cloud is present at altitudes above the -38 °C isotherm and below the 0 °C isotherm. As for the ice phase cloud in Figure 3.6b, it would be expected that some mixed cloud would exits outside the isotherms, as they are being averaged across all seasons. However mixed phase cloud is present almost everywhere, outside the expected seasonal variations of the isotherms.

As might be expected, Figure 3.6d shows that liquid phase cloud occurs in the bottom 2.5 km of the atmosphere near the poles, which increases to a maximum extent of just over 5km in the tropics. This is due to the temperature differences between the equator and the poles, as can be seen in the decrease of the 0 °C isotherm moving poleward. Liquid phase cloud has a maxima of 24% low to the ground (1.2 km above mean sea level) at a latitude of

40S. The isotherms shows liquid phase cloud at greater than the 0 °C isotherm. This does not give insight into whether 2BCL5 processes liquid phase cloud correctly, as supercooled liquid water exists below 0 °C. 2BCL5 does not differentiate between liquid water that is supercooled or not so further analysis cannot be produced.

Comparing the distributions of ice, mixed and liquid phase cloud, most clouds above 5km at the polar regions and 8km in the tropics are ice. This is where air temperatures get colder than the -38.5 °C threshold, below which the 2BCL5 processing algorithm only classifies cloud as ice phase. Another aspect to note is that the maximum of mixed phase cloud over the Southern Ocean corresponds to the maximum in the combined cloud for all phases. This suggests that understanding mixed phase cloud is a key part of correctly modelling clouds in the climate. A study by McCoy et al. (2015) investigated mixed phase cloud over the Southern Ocean in a number of GCMs. They found that the temperature at which the supercooled liquid and ice that make up the mixed phase cloud were equally partitioned varied by as much as 40 °K across models. This suggests that GCMs simulate mixed phase cloud and its processes poorly and better parameterizations of mixed phase cloud are needed to reduce this model uncertainty.

Bodas-Salcedo et al. (2016) did further work to investigate the contributions of cloud phases to the radiation bias in climate model over the Southern Ocean. They found that areas where the uppermost cloud layer contains supercooled liquid water contribute between 27% and 38% to the total amount of shortwave reflected radiation in the Southern Ocean. A lot of these supercooled liquid water cloud tops will exists in mixed phase clouds where ice is present deeper into the cloud. Since the partitioning between mixed phase and supercooled liquid is uncertain, their result categorized mixed phase and supercooled liquid water clouds together. This further highlights the needs for good mixed phase cloud representation in climate models. These two studies match results shown, where mixed phase cloud is poorly represented by 2BCL5, while being important over the Southern Ocean.

A notable feature of Figure 3.6a is a sharp reduction in the amount of cloud detected below an altitude of 1 km. This is more clearly illustrated in Figure 3.7, showing Figure 3.6a constrained between latitudes of 40S to 80S and altitudes below 2.5 km.

At 60S, cloud occurrence shows a maximum value of 60% at an altitude just above 1 km. Moving below 1 km the cloud occurrence drops sharply, reaching half the maximum of 30% at an altitude of 0.8 km. This limit is present across all latitudes and phases, although it is less pronounced for liquid phase cloud. It suggests that the 2BCL5 dataset is poor at detecting cloud below 1 km. CloudSat and CALIPSO are both known to be poor at detecting cloud at these heights. CloudSat is affected by surface clutter below approximately 1.2 km (Marchand et al., 2008; Tanelli et al., 2008) and the CALIPSO lidar signal cannot

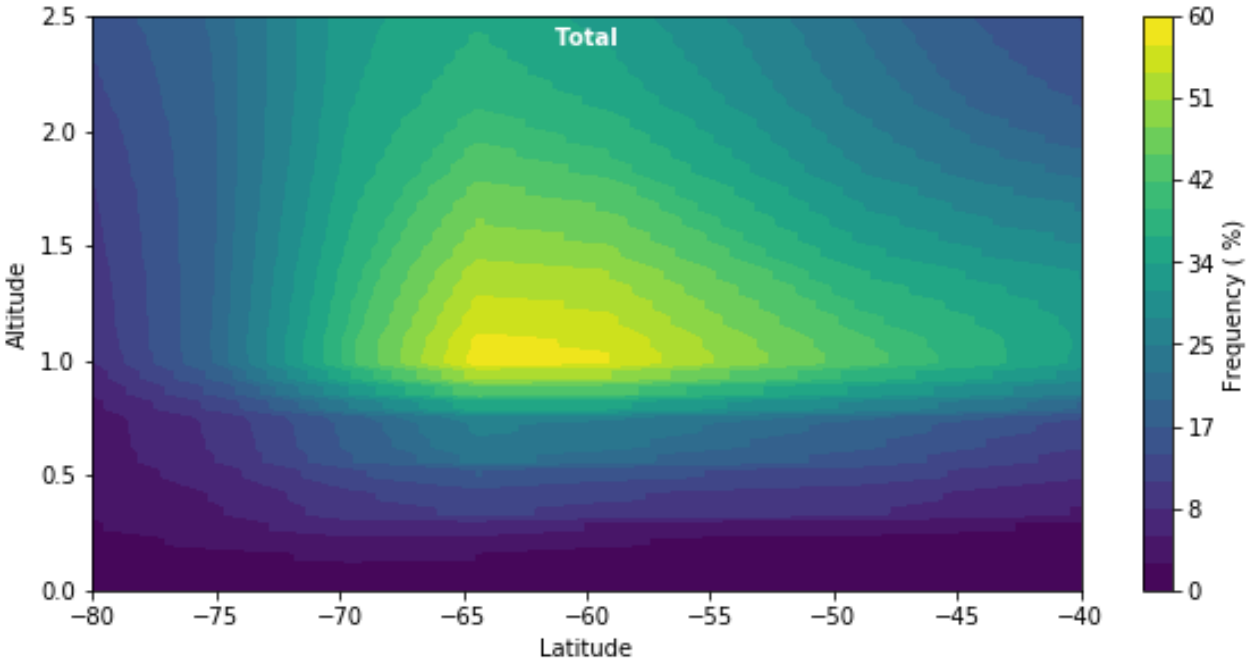

Figure 3.7: Subset of the latitudinal distribution of cloud occurrence for all phases plotted in Figure 3.6a. Latitude has been restricted to between 40S and 80S and altitude has been restricted to below 2.5 km.

pass through thick cloud. It is well known that both of the satellites that are combined to form the 2BCL5 dataset underestimate the amount of low level cloud. In order to get a complete picture of the vertical distribution of low level cloud a comparison with ground based observations are needed, which would allow an unattenuated detection of low level cloud. Another contributing factor is that some of the underestimation could be a result of the 2BCL5 processing algorithms, that would be absent with better processes. This has implications over the Southern Ocean where low level cloud is at its highest. In order to get verify this analysis of DARDAR, a secondary CloudSat/CALIPSO dataset is carried out and comparisons are drawn with 2BCL5.

3.3 DARDAR Processing

DARDAR data obtained from the ICARE Data and Services centre[4] also came in the HDF file format. Like 2BCL5, each of the HDF files contain 1 - 2 hours of combined CloudSat and CALIPSO observations with fourteen to fifteen observations in a day. The HDF files contain geolocation data fields that related to the spatial and temporal position the two satellites are observing, such as time, elevation above mean sea level, latitude, and longitude. Unlike 2BCL5, DARDAR cloud measurements are already grouped in a categorization

[4] `http://www.icare.univ-lille1.fr/projects/dardar`

mask that separates cloud into different atmospheric features. Figure 3.8 shows an example of this categorization for observations taken on the 26th May 2007 (Ceccaldi et al., 2013). The colours represent the different categories DARDAR pixels have been classified as. This includes cloud phases such as ice and liquid, as well as other features including aerosols and precipitation. The DARDAR classification also shows features that indicate limitations of the satellites. Radar clutter shows a lot of signal close to the ground where the quality of CloudSat measurement will be reduced. In reality the signal will be affected by ground clutter over a greater range of altitudes (Marchand et al., 2008; Tanelli et al., 2008). Lidar attenuation represented in black shows vertical columns where CALIPSO can not contribute to the identification of clouds, as CALIOP's lidar signal is being fully attenuated.

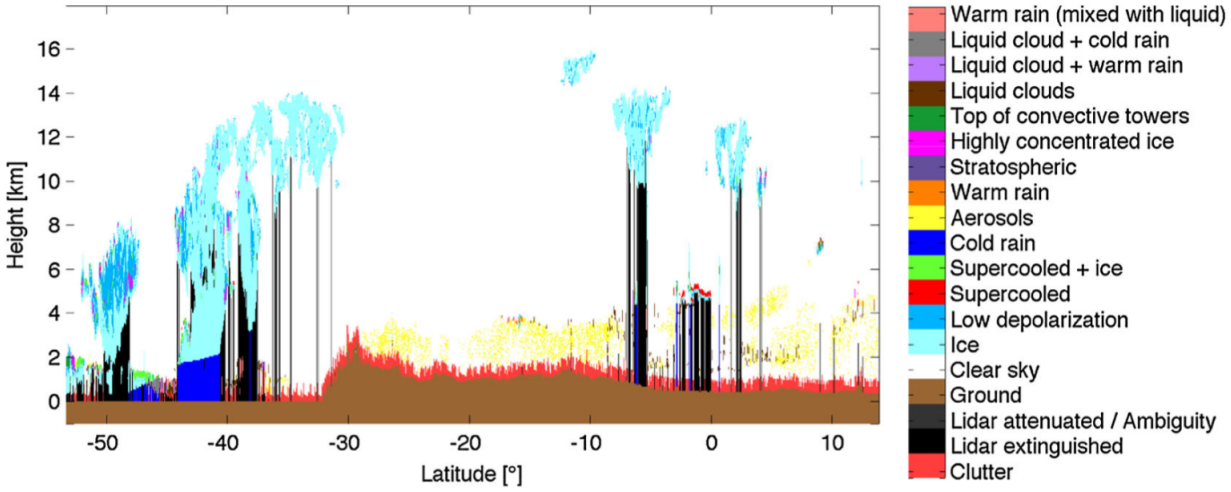

Figure 3.8: DARDAR classification showing features for observations taken on the 26th May 2007 (Ceccaldi et al., 2013).

Vertical profiles of cloud occurrence are then derived using the DARDAR classifications. The appropriate features are selected to partition the data into masks from different phases. The ice phase cloud mask is created by selecting the "ice" categorization as well as feature masks for "high ice concentration layers", "spherical ice" and the "tops of convective cloud towers". The mixed phase cloud mask is created by selecting the "supercooled liquid water and ice" categorization. The liquid phase cloud mask is created using the "supercooled liquid water", "liquid water", "warm rain & liquid cloud" and "cold rain & liquid" categorizations. Places where there is a detection are set to a cloud occurrence of 1 and elsewhere set to a cloud occurrence of 0.

Cloud occurrence profiles for each phase are then calculated at each altitude by summing the cloud occurrence at each vertical bin over the required time period. Similarly to 2BCL5, cloud occurrence profiles with phase information for each year, month and latitude bin are processed separately. The profiles can then be added together using a weighted sum which is then normalised using the total number of measurements in each profile. By masking the

DARDAR classification to cloud only detections the cloud fraction is also determined, giving the fraction of cloudy detections compared to the total number of detections. After the cloud occurrence and cloud fraction is determined, the processing of DARDAR measurements was completed using a similar process to the 2BCL5 measurements. Individual DARDAR files are sorted by month and then further split into latitude bins of five degrees.

3.4 DARDAR Analysis

3.4.1 Quality of DARDAR observations

DARDAR is selected to provide a reference to the 2BCL5 observations, where comparisons between the two are completed to assess their quality and decide which has a better representation of cloud. Because both are derived from CloudSat and CALIPSO you would expect they have the same amount of available data. Any differences would be due to their separate processing methods rather than the satellite data they input into their algorithms. DARDAR data used in this study ranges from January to December 2016 giving 12 possible months of data. While DARDAR observations exists for other years, 2016 was chosen to coincide DARDAR observations with the ground based AWARE measurements. CloudSat had measurements during all of 2016, but a CALIPSO outage from the end of January to the start of March meant that there was no DARDAR data for February, leaving 11 months of observations.

The amount of DARDAR observations gathered each month is investigated, as shown in Figure 3.9. Like Figure 3.1, it shows the total number of days in each month where measurements were taken by the satellites. Gaps indicate months with no data due to the satellite not being in operation. It shows no data for February 2016 as expected, but also shows only 6 days worth of data for April 2016.

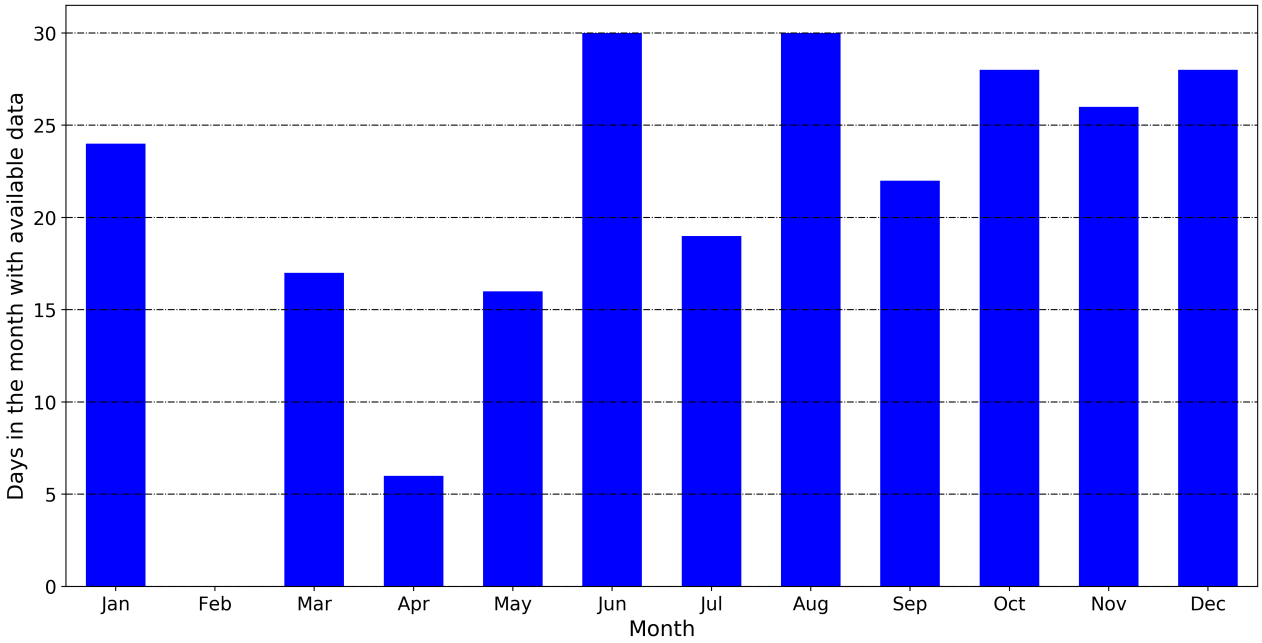

Figure 3.9: Days with available DARDAR data for each month during 2016. Gaps indicate months with no DARDAR data.

Figure 3.10 shows differences in the data availability between DARDAR and 2BCL5 during 2016. Red bars represent DARDAR, blue bars represent 2BCL5, and purple bars represent where the two overlap. The only month where DARDAR shows more data than 2BCL5 is July, where 2BCL5 does not have any days with valid cloud observations. During all other months DARDAR shows a lesser or an equal amount of days with available data. The largest reductions in the amount of observations are present during April, May and September.

It suggests 2BCL5 overall is more complete as less observational data is removed when the CloudSat and CALIPSO observations are combined, although the lack of measurements during July is unusual. Looking into a similar product to 2BCL5 that does not include CALIPSO lidar measurements, 2B-CLDCLASS R05, CloudSat data is available during July. This means that the gap in 2BCL5 during July 2016 may be an issue with the CALIPSO data. However, CALIPSO measurements are available during this time and DARDAR can combine CloudSat observations with them in their product. This gives an indication that the gap in July is indicative of a problem in 2BCL5's processing rather then a lack of data from either satellite.

The differences between the availability of 2BCL5 and DARDAR measurements might also mean that DARDAR has stricter quality control methods that remove more data, and is therefore a more representative dataset. There are six months such as August and December where the two are either in agreement or have a difference in the number of available observations of a day, so this is unlikely.

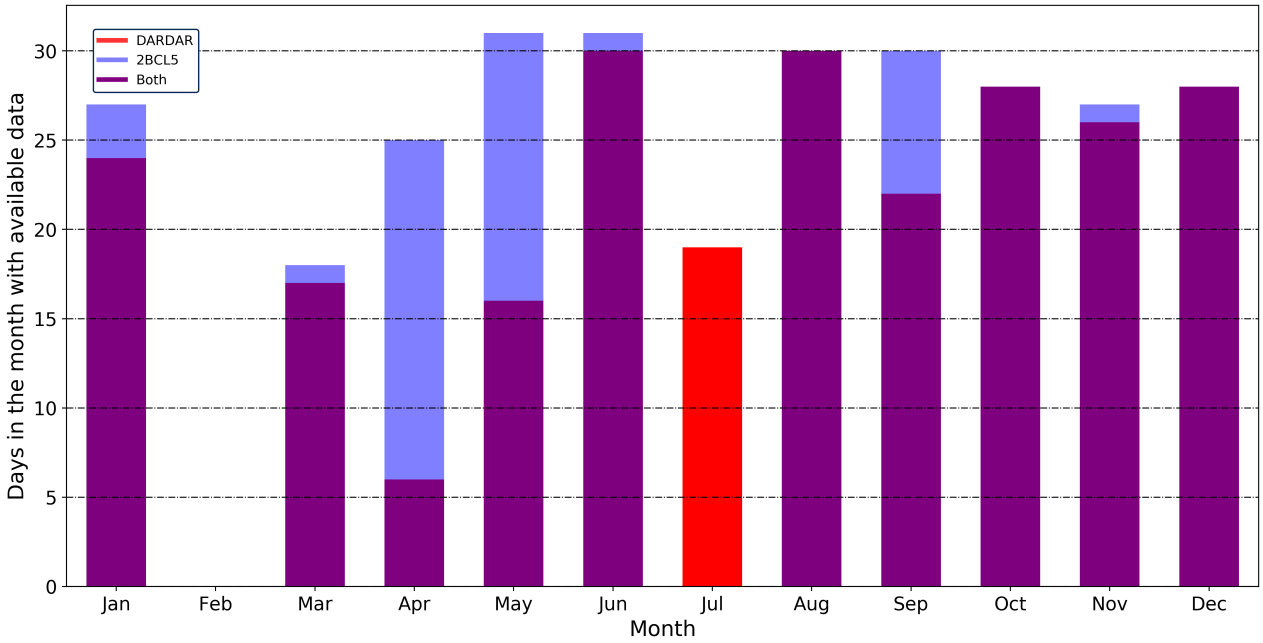

Figure 3.10: Days with available data for each month during 2016 for both DARDAR and 2BCL5. Red bars indicate DARDAR, blue bars indicate 2BCL5. Purple bars indicate overlap between the two. Gaps indicate months with no DARDAR data.

3.4.2 Latitudinal cross sections of DARDAR cloud occurrence

The latitudinal distribution of cloud occurrence as a function of altitude for the total cloud as well as the separate phases was created for DARDAR in Figure 3.11. This was completed using a process identical to Figure 3.6 where profiles of cloud occurrence in each latitude were joined together to make a contour plot.

Figure 3.11a shows the global distribution of cloud occurrence for all phases across each latitude and altitude. A maximum cloud occurrence of 48% at an altitude of 1 km is located at approximately 65S. This shows globally cloud is dominated by low level boundary layer cloud. Other places where Figure 3.11 shows local maxima are in the tropics at 10N, at a height of 11.5 km, and 60N at a height of 4 km.

Figure 3.11b-d shows that cloud is dominated by ice phase cloud with the Southern Ocean maximum of 48% consisting of approximately 35% ice, 8% liquid and 5% mixed phase cloud. Globally, ice is dominant except at mid to low latitudes where ground level clouds are primarily liquid phase. There is mixed phase cloud with a maximum of 4.5% over the Southern Ocean, but this is a small amount compared to the ice cloud at these heights. Liquid phase cloud is present in the bottom 5 km of the atmosphere which lowers around 40N/S. Liquid phase cloud has a maximum of 12% at an altitude of 1.2 km and a latitude of 40S.

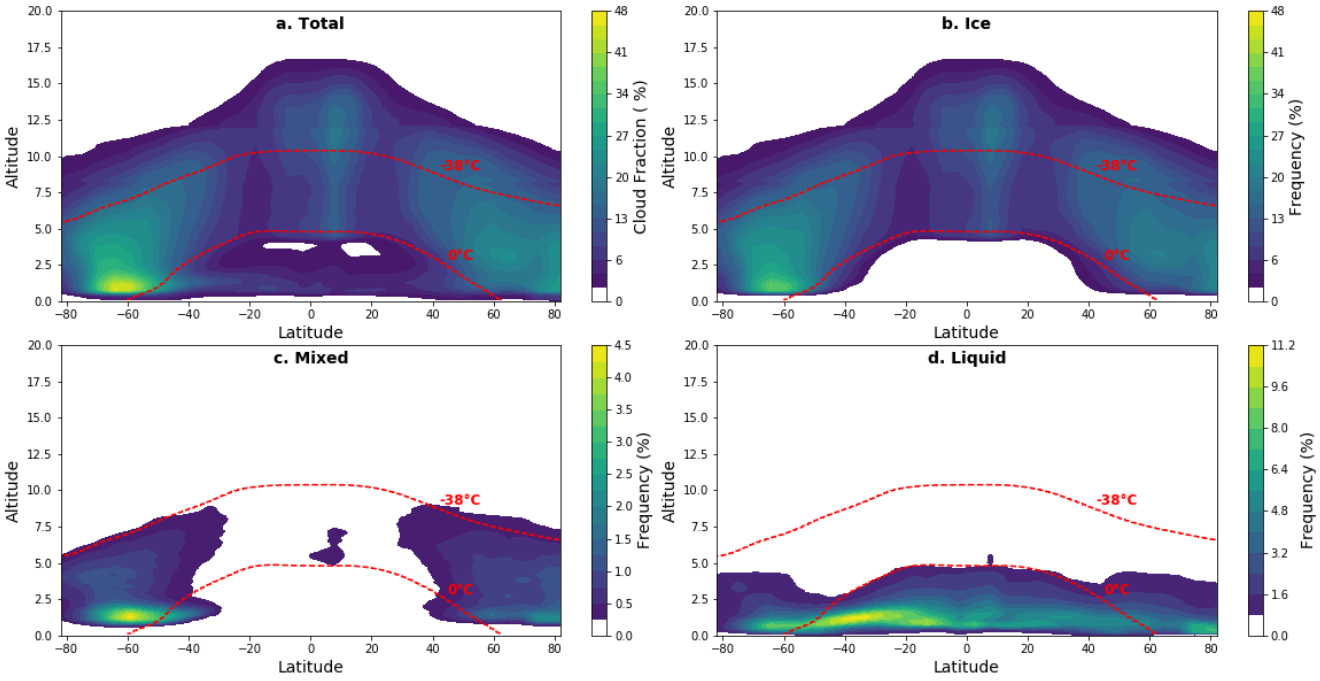

Figure 3.11: Latitudinal distribution of cloud occurrence as a function of altitude for the total cloud (a.) as well as the ice (b.), mixed (c.) and liquid (d.) phase cloud for DARDAR cloud observations.The red dashed lines indicate isotherms of constant temperature. Note that the scales are different on subplots c. and d. to highlight where cloud occurs.

Comparing the distribution of the ice, mixed and liquid phase cloud, above an altitude of 5 km cloud consists of ice, apart from a small proportion of mixed phase cloud. Below 5 km cloud consists of liquid between 0 to 40N/S and a combination of liquid, ice and mixed phase cloud poleward of this latitude. Apart from a sizable low level liquid distribution stretching to 60S, this is mostly ice. According to the isotherms, ice is located in places where you would expect temperatures to be below 0 °C. Small amounts of ice phase cloud are present below the 0 °C isotherms, but as in the case for 2BCL5 this can be explained by variations in the position of the isotherms due to seasonal cycles in the temperature. Mixed phase cloud is located at high latitudes where sub zero conditions allow the combination of ice crystals and supercooled liquid water to exist. Mixed phase cloud matches well with the 0 °C and -38 °C isotherms, within what would be excepted due to seasonal variations in temperature. Mixed phase clouds are present at all latitudes (Korolev et al., 2017) but are lowest over tropical latitudes (Mülmenstädt et al., 2015; Korolev et al., 2017; Wang, 2019). However, mixed phase cloud is absent between 40N/S and only has an occurrence of up to 5% elsewhere. This suggests that DARDAR may under-represent tropical mixed phase cloud. Liquid cloud extends to an equal height at both the equator and poles, but has a dip over mid latitudes. As the height of the 0 °C isotherm is higher in the tropics than at the poles due to warmer temperatures, you would expect that the liquid phase cloud would extend to a greater altitude at the equator.

Similarly to 2BCL5, DARDAR cannot completely resolve cloud down to the ground. To highlight this Figure 3.11a is constrained between latitudes of 40S to 80S and altitudes below 2.5 km, shown on Figure 3.12. Here cloud falls away below 0.8 km with little cloud below 0.5 km, and almost no cloud below 0.25 km. The maximum amount of cloud is at an altitude of 1 km. This shows a clearer picture low level cloud than seen in Figure 3.7 for 2BCL5. 2BCL5 shows a maximum above 1 km where cloud falls off significantly below this point. DARDAR has a much smoother resolution close to the ground and sees a better representation of the cloud.

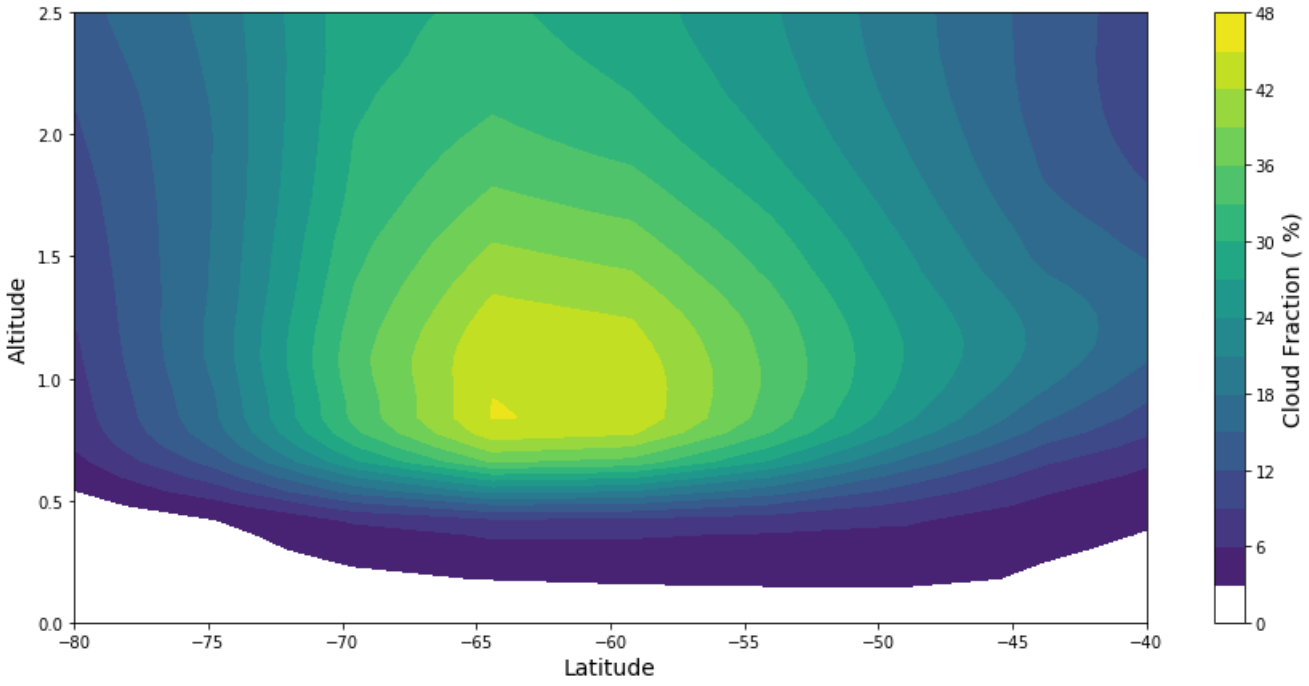

Figure 3.12: Subset of the latitudinal distribution of cloud occurrence for all phases, plotted in Figure 3.11a. Latitude has been restricted to between 40S and 80S. Altitude has been restricted to below 2.5 km.

Something that is present in Figure 3.11a is an irregularity in the cloud occurrence at an altitude of just below 12.5 km. At this height the contours pinch inwards, which is coming from Figure 3.11b for the ice phase cloud. While assessing the second version (v2) of DARDAR compared to the first (v1), Ceccaldi et al. (2013) investigated the differences in cloud occurrence depending on latitude and altitude. Figure 3.13 shows the result of this analysis, where distributions of cloud occurrence were produced using DARDAR observations from January, February and March 2010.

Figure 3.13c, assessing the difference between DARDAR v1 and v2 shows a dark line just below 12.5 km where less cloud is detected in v2 at this height. This irregularity is a result of v2's processing and matches the similar pattern seen in Figure 3.11b.

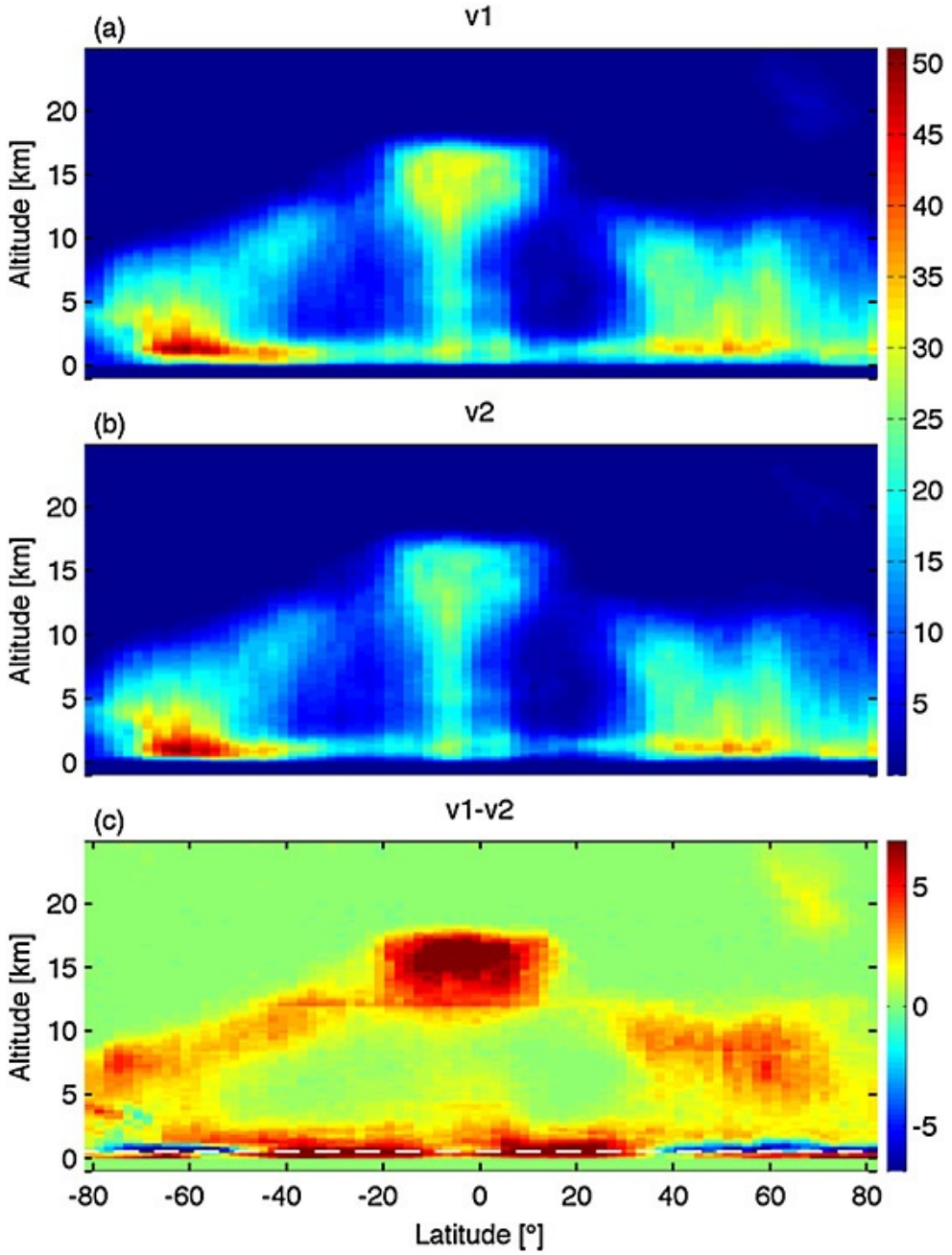

Figure 3.13: Comparison of hydrometeor occurrence between DARDAR v1 and v2 for January, February and March 2010 for (a.) Hydrometeor occurrence with respect to latitude and altitude for DARDAR v1. (b.) Same as a. but for DARDAR v2. (c.) The difference between DARDAR v1 and DARDAR v2. A positive difference means DARDAR v1 detects a greater amount of cloud (Ceccaldi et al., 2013).

To verify the results obtained in this study the Ceccaldi et al. (2013) representation of DARDAR v2 (Figure 3.13b) cloud was compared to the representation of DARDAR produced in Figure 3.11. Ceccaldi et al. (2013) shows a maximum of cloud over the Southern Ocean of approximately 50%. This matches with what is seen in Figure 3.11 with a 48% maximum over the Southern Ocean. Although both figures have produced DARDAR cloud occurences

for different temporal periods, they show global structures that represent the cloud similarly. The difference between the two is that Figure 3.13b shows a much greater amount of cloud in the bottom 5 km between 40N and 40S. Figure 3.13 represents all hydrometeors (which include both cloud and precipitation). Figure 3.11 was created ignoring features that have been classified by DARDAR as precipitation, as cloud was to be looked at directly.

To compare the two more directly, the DARDAR categorisations of "warm rain" and "cold rain" were included in the liquid phase cloud mask. Figure 3.14 shows latitudinal profiles of occurrence for all hydrometeors, compared to Figure 3.11 that ignored precipitation. Previously an issue was identified in the extent of the liquid phase cloud, where it appeared too high at the poles. The liquid phase hydrometeor occurrence in Figure 3.14d has dropped towards the poles from 5 km in Figure 3.11 to below 2.5 km, which matches better with the isotherms. The maximum in the liquid phase cloud still occurs in the same place of 40S, but has doubled from 12% to 24%. The amount of liquid has increased, mostly in the tropical and subtropical regions between 40S and 40N. This change in the liquid occurrence is also reflected in Figure 3.14a, where the gaps below 5 km at low to mid latitudes have been filled in. Given that both plots are derived from DARDAR measurements of both cloud and precipitation, it is unsurprising that the match with Figure 3.13 is much better for Figure 3.14 compared to Figure 3.11. This provides verification that the processing of the DARDAR observations and subsequent graphs are accurate as differences seen can be corrected by adding precipitation.

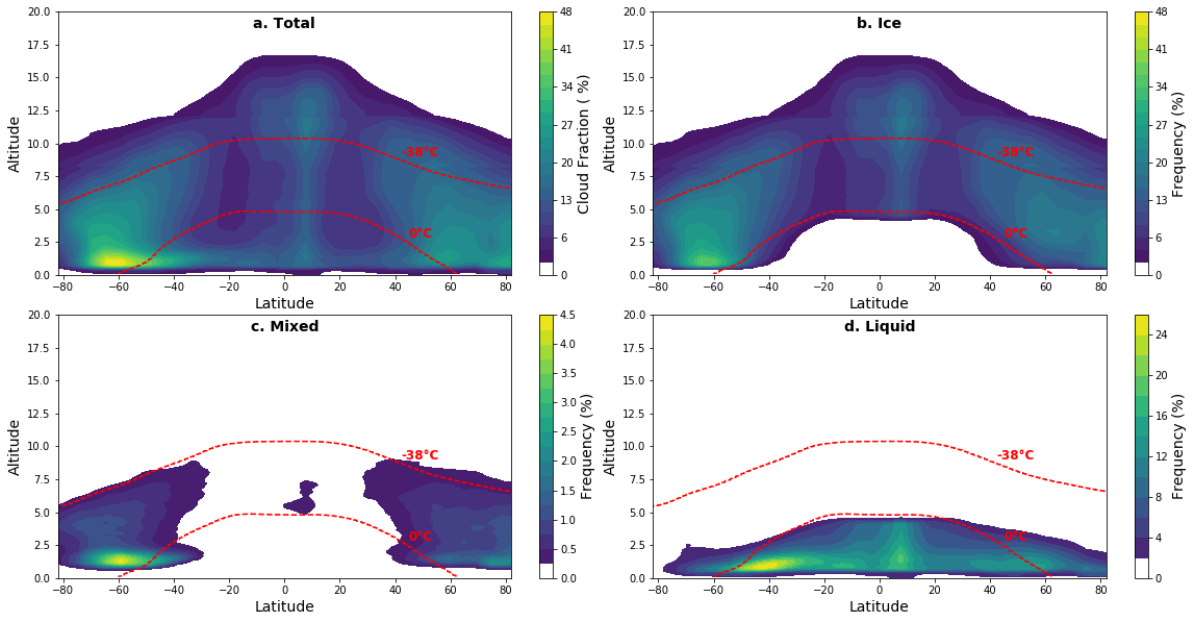

Figure 3.14: Latitudinal distribution of all hydrometeors as a function of altitude for the total hydrometeor occurrence (a.) as well as the ice (b.), mixed (c.) and liquid (d.) phase hydrometeor classifications for DARDAR observations. Hydrometeors include detections of clouds and precipitation. The red dashed lines indicate isotherms of constant temperature.

3.5 Comparing 2BCL5 & DARDAR

3.5.1 Differences in latitudinal cloud occurrence

Both 2BCL5 and DARDAR have been used to derive global distributions of cloud occurrence. Both show a reasonable picture of the total cloud, observing the highest extent of the cloud top well and showing the greatest amounts of cloud in similar places. The biggest difference between the relative shapes of Figure 3.6a and Figure 3.11a is the amount of subtropical and tropical cloud. 2BCL5 shows a large amount of cloud here, whereas DARDAR observes little. Instead representations of 2BCL5 cloud will be compared with DARDAR cloud and precipitation features, which corrected subtropical and tropical cloud deficiencies identified in Figure 3.11.

Initially, it was thought that the 2BCL5 excluded precipitation in its cloud mask determination. The 2BCL5 processing document (Wang, 2019) states that one of the primary inputs for cloud determination in 2BCL5 is a cloud mask from another CloudSat product named 2B-GEOPROF. This "cloud mask" indicates where radar reflectivity measurements are likely due to real hydrometeors, that is clouds or precipitating particles. It does not distinguish between cloud and precipitation, which transferred to the 2BCL5 cloud masks. With this in mind, comparison between 2BCL5 and DARDAR will include the precipitation feature masks in the DARDAR cloud distribution.

Even with precipitation included in both products, the two show large differences in the total amount of cloud, how it is partitioned between the ice, mixed and liquid phases, and how each phase is globally distributed (See Figures 3.6 and 3.14). This is either due to different processing algorithms, or a result of the different temporal periods of the two datasets; The first point is likely to be dominant. 2BCL5 was analysed between 2006 and 2017 while DARDAR was analysed only during 2016 to match the AWARE ground based dataset. To remove the temporal differences between the two the 2BCL5 measurements were restricted to 2016 only. Due to similarities with Figure 3.6, the figure for the 2016 2BCL5 latitudinal cloud occurrence can be found in Appendix C. Absolute differences between the two are displayed on Figure 3.15 which shows the 2016 2BCL5 measurements subtracted from the 2016 DARDAR measurements, including precipitation. A positive difference indicates that DARDAR is reporting more hydrometeors and likewise, a negative difference indicates 2BCL5 reports more hydrometeors.

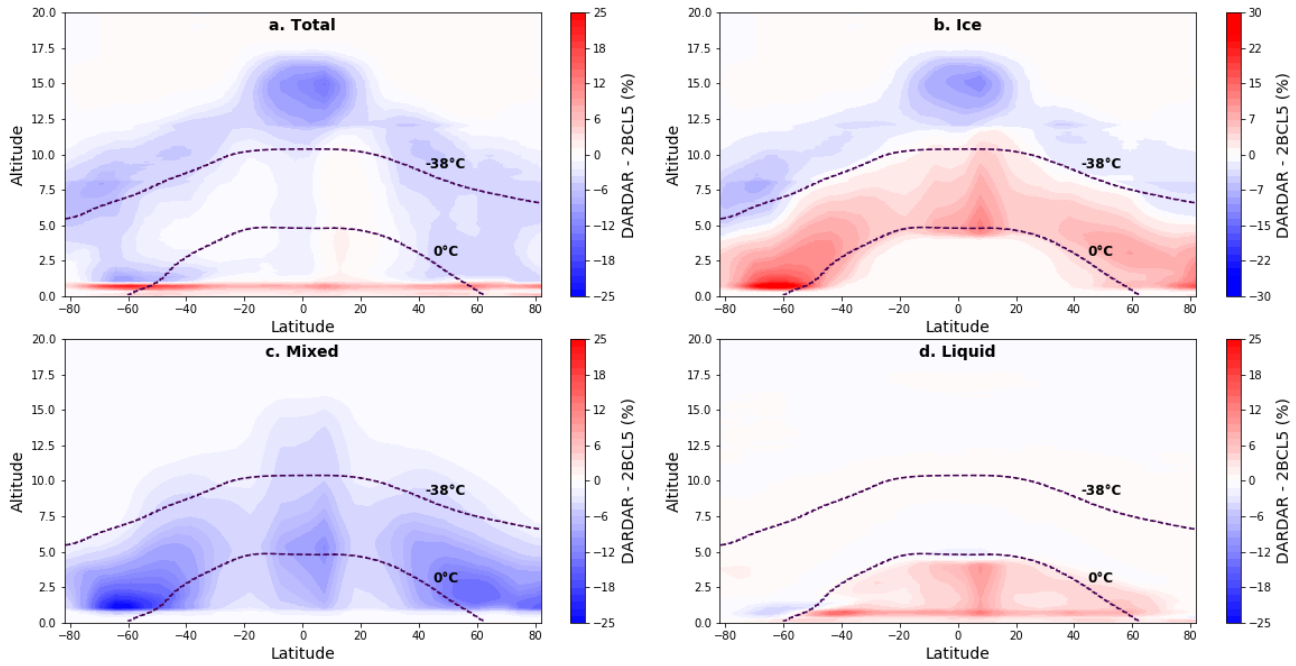

Figure 3.15: Differences in hydrometeor (cloud and precipitation) occurrence between DARDAR and 2BCL5 during 2016, broken into (a.) the total amount of hydrometeors and the difference phases (b.) ice, (c.) mixed and (d.) liquid. A positive difference indicates DARDAR is greater and a negative difference indicates 2BCL5 is greater. The black dashed lines indicate isotherms of constant temperature. Note that subplot b. has a larger scale on the colour bar.

Figure 3.15a shows that overall 2BCL5 detects more hydrometeors than DARDAR, except closest to the ground where DARDAR shows a greater amount of hydrometeors in the bottom 1 km. Figure 3.15c shows that 2BCL5 always detects more mixed phase hydrometeors, with an absolute difference up to 25% over the Southern Ocean maximum. DARDAR classifies these hydrometeors as either ice or liquid depending on geographical positions, as can be seen in Figure 3.15b/d. Figure 3.15b shows a clear separation between the blue region where 2BCL5 detects more hydrometeors and the red region where DARDAR detects more hydrometeors. This matches well with the position of the -38 °C isotherm. DARDAR detects more ice phase hydrometeors in between the isotherms, where mixed phase hydrometeors are able to be present. 2BCL5 instead classifies this cloud as mixed phase. Figure 3.15d shows that DARDAR detects more liquid phase hydrometeors below the 0 °C isotherm, while 2BCL5 classifies this as mixed phase hydrometeors. Strong matches with the 0 °C and -38 °C isotherms suggest a large dependence on temperature for both 2BCL5 and DARDAR when classifying phase, and points to difference between 2BCL5 and DARDAR in how they determine cloud phase.

3.5.2 Differences in 2BCL5 and DARDAR phase determination

Both 2BCL5 and DARDAR represent ice and liquid phase cloud well with respect to temperature constraints (Figures 3.6 and 3.14). The biggest differences between the two lie in the datasets representation of mixed phase cloud. DARDAR mixed phase cloud falls within the 0 °C and -38 °C isotherms well, but there is a gap in the coverage of mixed phase cloud over the tropics. Mixed phase clouds are present at all latitudes (Korolev et al., 2017) but are lowest over tropical latitudes (Mülmenstädt et al., 2015; Korolev et al., 2017; Wang, 2019). This suggests that DARDAR under-represents tropical mixed phase cloud. 2BCL5 instead shows mixed phase cloud at all latitudes, ranging from a vertical extent of 5 km over the polar regions to 15 km over the equator. Their representation of mixed phase cloud occurs commonly below the 0 °C isotherm and above the -38 °C isotherm. Because the isotherms are produced by taking an average, they do not account for the seasonal cycle in temperature shifting their positions. However mixed phase cloud is present almost everywhere, outside the expected variations of the isotherms. This suggests that 2BCL5 is incorrectly classifying cloud mixed phase cloud.

In order to determine cloud phase, 2BCL5 uses a process primarily driven by the temperatures of the cloud top and cloud base. They classify detections as ice if both the cloud base and cloud top are below a temperature of -38.5 °C. At temperatures both this also uses a temperature dependent radar reflectivity (Z_e) threshold and an integrated attenuated backscattering coefficient threshold to classify phase (D. Zhang et al., 2010). This splits the cloud into liquid, ice and mixed phase. DARDAR also uses a temperature dependent classification scheme. Above 0 °C detections are classified as water and below -40 °C detections are classified as ice. In between these two temperatures, the strength of the lidar backscatter signal to locate any attenuating high backscatter layers. They then attempt to classify these layers, based on temperature, cloud thickness, radar reflectivity, and altitude (Ceccaldi et al., 2013). Both 2BCL5 and DARDAR use temperature dependent processes for the same reason: The lidar depolarisation ratio that can be use to classify phase is too noisy to all phase identification with enough certainty. The same CloudSat product of ECMWF-AUX is used by both 2BCL5 and DARDAR to get temperature information.

The biggest differences between the two lie in how they assign phase to cloud detections. 2BCL5 splits cloud into layers with distinct cloud tops and bottoms. Each cloud layer is assigned a phase based on the 2BCL5 classifications algorithms. DARDAR classifies each pixel separately, so a cloud layer identified by 2BCL5 might have multiple classifications given by DARDAR. This offers an explanation to the differences in the mixed phase partitioning between 2BCL5 and DARDAR, where mixed phase 2BCL5 detections are classifies as ice/liquid by DARDAR. While 2BCL5 will generalise a whole cloud layer as mixed phase cloud if it detects both ice and supercooled liquid water, DARDAR will classify the parts of cloud that are ice, liquid and mixed phase separately. Figure 3.11 identifies that DARDAR

classifies little cloud as mixed phase cloud and Figure 3.6 identifies that 2BCL5 classifies mixed phase cloud outside the 0 °C and -38 °C isotherms. These changes are explained by the different classifications of cloud phase by 2BCL5 and DARDAR.

3.5.3 Importance of cloud over the Southern Ocean

Both 2BCL5 and DARDAR show the greatest amount of cloud over the Southern Ocean. Chapter 1 identified the Southern Ocean as an area of importance, due to a high shortwave radiation bias causing increased sea surface temperatures. The Southern Ocean also has an almost constant presence of cloud, which climate models represent poorly.

Figure 3.16 shows differences in cloud occurrence between DARDAR and 2BCL5 for different latitudinal regions. It shows the difference is greatest over the Southern Ocean (50S - 75S; blue curve) compared to other regions (grey curve). An 18% difference is seen just below 1 km, where DARDAR shows more cloud above 2BCL5. Above 1 km 2BCL5 shows a more cloud, with a 6% difference seen at 1.5 km and 8 km. This further highlights the importance of cloud over the Southern Ocean. If observational products derived from the same set of satellite measurements show significant differences, climate models will have difficulties representing cloud accurately.

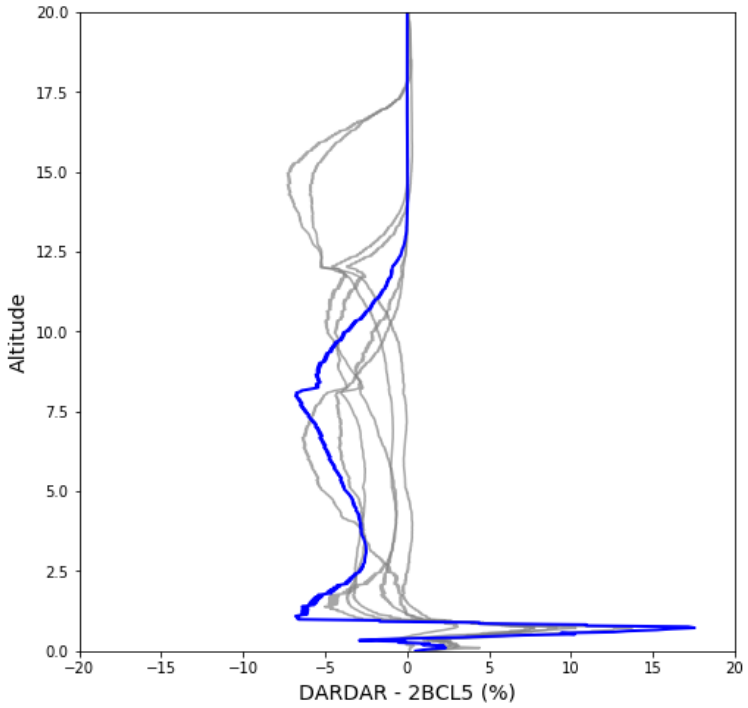

Figure 3.16: The difference in cloud occurrence between 2BCL5 and DARDAR as a function of altitude. Grey lines represent different latitudinal regions, with the Southern Ocean (50S - 75S) highlighted in blue.

Another comparison can be made looking at the cloud fraction, which indicates the presence or absence of cloud. Figure 3.17 shows cloud fraction as a function of latitude for 2BCL5 and DARDAR observations during 2016. 2BCL5 and DARDAR match well overall, observing the same pattern in the cloud fraction. A peak in cloud fraction over the Southern Ocean of 94% matches with previous studies that found the annual mean of cloud fraction over the Southern Ocean to be 80% - 90% (Kay et al., 2012; McCoy et al., 2014; Matus & L'ecuyer, 2017). Figure 3.18 shows the difference between the two curves. The match is best over the Southern Ocean, with up to a 10% difference elsewhere. Above 50N DARDAR has a higher cloud fractions and below 50N 2BCL5 has a greater cloud fraction, except for over the Southern Ocean.

While the cloud fraction for 2BCL5 and DARDAR matches well over the Southern Ocean, Figure 3.16 shows the differences in cloud occurrences are greatest over the Southern Ocean. Both satellites are differentiating between clear/cloudy sky well but differ in what altitudes cloud is occurring at and how much cloud is present.

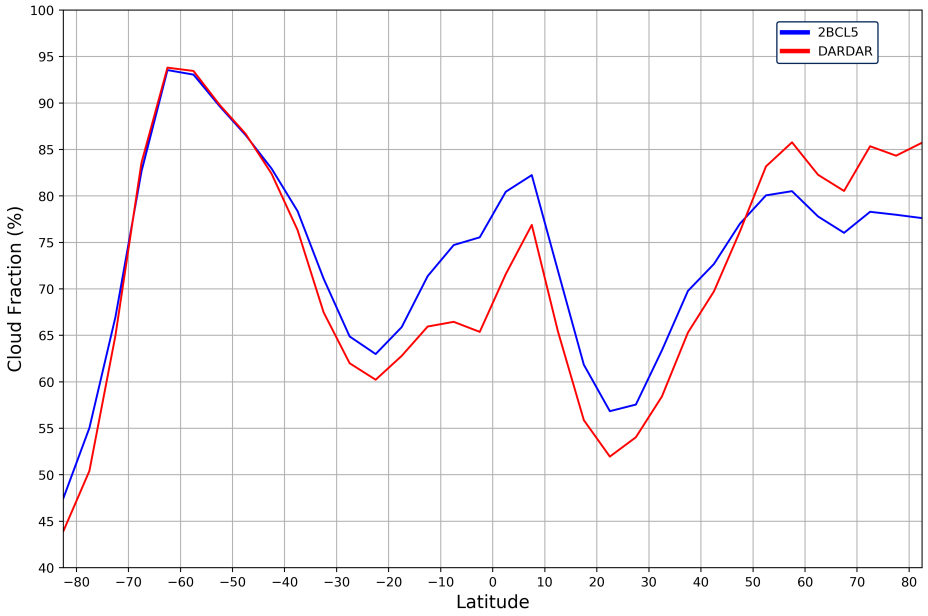

Figure 3.17: Latitudinal distribution of 2BCL5 and DARDAR cloud fraction observed measurements during 2016.

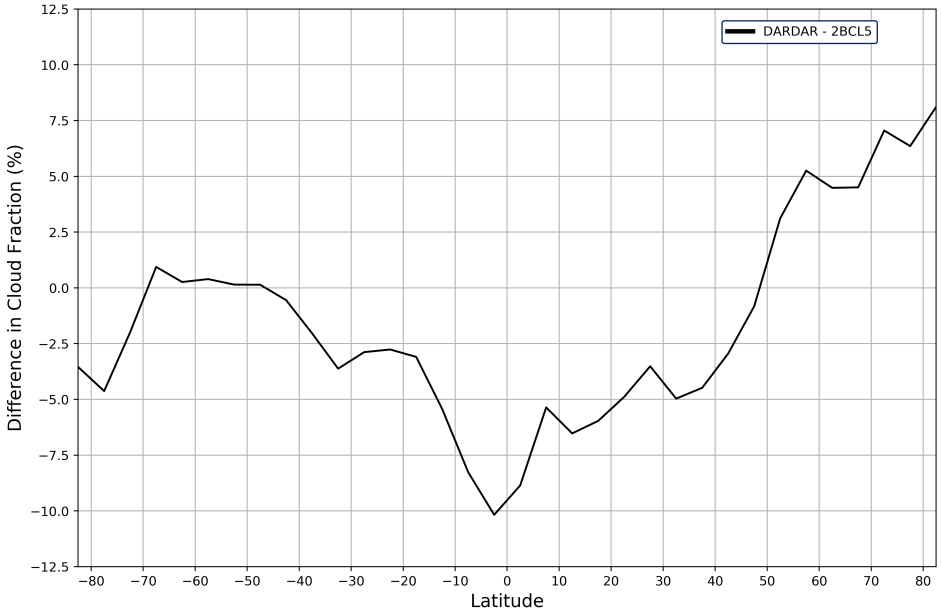

Figure 3.18: Differences in 2BCL5 and DARDAR latitudinal cloud fraction measurements during 2016.

3.5.4 Validation with external studies

Both 2BCL5 and DARDAR show differences in how they detect cloud and cloud phase. In order to determine which dataset is better representing cloud further comparisons need to be made to external studies and datasets. In the Cloud and Aerosols chapter of the IPCC Fifth Assessment Report, Boucher et al. (2013) discusses the abilities of instruments aboard the CloudSat and CALIPSO satellites to classify the vertical profiles of cloud occurrence. Figure 3.19 shows latitude-height sections of annual cloud occurrence (including precipitation falling from cloud). The dashed curves show the annual mean 0 °C (liquid) and -38 °C (ice) isotherms, that indicate the edges of the phase regimes.

Both isotherms agree well with those generated by this study using ERA5 temperature reanalysis. The 0 °C isotherm has a peak height of 4.5 km and slopes downward towards the ground at 60N/S, matching with the 0 °C isotherm on Figure 3.15. The -38 °C isotherm has a peak height of 10 km that slopes down similarly to the 0 °C isotherm, which also agrees with Figure 3.15. The distribution of cloud occurrence matches better with 2BCL5 than DARDAR. A peak occurrence of 60% at 60S matches with Figure 3.6 and the shape of the distribution shows better agreement. However, it is unsurprising that 2BCL5 matches much better than DARDAR. Figure 3.19 was made using the 2B-GEOPROF-LIDAR dataset for observations between 2006 to 2011. Because this product is part of the CloudSat Data Processing Centre, cloud occurrence will be heavily biased towards 2BCL5 results, which use the same processing algorithms. It is unfair use the cloud occurrence here to determine whether 2BCL5 or DARDAR is more representative.

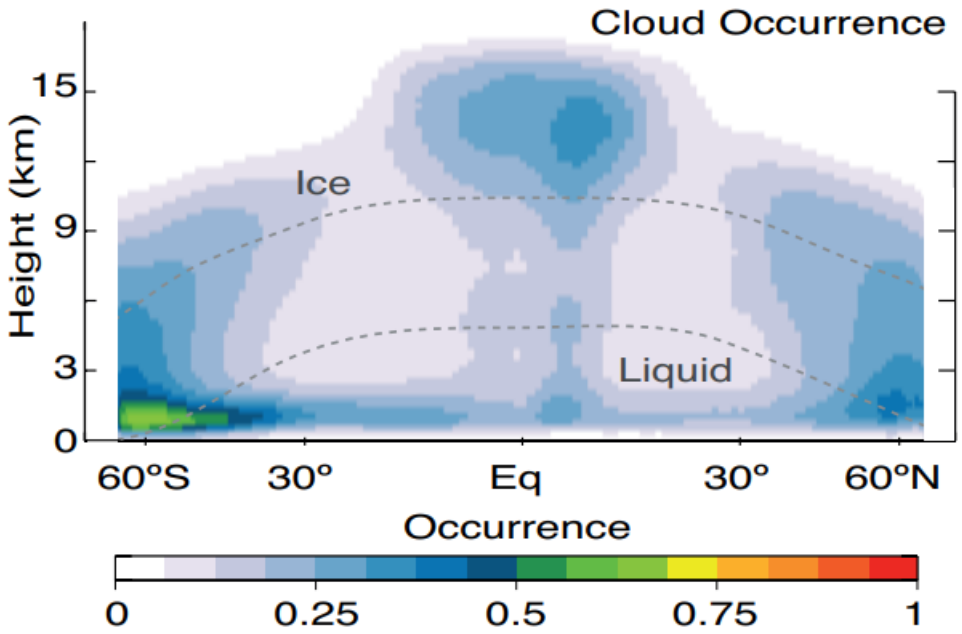

Figure 3.19: Latitude-height sections of annual cloud occurrence that includes precipitation falling from cloud, made from the 2B-GEOPROF-LIDAR dataset for 2006 to 2011. The dashed curves show the annual mean 0 °C (liquid) and -38 °C (ice) isotherms, that indicate the edges of the cloud phase regimes (Adapted from Boucher et al., 2013).

This is not an isolated occurrence. While there are combined radar/lidar cloud studies that could be used to determine which dataset is representing cloud occurrence and cloud phase better, they have significant biases in the datasets used. CloudSat and CALIPSO are unique in their abilities to measure the vertical distribution of clouds, so studies are completed using their products. Studies using 2BCL5 or similarly processed datasets show cloud occurrences comparable to what has been found here (Mace et al., 2009; Wang, 2019) with the similar agreement for studies that use DARDAR observations (Mülmenstädt et al., 2015).

3.5.5 Summary and Conclusions

The 2BCL5 and DARDAR datasets have apparent strength and weakness. Both represent the show similar observations for the cloud fraction and show reasonable shapes of global cloud occurrence. They disagree on how this is distributed depending on both latitude and altitude. DARDAR detects a greater cloud occurrence below 1 km and 2BCL5 has a greater cloud occurrence elsewhere. When it comes to how 2BCL5 and DARDAR partition between the cloud phases, both represent ice and liquid phase cloud well with respect to temperature constraints. Differences lies in how DARDAR and 2BCL5 determine mixed phase cloud. They agree that the most mixed phase cloud is over the Southern Ocean but disagree with the amount, up to 25%. DARDAR classifies cloud detected as mixed phase by 2BCL5 as either ice or liquid depending on altitude and latitudinal positions, and misses mixed phase

cloud over the tropics. 2BCL5 classifies cloud as mixed phase incorrectly where it exists below the 0 °C isotherm and above the -38 °C isotherm. 2BCL5 splits cloud into layers with distinct cloud tops and bottoms while DARDAR classifies each pixel separately. This means 2BCL5 will generalise a whole cloud layer as mixed phase cloud if it detects both ice and supercooled liquid water while DARDAR will classify the parts of cloud that are ice, liquid and mixed phase separately. This offers an explanation to the differences without a clear picture of whether either one is better.

Overall, it is hard to classify either 2BCL5 or DARDAR as a more representative dataset without another dataset for comparison, independent of the processing of either. Using external studies to validate whether 2BCL5 of DARDAR is better proves difficult, as they tend to use observational products related to 2BCL5/DARDAR that bias comparisons. This is where the motivation for using ground based radar/lidar measures of cloud comes from, as well as the satellites inability to completely resolve cloud closest to the ground. Work in this chapter identifies the Southern Ocean as an area of interest. The Southern Ocean has maxima in cloud occurrence and cloud fraction. It also has the biggest differences between 2BCL5 and DARDAR cloud occurrence while the cloud fraction observations are in agreement. However, ground based measurements vertically resolving cloud and cloud phase over the Southern Ocean are uncommon due to the logistical issues of collecting measurements in a region dominated by ocean.

Ground based measurements from the AWARE campaign over McMurdo Station in Antarctica provide a comparison with 2BCL5/DARDAR observations, and are discussed in detail in Chapter 4. The first climate-related field campaign in West Antarctica in more than 40 years, AWARE provides a rare surface based dataset in the region. This independent dataset will provide valuable information in determining whether 2BCL5 or DARDAR is the better dataset to use for classifying cloud phase.

Chapter 4

Processing and analysis of ground based observations

4.1 Processing

4.1.1 AWARE processing

The data used from the AWARE campaign came in the form of hourly cloud occurrences based on measurements from the KAZR and HSRL instruments. Each profile has a vertical resolution of 7.5 m and were collected from McMurdo Station during the whole of 2016. The AWARE data has several types of masks defined: liquid (liquid-bearing air volumes, based on HSRL lidar detections), all detected hydrometeor (ice + liquid, based on HSRL lidar + KAZR radar detections), as well as radar/lidar only masks with detected hydrometeors based exclusively on HSRL/KAZR data. The AWARE dataset also contains KAZR/HSRL data availability metadata and HSRL hourly-mean extinction altitude profiles. Both the KAZR and the HSRL datasets are rather complete, with more than 97% data availability during 2016 (Silber et al., 2018).

In order to use the cloud masks the KAZR/HSRL data availability had to be considered. The hourly cloud statistics were formed using smaller profiles sampled every 10s. Hours with small amounts of detected data might cause a potential low-sampling bias. An investigation was completed into the proportion of AWARE observations that were removed using different thresholds for the quality of the hourly cloud occurrence. Both KAZR and HSRL measurements needed to have an availability higher than the threshold or be excluded. A higher quality threshold means a higher proportion of observations must be available for that hour, with a threshold of one representing that 100% of both HSRL and KAZR measurements are available. Figure 4.1 shows the percentage of observations that are removed for different quality thresholds. Up to a threshold of 0.65, a small amount of observations (just over 1%) are removed. This increases steadily between thresholds of 0.65 and 0.85 to around 3%, then increases sharply until approximately 19% of AWARE observations are removed for a quality threshold of 1. A 75% availability for both the KAZR and HSRL datasets each hour was decided upon, as it removed low quality data while still leaving a sizable amount for analysis. This threshold, shown as the black dotted line on Figure 4.1, resulted in an exclusion of 2.3% of hourly measurements over the entire year.

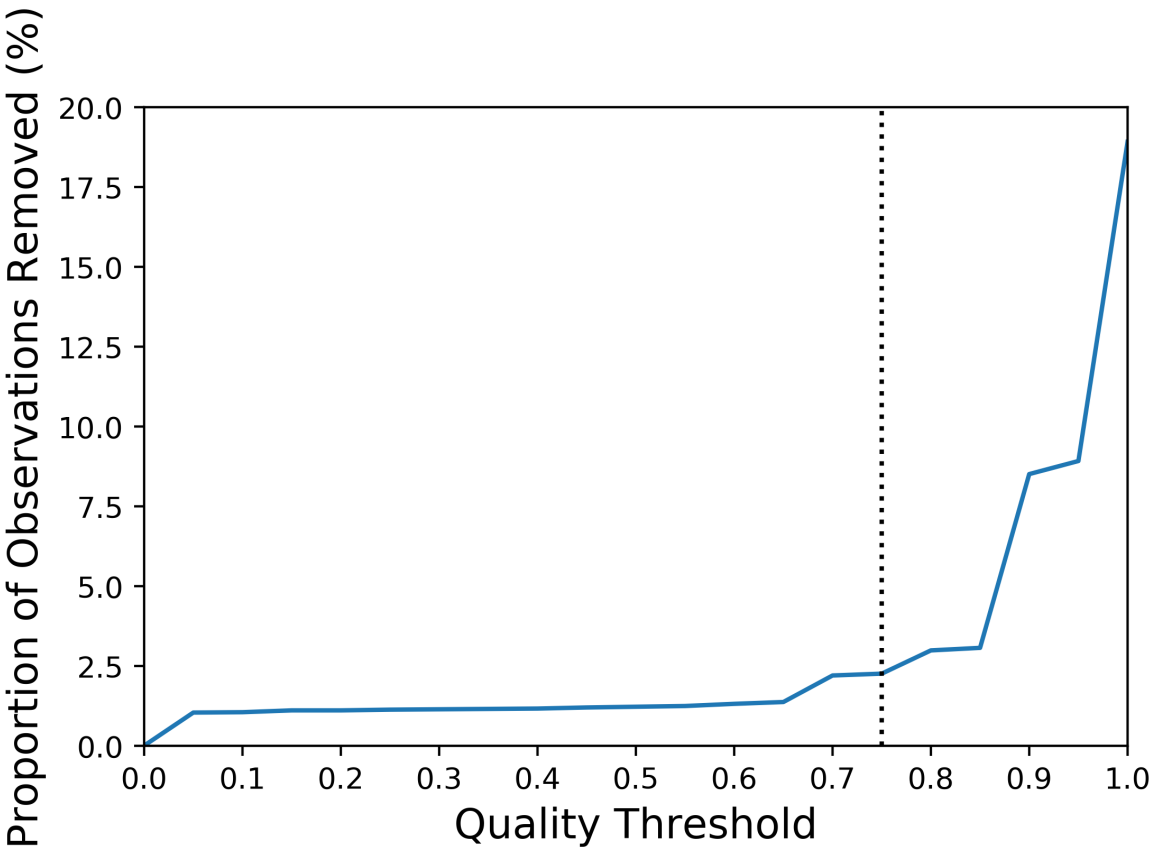

Figure 4.1: Proportion of AWARE observations removed for different threshold in the hourly availability of KAZR and HSRL measurements. The black dotted line indicates the chosen threshold of 0.75.

4.1.2 2BCL5, DARDAR and AWARE combined processing

Further processing was carried out upon the AWARE, 2BCL5 and DARDAR measurements so that they could be compared. Observations are required to be matched both spatially and temporally. To allow coincident measurements to be examined the satellite data was masked so that only observations falling within an area centered around McMurdo Station were used. The AWARE data was masked so that only measurements occurring within a set number of hours before or after a CloudSat/CALIPSO pass over McMurdo are considered. All measurements from CloudSat/CALIPSO and the AWARE datasets used include both cloud and precipitation in their cloud masks. Because AWARE and 2BCL5 cannot distinguish between the two, they shall be considered together and DARDAR observations shall also include precipitation.

In order to determine a region within which satellite observations would be considered, the geography around McMurdo was examined. A balance is needed between a region that allows the greatest amount of satellite data while still being representative of conditions over McMurdo. Figure 4.2 shows McMurdo Station, indicated by the red point, and the topogra-

phy of the surrounding area. The black box indicates a 5 degree grid centered on McMurdo. This is chosen for the spatial region examined for the 2BCL5 and DARDAR data as it was large enough to have a considerable number of satellite passes over the region, while it also excluded the Trans-Antarctic mountains to the west. Inclusion of the the Trans-Antarctic mountains would have biased the low-level cloud values examined.

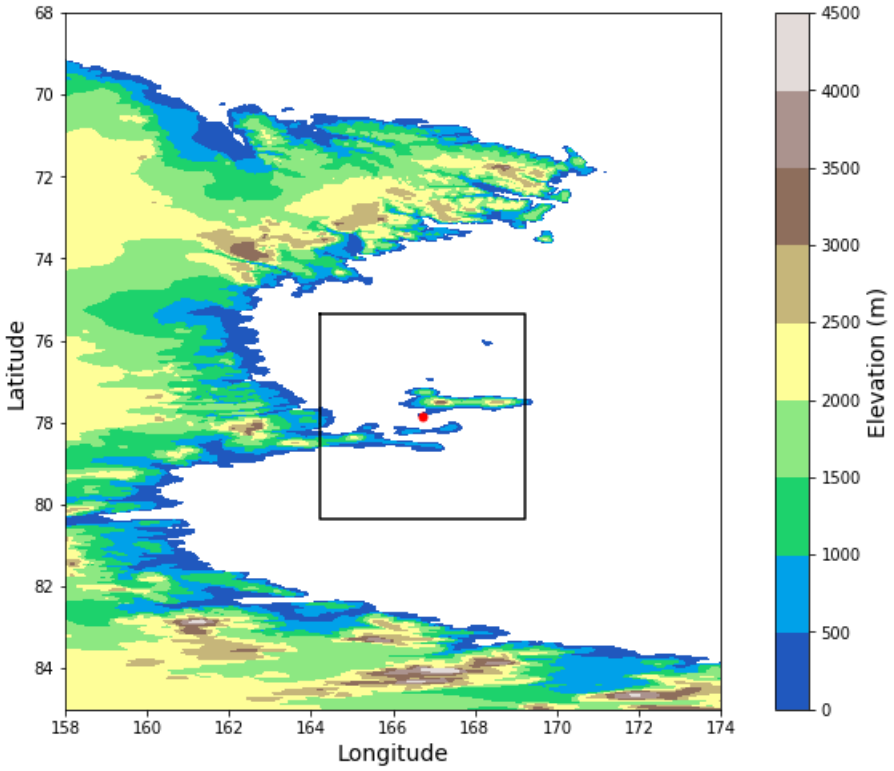

Figure 4.2: Topographical map of the area surrounding McMurdo Station, indicated by the red point. The black box is the chosen 5 degree region within which satellite observations are considered.

For the temporal resolution of the AWARE data, a greater resolution provides more hourly AWARE profiles that correspond to a 2BCL5 pass, but also could mean that the cloud observed by the different instruments might be associated with distinct weather patterns. The two distinct patterns would be averaged together to produce a result that is unrepresentative of either. A previous study by Coggins et al. (2014) was used to help determine an appropriate number of hours either side of a 2BCL5/DARDAR pass where AWARE profiles would be considered. The study used a k-means clustering technique to produce a synoptic climatology of the Ross Sea and Ross Ice Shelf regions. One aspect that their study investigates was the characteristic time periods of each cluster, defined as the length of time where a certain state in the region occurs uninterrupted before changing into another state. They found that for most of the clusters the mean time period fell between 13 and 20 hours. A follow on study by Jolly et al. (2018) used this synoptic climatology to quantify the vertical distribution of cloud occurrence, phase, and type over the Ross Ice Shelf and southern Ross Sea,

which encompasses McMurdo Station. They found large differences between the synoptic regimes relative to seasonal variation for the cloud occurrence as a function of altitude. This suggested the synoptic regimes are important for clouds in this region. However, they also found that the cloud phase was strongly modulated by season, rather than synoptic regime. This suggested the most important control on cloud phase in the region is still temperature. A more specific study of cloud persistence using the AWARE data was carried out by Silber et al. (2018). They investigated the persistence of all cloud layers, as well as those consisting only of liquid. AWARE measurement showed that the mean cloud persistence is between 5 to 10 hours depending on the month. However liquid cloud layers have a much smaller mean persistence of 2.7 hours and 54% do not last for more than 1 hr. As liquid cloud is the only phase that can be easily compared between the three datasets, a temporal threshold of 1 hour either side of the closest AWARE measurement during a satellite overpass is chosen (3 hours in total).

The satellite observations are then broken into each CloudSat/CALIPSO pass though the selected 5 degree region around McMurdo. The AWARE observations are matched within an hour either side of these passes to generate a set of spatially and temporally co-located and coincident measurements for both 2BCL5/AWARE and DARDAR/AWARE. Only the months of January, March, September, October, November and December had any overlap between the satellite and ground based observations. No data was available for February for either 2BCL5 and DARDAR due to a lack of CALIPSO observations. Cloud occurrence, cloud fraction and cloud phase could not be determined for the remaining months of April, May, June, July and August. This is due to limitations of CloudSat being able to only operate during the sunlit portion of its orbit, as shown in Figure 3.3.

Because of the differing availability of 2BCL5 and DARDAR, each dataset produces a different amount of passes over McMurdo throughout 2016. 2BCL5 has 238 satellite passes that match with AWARE observations while DARDAR has 202. Figure 4.3 shows how these passes are split between the six months of overlapping satellite and ground based cloud observations. 2BCL5 shows the most passes across all months, which makes sense as it has more data available than DARDAR in general, which suggests that the DARDAR quality control criteria are more demanding. Figure 3.10 displays the differences in the days in the month with available measurements between 2BCL5 and DARDAR. It shows that for the months with satellite/ground overlap, January and September have the differences between 2BCL5 and DARDAR. This matches well with Figure 4.3, where January and September once again show the biggest differences between 2BCL5 and DARDAR. March and September show the least passes so comparisons here may be biased due to a smaller sample size. Comparing when both 2BCL5 and DARDAR both show a pass over McMurdo at the same time, four of the months show equality between the DARDAR passes. That means for these months all the DARDAR passes are seen by 2BCL5, and are a subset of the 2BCL5 passes. However,

two months show less overlapping passes than the amount of DARDAR passes. This means there are times that DARDAR reports a pass while 2BCL5 does not. The passes used for comparison with AWARE were further filtered to only include passes that both satellites were seeing, which reduced the total to 194.

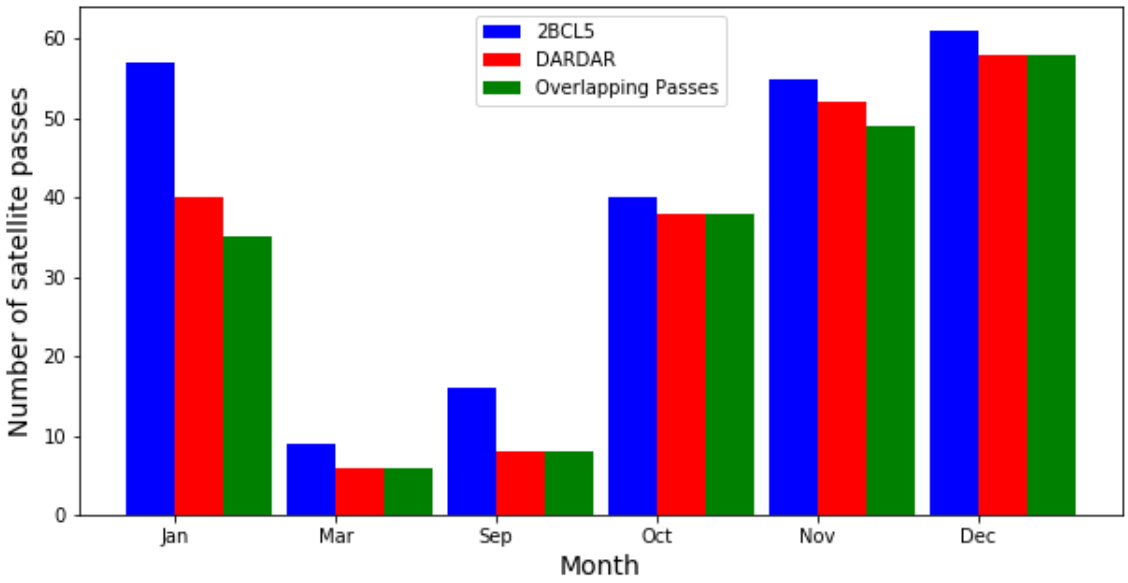

Figure 4.3: Satellite passes over McMurdo Station during 2016 for 2BCL5, DARDAR and overlapping passes between the two.

4.2 Analysis

4.2.1 AWARE vertical temperature profiles

Figure 4.4 shows vertical temperature profiles for the AWARE dataset across 2016. The black line indicates the edge of the homogeneous freezing regime at -38 °C (Lamb & Verlinde, 2011), above which any supercooled liquid in the cloud will freeze readily. Temperature profiles were generated using radiosonde soundings over McMurdo as discussed in Chapter 2.2.1.

McMurdo Station shows a seasonal change in temperature where the summer months are warmer. Overall surface temperatures rarely get above 0 °C, so liquid present is likely to be supercooled. The -38 °C isotherm follows the same seasonal pattern where its height is raised in the warmer months due to the greater temperatures, however large variations are present. Silber et al. (2018) carried out similar analysis of temperature soundings and found near identical results.

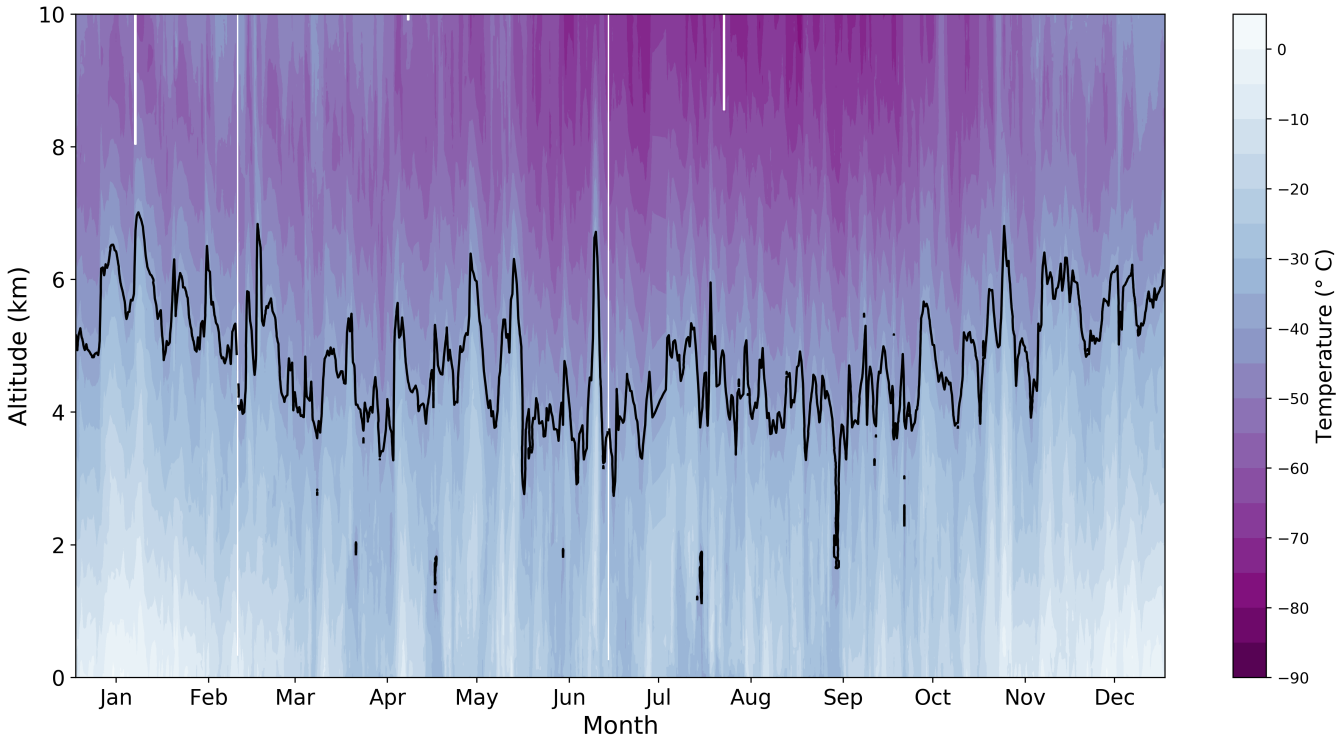

Figure 4.4: Vertical temperature profiles at McMurdo station during 2016 obtained from twice-daily temperature measurements taken during the AWARE campaign. The verge of the homogeneous freezing regime at -38 °C is indicated by the black curve.

4.2.2 AWARE cloud occurrence

The cloud occurrence over McMurdo Station for the 2016 AWARE measurements is shown in Figure 4.5. AWARE observations that coincide with 2BCL5 and DARDAR have been displayed for January, October, November and December. March and September have been excluded from this graph due to their small number of passes. Measurements have been split into different cloud phases as detected by AWARE. The red dashed line is the liquid phase cloud, the green dashed line is the ice phase cloud, and the black dashed line is the cloud occurrence for all phases. The area between the green and black lines represents the phase that AWARE classified as 'unknown'. As talked about in Chapter 2 this was due to a lack of lidar observations. The HSRL lidar instrument is attenuated by low level clouds, which is needed for AWARE to classify the phase. While it is possible that lidar observations could be missing due to equipment malfunction, Silber et al. (2018) reports that both the KAZR and the HSRL datasets are rather complete, with more than 97% data availability during 2016. They also note that the unknown phase is likely to mostly represent ice phase cloud, although some supercooled liquid water will be present in the unknown classification. The purple line represents the level of the -38 °C isotherm, the edge of the homogeneous freezing regime. This was produced by taking the average temperature profile across all passes using the twice-daily radiosonde observations over McMurdo. The closest of the twice-daily temperatures observations was assigned as each pass as a temperature profile.

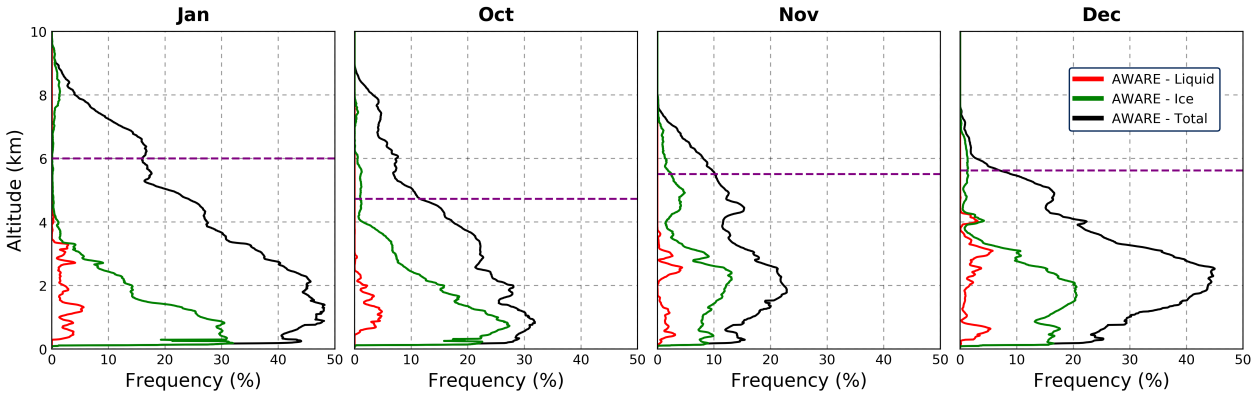

Figure 4.5: Cloud occurrence for 2016 AWARE data overlapping with 2BCL5 and DARDAR. Observations are partitioned between the phases, where the red dashed line is the liquid phase cloud, the green dashed line is the ice phase cloud, and the black dashed line is the total cloud for all phases. The purple line represents the level of the -38 °C isotherm, the edge of the homogeneous freezing regime.

The AWARE cloud profiles show liquid phase cloud occurring in the bottom 4 km of the atmosphere, except for December where liquid phase cloud up to an altitude of 4.5 km is observed. It shows a maximum of 5%, with no pattern of where it peaks between the months. For all months liquid phase cloud falls below the -38 °C isotherm, so the AWARE phase algorithm is classifying liquid correctly with respect to temperature. The ice cloud phase extends much higher than the liquid phase cloud, but shows reduced frequency after an altitude of 4 km. This matches with an increase of unknown phase cloud. Ice phase cloud peaks at an altitude below 1 km during January and October, but is higher at 2 km - 2.5 km during November and December. The unknown phase cloud dominates the cloud occurrence above altitudes of 4 km, due to the extinction of the lidar signal preventing classification of the cloud phase. The altitudes at which the unknown phase show maxima in the cloud occurrence match well with the altitudes at which ice phase cloud show maxima in the cloud occurrence. This further highlights that the unknown phase cloud is likely to be ice. AWARE shows high cloud occurrences down to the surface.

Figure 4.5 appears to show artifacts in the cloud occurrence of ice phase cloud below an altitude of 1 km for January and October. Figure 4.6 shows a subset where the altitude has been restricted to below 1.5 km. This clearly highlights an irregular decrease in ice cloud occurrence of approximately 10% at an altitude of 300 m. These are likely to be a result of the AWARE processing, but could be a result of the temporal restrictions placed on the AWARE dataset. The AWARE dataset was constricted to only observations that coincide with the 2BCL5/DARDAR satellite passes over McMurdo. In their evaluation of the AWARE dataset, Silber et al. (2018) produces vertical profiles of AWARE cloud similar to the cloud occurrence profiles in this study. They also show artifacts in the ice phase cloud

at an altitude of 300 m where the cloud occurrence drops by 10%. They also see an increase in the unknown phase cloud at an altitude of 800 m, which can be seen in the January and December sub-figures of Figure 4.6. Their profiles of cloud are averaged across the whole AWARE dataset, so the artifacts seen in Figure 4.6 are present throughout the whole dataset. To verify their results profile of cloud occurrence for the whole of the AWARE dataset are shown in Appendix D. The profiles have artifacts present, which reinforces the conclusion that artifacts in the ice phase cloud are not isolated to the 2BCL5/DARDAR passes the AWARE observations are restricted to in this study.

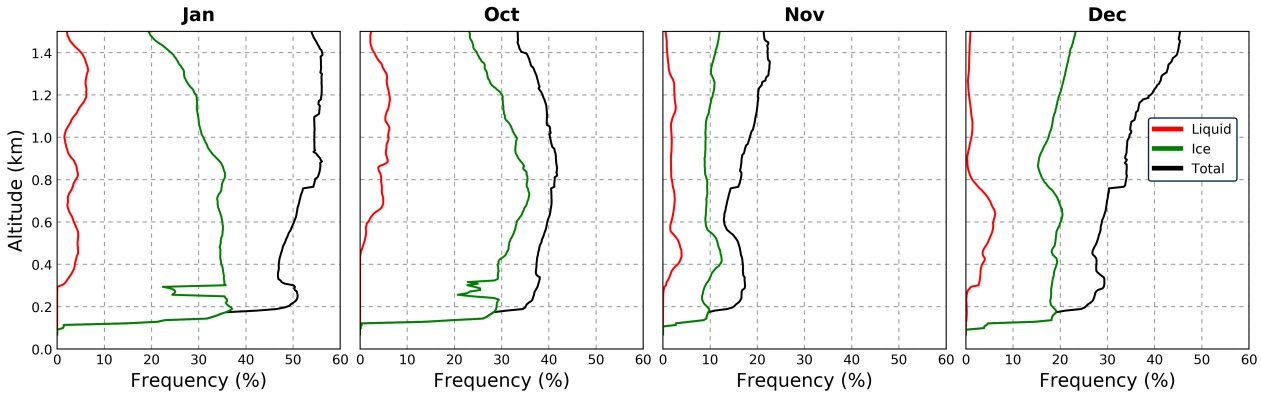

Figure 4.6: Cloud occurrence for 2016 AWARE data overlapping with 2BCL5 and DARDAR an in Figure 4.5, but restricted to altitudes below 1.5 km to highlight artifacts in the ice phase cloud.

4.2.3 Comparison of 2BCL5, DARDAR and AWARE cloud occurrence

The cloud occurrences over McMurdo Station comparing AWARE with 2BCL5 and DARDAR at each altitude are shown in Figure 4.7. Cloud profiles for each pass are averaged together and split into the various phases for each dataset. As in the case of Figure 4.5, observations during January, October, November and December are displayed; Observations during March and September have been excluded (See Appendix E). The filled curves represent the DARDAR (Figure 4.7a-d) and 2BCL5 (Figure 4.7e-h) where the darkest blue shaded region indicates liquid phase cloud, the lightest blue shaded region represents ice phase cloud, and in between the two represents the mixed phase cloud region. The dashed curves represent the AWARE data as displayed in Figure 4.5. Annotated alongside the month at the top of the figure are the number of passes in each of the months for reference purposes. The purple line represents the altitude of the -38 °C isotherm, the edge of the homogeneous freezing regime across all passes. Because Figure 4.4 shows large variations in the edge of the homogeneous freezing regime, the maximum altitude of the -38 °C isotherm is also considered (dashed line).

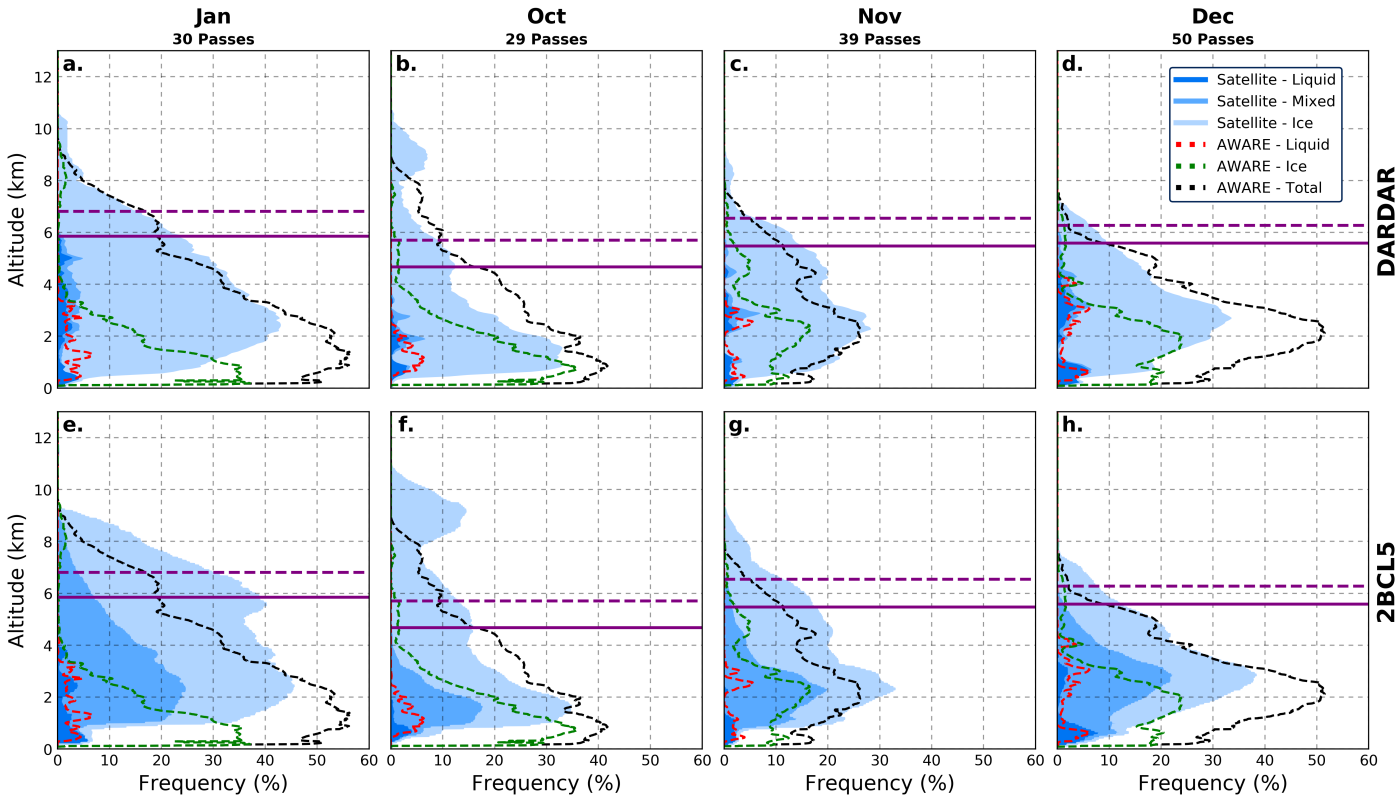

Figure 4.7: Mean vertical profiles of cloud occurrence for different cloud phases derived from observations over McMurdo Station during 2016. The dashed lines represent the AWARE cloud occurrence and the filled curves represent DARDAR (a - d) and 2BCL5 (e - h) cloud occurrences. Each month as well as the number of passes are annotated at the top of the figure. The purple lines represents the mean (solid) and maximum (dashed) altitudes of the edge of the homogeneous freezing regime across all passes.

Figure 4.7a-d shows DARDAR cloud occurrence profiles have liquid phase cloud that extends up to an altitude of 6 km and a maximum amount of just over 5%. There is mixed phase cloud where liquid cloud is detected, but only a few percent at the most. The majority of DARDAR cloud is classified as ice phase, extending up to an altitude of 10 km. Maxima in the ice phase cloud (which corresponds to the maximum of the cloud occurrence) generally occur between 2 km and 3 km for January, November and December, but occur at a lower altitude during October of just above 1 km. Below the maxima DARDAR cloud occurrence falls off rapidly, where below 1 km cloud occurrence has a frequency of less than 10%.

No liquid appears to be located above the mean -38 °C isotherm, but a proportion of the mixed phase cloud is located above this altitude. The mean isotherm is taken from an average across all passes, so the isotherm for the maximum altitude across all passes needs to be considered. No mixed phase cloud for DARDAR is present above the maximum level of the -38 °C isotherm which shows DARDAR is representing liquid and mixed phase cloud

correctly with respect to temperature constraints.

Figure 4.7e-h for 2BCL5 shows up to a 10% frequency of liquid phase cloud between altitudes of 0 km and 5 km, with the maxima in cloud occurrence occurring between 0.3 km and 1 km. Liquid phase cloud tends to drop off rapidly at altitudes above the maxima, although the summer months of December and January show increased cloud occurrence at higher altitudes due to warmer temperatures.

All months show mixed phase cloud with maxima in the cloud occurrence at altitudes between 2 and 3 km. October has the least amount of mixed phase cloud and shows none above 4 km, reflected by the lowest position of the -38 °C isotherm. The other months show mixed phase cloud above the mean altitude of the -38 °C isotherm where liquid water should not be present. November and December show mixed phase cloud up to a height of 6.5km, which can be explained when looking at the maximum level of the isotherm across all passes. January however, shows the presence of mixed phase cloud up to an altitude of 9 km. This is much higher than the 7 km maximum of the -38 °C isotherm observed in Figure 4.7. This points to limitations with how the 2BCL5 mixed cloud phase is determined. In all months the mixed phase cloud occurrence shows a rapid decrease below 2 km with little mixed phase cloud present in the boundary layer below 1 km. This likely due to the satellites underestimating cloud occurrence rather than an absence of low level mixed phase cloud.

Ice phase cloud is consistently present in all months up to heights of 11 km, although only October shows a large occurrence of ice clouds above 9 km. Looking at the 2BCL5 cloud as a whole, the maximum for the monthly cloud occurrence occurs between altitudes of 1.5 and 3 km. All of these coincide with where the mixed phase cloud is also the greatest. Below the maxima, cloud occurrence falls off swiftly with little cloud below an altitude of 1 km, as in the case for DARDAR.

Representation of DARDAR cloud matches better with constraints set by the altitude of the -38 °C isotherm. 2BCL5 shows a large amount of mixed phase cloud above this level, which is most prominent in the warmest month of January. Comparing DARDAR and 2BCL5 as a whole, profiles for the cloud occurrence for all phases from Figure 4.7 are shown on Figure 4.8. The black line represents 2BCL5 and the filled curve DARDAR. Only passes where both 2BCL5 and DARDAR detect cloud are considered. 2BCL5 systematically has a higher occurrence of cloud than DARDAR, except below 1 km where DARDAR systematically has a higher occurrence of cloud than 2BCL5. Although they differ in the amount of cloud observed, the shapes of their profiles are similar with areas of high and low cloud occurrence at the same altitudes. This might be expected as these two products are derived from the same satellite measurements. This matches with what was found for the global cloud distributions (Figure 3.15), but discrepancies between the two points towards differences in the

way 2BCL5 and DARDAR process the CloudSat/CALIPSO observations.

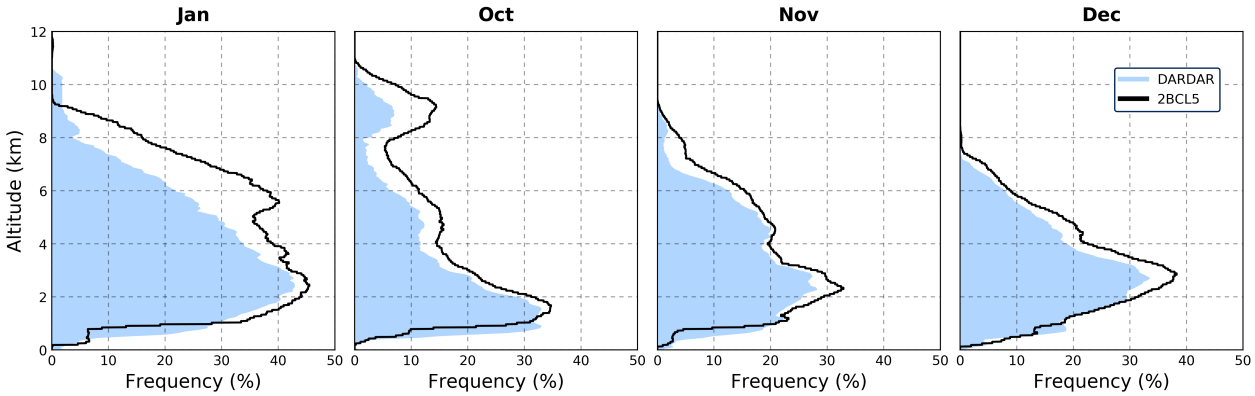

Figure 4.8: Cloud occurrences for 2BCL5 (Black line) and DARDAR (Filled blue curve) as shown on Figure 4.7.

The liquid phase profiles from Figure 4.7 for AWARE match with DARDAR during November (c) and December (d), but DARDAR shows a decreased amount of low level liquid cloud and a greater amount of high level liquid cloud during January (a) and October (b). 2BCL5 matches well with AWARE closest to the surface, but shows a lower amount of the high level liquid phase cloud (e - h). Overall neither 2BCL5 or DARDAR do a consistent job detecting the liquid phase cloud reported by the AWARE dataset, although Figure 4.7d/h shows that during December both DARDAR and 2BCL5 are in agreement with AWARE.

AWARE cloud occurrence shows that at higher altitudes there is an underestimation of cloud compared to that detected by 2BCL5 and at lower altitudes there is an overestimation of cloud compared to both DARDAR and 2BCL5. The satellite based data appears to be unable to detect as much cloud below an altitude of 1 km. Conversely the ground based data appears to be unable to detect as much cloud as 2BCL5 higher than 4km, although AWARE and DARDAR appear to match better than AWARE and 2BCL5. AWARE observations will be attenuated at this height, so a good match with DARDAR might suggest that DARDAR is also underestimating the cloud at altitudes greater than 4 km. This matches with Figure 3.15 where DARDAR has been seen to measure less cloud than 2BCL5 above altitudes of 1 km. The maxima in the cloud occurrence are also at a lower altitude for the AWARE measurements compared to both 2BCL5 and DARDAR. That neither the satellite or ground based instrument see a peak in the cloud occurrence at the same altitude is a sign that neither gets a complete picture of the cloud.

A similar study investigating cloud phase using four years of 2BCL5 data over the Ross Sea and Ross Ice Shelf regions was carried out by Jolly et al. (2018). Their study does not use any ground based measurements or another satellite dataset such as DARDAR, but instead provides a reference point for similarly located measurements for 2BCL5. Although their

cloud occurrence profiles are smoother due to a larger sampling of data, their results show reasonable agreement with the results of the 2BCL5 data obtained in this study. They show that January and December have higher occurrences of mixed phase cloud and liquid phase cloud extending to an altitude of 4 km which is absent during October and November. Maxima in the cloud occurrence of 30% - 40% are dominated by mixed phase cloud, although the altitudes at which this occurs is higher in some cases. Their results also show the bottom 1km being dominated by liquid phase cloud, as well as a sharp decrease in cloud occurrence below 1km. Overall their analysis is consistent with the results obtained here for 2BCL5.

The cloud occurrence for all phases shows maxima for between 1.5 km and 3 km for both 2BCL5 and DARDAR. Below this level cloud occurrence falls off rapidly with little cloud below a height of 1 km for 2BCL5 and 0.5 km for DARDAR. AWARE displays a maximum in the cloud occurrence at a slightly lower altitude (between 1 and 2.5 km), but also shows a sustained presence of low level cloud. Because CloudSat is affected by surface clutter below approximately 1.2 km (Marchand et al., 2008; Tanelli et al., 2008) and the CALIPSO lidar signal cannot pass through thick cloud, it is likely that both instruments that are used to form the 2BCL5 and DARDAR datasets underestimate the amount of low level cloud. Above the maxima, AWARE tends to fall off faster than 2BCL5/DARDAR, which shows clouds extending to higher altitudes. With the lidar signal used within the AWARE dataset being mostly attenuated above 4 km, detection of the high level cloud is reduced. While the KAZR radar could still detect much of this cloud, it struggles to detect high level ice clouds with small optical depths (Sassen & Khvorostyanov, 1998). Neither 2BCL5, DARDAR or AWARE appears to be able to observe the complete vertical structure of cloud. In order to get a full picture a combination of ground and satellite based measurements are needed.

To better compare the phases between 2BCL5, DARDAR, and AWARE, twice-daily temperature measurements taken at McMurdo Station during 2016 were used to reproduce the comparisons between different datasets displayed in Figure 4.7 as a function of temperature rather than altitude. Cloud occurrence was summed across all altitudes and assigned to a temperature. Cloud occurrence at each temperature is normalised, where all phases sum to 100% at each temperature. This shows the relative amounts between each of the phases. Figure 4.9 shows the normalised occurrence of cloud phase at each temperature. 2BCL5 and DARDAR are split into the ice, mixed and liquid phases, and AWARE into the ice, liquid and unknown phases. The dashed line indicates the edge of the homogeneous freezing regime at -38 °C.

The top panel of Figure 4.9 for 2BCL5 shows at high temperature supercooled liquid water dominates, but quickly falls off as the proportions of mixed and ice phase cloud increase at colder temperatures. Mixed phase cloud starts to fall off below -25 °C but shows sustained presence up until -54.5 °C, below which no further cloud is detected. Ice phase cloud dom-

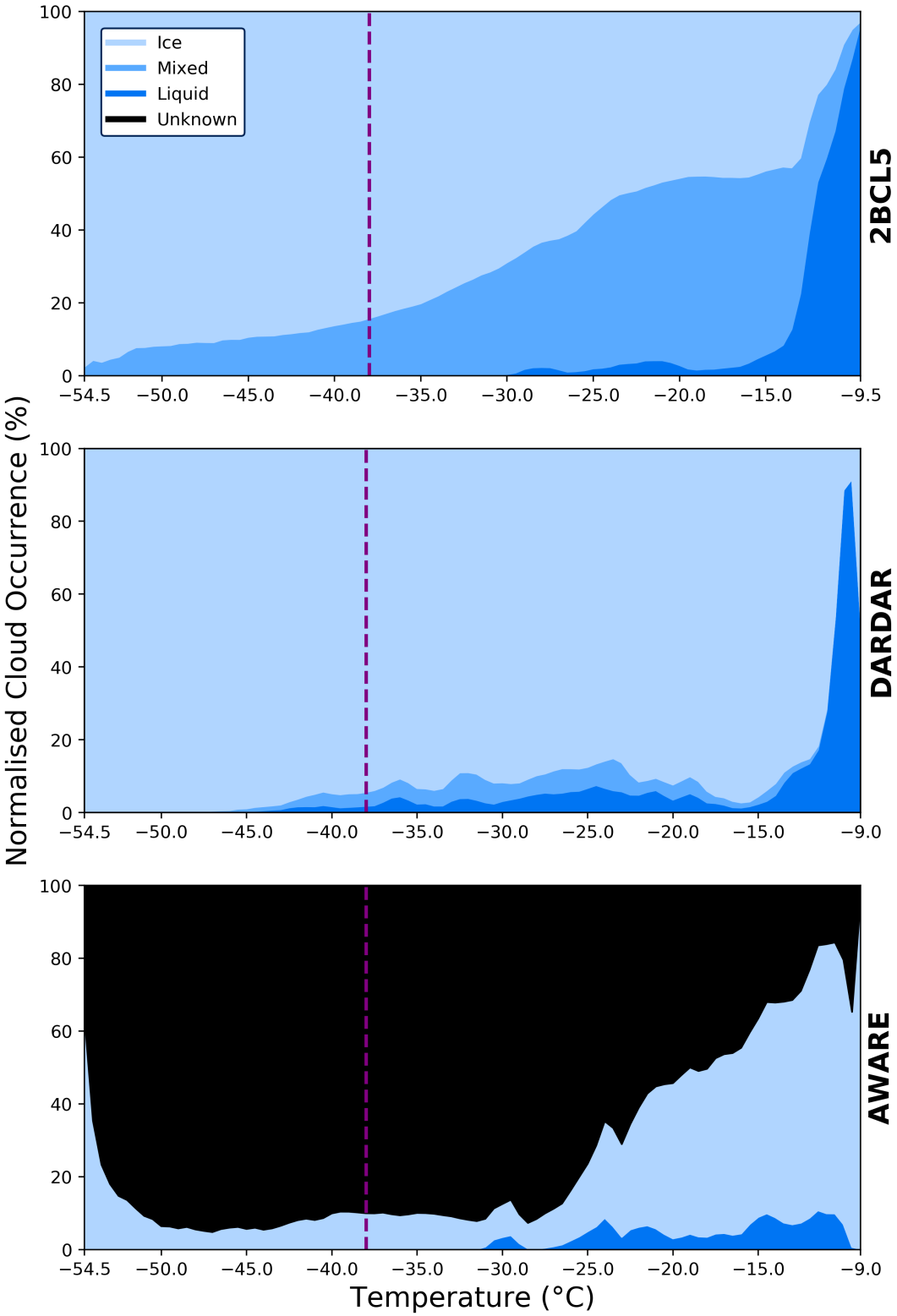

Figure 4.9: Normalised cloud occurrences for 2BCL5, DARDAR and AWARE from Figure 4.7 as a function of temperature. Cloud occurrence is split into ice, mixed and liquid phase cloud for 2BCL5 and DARDAR. Cloud occurrence is split into ice, liquid and unknown phase cloud for AWARE. The dashed line indicates the edge of the homogeneous freezing regime at -38 °C.

inates the coldest temperatures but lessens as the temperature rises. The middle panel for DARDAR shows that apart from a large presence of liquid phase cloud at -10 °C, ice phase cloud dominates. There are small amounts of mixed and liquid phase cloud present down to temperatures of -45 °C. Matching between the two is limited to both showing large amounts of ice phase cloud at the coldest temperatures and liquid phase cloud at the warmest temperatures.

2BCL5 and DARDAR do not agree with the physical limitations inferred from the verge of the homogeneous freezing regime. 2BCL5 shows that of the cloud classified as mixed phase at any temperature, 13.9% occurs at temperatures below the -38 °C isotherm. 2BCL5 does not show any liquid phase cloud below -38 °C. This matches what was found in Figure 4.7 where mixed phase cloud is found below the edge of the homogeneous freezing regime, but liquid phase cloud is not. DARDAR shows 3.4% of cloud classified as liquid phase and 13.8% of cloud classified as mixed phase at any temperature occurs below the -38 °C isotherm. This disagrees with Figure 4.7 where DARDAR only showed a little mixed phase cloud below the verge of the homogeneous freezing regime. It was suggested that this could be due to variations in the positions of the regime as mixed/liquid phase DARDAR cloud falls within the maximum isotherm across all passes, as seen on Figure 4.7. Using temperature directly removes this uncertainty on how phase is distributed as a function of temperature and shows that DARDAR also incorrectly classifies mixed phase cloud. 2BCL5 shows a higher proportion of mixed phase cloud below the -38 °C isotherm compared to DARDAR, which extends to temperatures colder than -50 °C. However, DARDAR shows a higher amount of mixed and liquid phase cloud above the -38 °C isotherm relative to the amount below than 2BCL5. Looking at the proportion of cloud below the -38 °C isotherm that is incorrectly classified, 2BCL5 classifies 9.8% of cloud incorrectly as mixed phase cloud. DARDAR classifies 1.8% of cloud below the -38 °C isotherm as either liquid of mixed phase cloud. Both 2BCL5 and DARDAR are incorrectly determining cloud phase based on physical limitations set by temperature.

Both 2BCL5 and DARDAR use the same product of ECMWF-AUX to get temperature information, yet 2BCL5 is worse at identifying cloud phase compared to temperature observations than DARDAR. It was identified in Chapter 3 that differences in how 2BCL5/DARDAR assign phase to their cloud may play a role in why their phase determinations are different. For 2BCL5, each cloud layer with a distinct top and bottom is assigned a single phase. DARDAR classifies each pixel in a cloud layer separately, so a cloud layer identified by 2BCL5 might have multiple classifications given by DARDAR. This could allow 2BCL5 to identify mixed phase above the -38 °C isotherm, as 'mixed' for 2BCL5 means that a combination of ice and supercooled liquid water exits in the cloud layer, rather than the whole cloud being mixed phase cloud. If mixed phase cloud exists at the cloud base where temperatures are warmer, 2BCL5 would also assign a mixed phase to the cloud top where temperatures are

colder.

The bottom panel in Figure 4.9 shows that for AWARE most of the cloud cannot be classified, and is instead assigned as a unknown phase. Liquid phase cloud is present in small amounts until approximately -30 °C. Ice phase cloud shows a greater proportion relative to the liquid and unknown phases at the warmest temperatures but falls off significantly below -25 °C as the unknown dominates. This matches what is seen in Figure 4.5 where the the ability to classify phase falls off as altitude increases (and conversely the temperature decreases), due to attenuation of the HSRL lidar. AWARE matches well with the verge of the homogeneous freezing regime at -38 °C. This result is uncertain due to the majority of the cloud here being unclassified, though as identified previously most unknown cloud is assumed to be ice in the AWARE dataset.

Due to a large part of the AWARE cloud being classified as an "unknown" phase, and 2BCL5/DARDAR classifying some cloud as mixed phase, it becomes difficult to draw comparisons between cloud phases for the satellite and the ground based datasets. 2BCL5 uses a process primarily driven by the temperature of the cloud top and cloud base, but also uses a temperature dependent radar reflectivity (Z_e) threshold and an integrated attenuated backscattering coefficient D. Zhang et al. (2010). This splits the cloud into liquid, ice and mixed phase cloud containing a combination of ice and liquid. Contrastingly, DARDAR uses the strength of the lidar backscatter signal to locate any attenuating high backscatter layers. They then attempt to classify these layers, based on temperature, horizontal extent of layer, thickness, reflectivity, and altitude. The algorithms used on the AWARE dataset use particulate backscatter cross-section and linear depolarization ratio to split the lidar observations of cloud into liquid and ice cloud. Due to attenuation of their lidar instrument, much of their cloud observations can not be classified and are instead defined as unknown. In order to draw better comparisons between the phases better, consistent processing algorithms would need to be applied to the raw radar/lidar measurements rather than trying to match separately processed products together.

4.2.4 Interannual variability of 2BCL5

It is seen that 2BCL5/DARDAR detect different amounts of cloud compared to AWARE. Something that was investigated was whether the differences between the satellite and the ground based measurements could be explained by geophysical interannual variability within the data. If the differences between the satellite and ground based measurements are smaller than the variability, then the two might represent each other well.

While AWARE data exists for 2016 only, 2BCL5 data is currently available from 2006 to 2017. For each of the six months with overlapping data, 2BCL5 cloud occurrence profiles for each year were compared to analyse the geophysical variability in cloud occurrence between years. This allows us to understand the geophysical interannual differences within 2BCL5 dataset relative to the 2016 AWARE dataset, and see if they might represent each other well despite differing in the amount of cloud they observe.

Figure 4.10 shows the variability in the 2BCL5 cloud occurrence for the month of November, chosen because of its representative nature across the period examined. Similar figures for the other months can be found in Appendix F. The 2016 average for AWARE is also shown as a dashed red line on the figure. The profiles for each year of 2BCL5 observations are shown on each sub-figure, with the target year highlighted as the filled blue curve. The total amount passes over McMurdo and days in the month with 2BCL5 measurements are annotated on each sub-figure. The number of passes represent the quality of the profile compared to the yearly average. A low amount of data would produce a profile that is unrepresentative of that year due to a low sampling bias, which can be seen in the Figure for the remaining months in Appendix F.

There is a high amount of variability between the total amount of cloud. 2006, 2007 and 2009 show large amounts of cloud, with maxima in cloud frequency above 30%. This contrasts to 2008, 2010 and 2012 which show maxima in the cloud occurrence of less than 20%, just above 10% in the case of 2010. The other years show maxima in the cloud occurrence between 20% and 30%. What is also interesting is the variations between the highest altitude where the cloud is detected. For 2014 this altitude is just 7.5 km but for the 2009, 2007 and 2009 cloud remains present up to an altitude of above 11 km. As might be expected, the 2BCL5 data underestimates the amount of clouds at low altitudes compared to AWARE and AWARE underestimates the amount of cloud at higher altitudes compared to 2BCL5 across all years. The shape of the AWARE curves matches well with the shape of the 2016 2BCL5 curve. This suggests that the geophysical variation in 2BCL5 is not the cause of the difference in cloud occurrence between 2BCL5 and AWARE.

What is interesting about the geophysical interannual variability for 2BCL5 is the possible presence of a limit in the amount of cloud detected below an altitude of 1 km. Figure 4.10 shows that cloud occurrence decreases rapidly at this level, where the 2011 sub-figure illustrates a darkening at the lower portion of the sub-figure. This indicates that the cloud occurrence profiles show the same amount of cloud at this level across all years, seemingly independent of the amount of cloud detected above. This darkening is not just limited to November and can be seen across the other months.

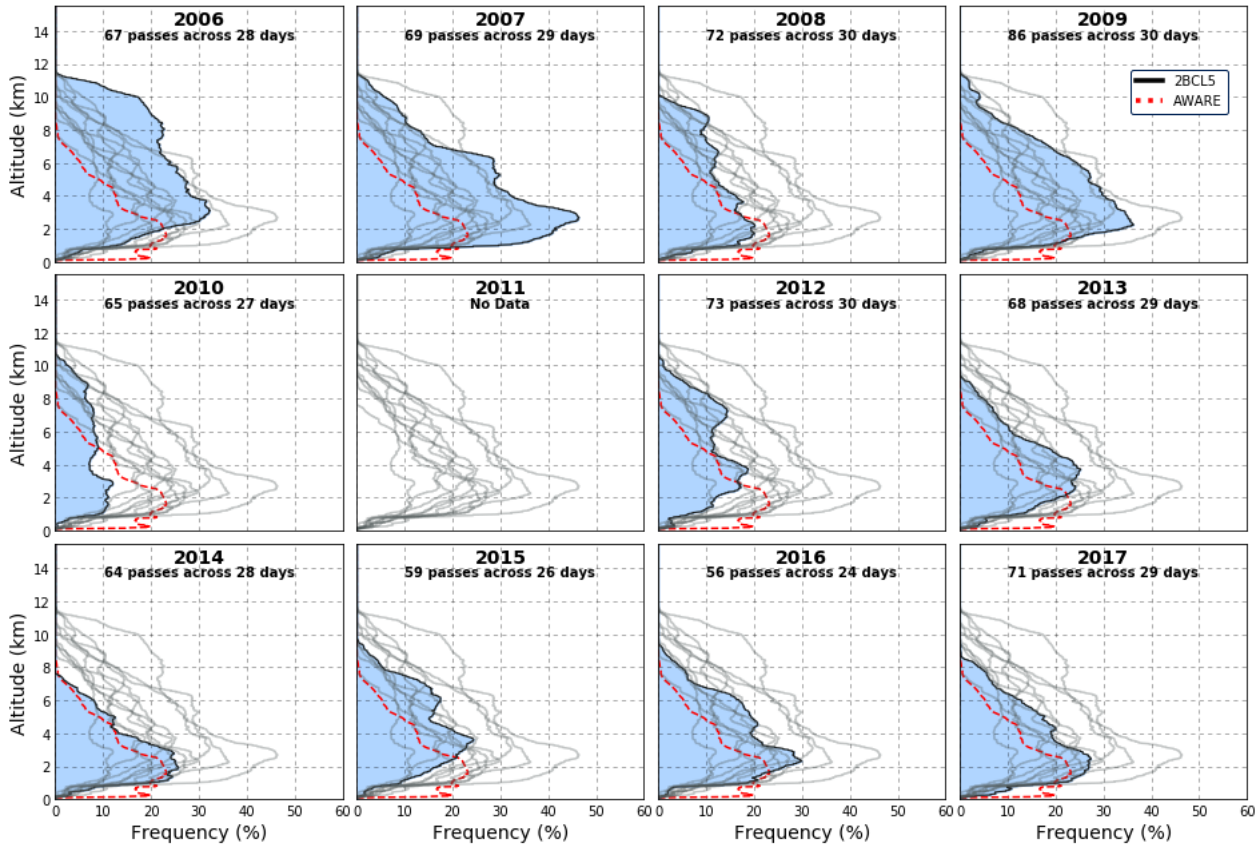

Figure 4.10: Geophysical variability of the 2BCL5 cloud occurrence between 2006 and 2017 for the month of November. The target year is indicated by the filled blue curve with the grey lines representing the profiles from the other sub-figures. The total amount passes over McMurdo and days in the month with 2BCL5 measurements are annotated at the top of each sub-figure. AWARE data is only available in 2016 as represented by the red dashed curve, highlighted on each plot for comparison.

Similar figures were made for the other months, the results of which are summarized in Figure 4.11. It displays a box and whisker diagram showing the geophysical interannual variability in 2BCL5 cloud occurrence across each month for 3 km altitude bins, as well as the cloud averaged across all altitudes (0 km - 12 km). The 0 km to 3 km altitude bin is split because of important differences in the cloud occurrence below and above 1 km. The black boxes represent the six individual months of overlapping AWARE and 2BCL5 data. In order from left to right the boxes represent the months of January, March, September, October, November, then December. The green line represents the monthly mean for the 2016 AWARE data and the purple line the monthly mean for the 2016 2BCL5 data. The means were calculated by summing the average cloud occurrence in each altitude bin, using the monthly cloud profiles for 2BCL5 and AWARE during 2016, as shown on Figure 4.10.

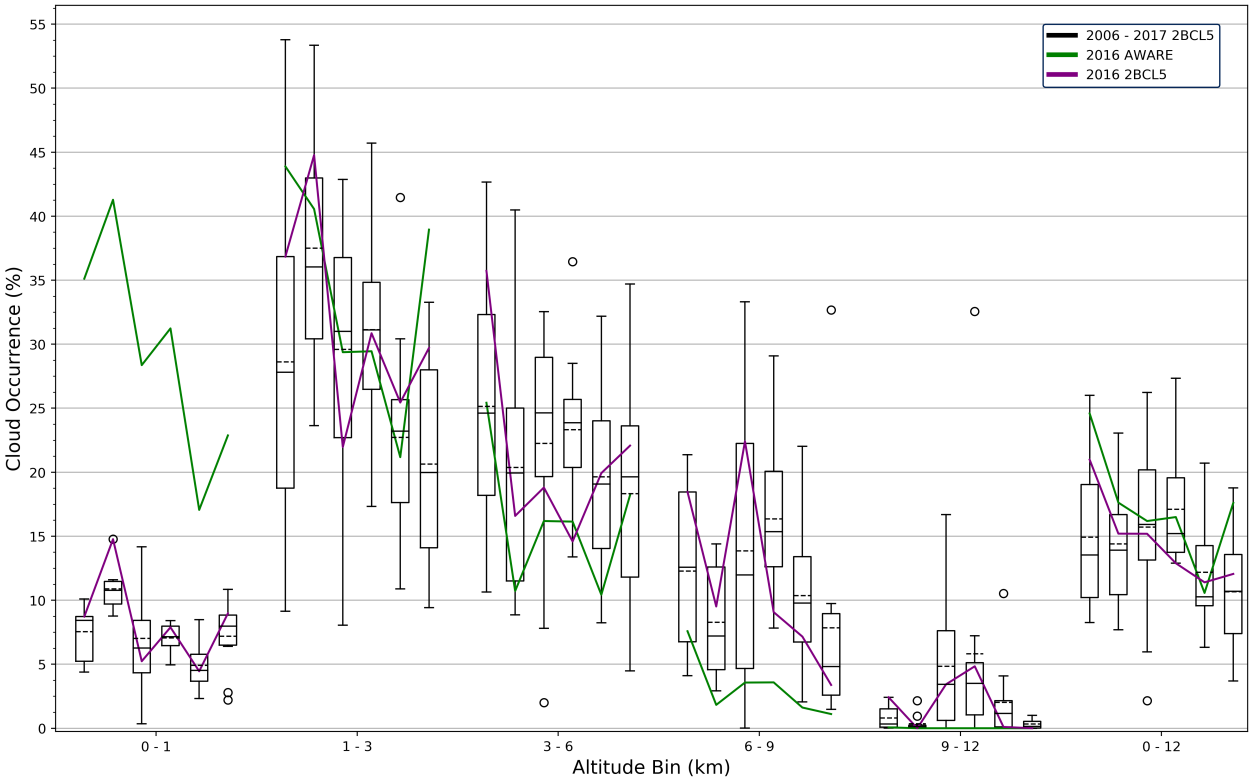

Figure 4.11: Geophysical interannual variability (2006 - 2017) in 2BCL5 cloud occurrence between different altitude bins across each month. It designates the median (thick line), 1st and 3rd quartiles (box's edges), 5th and 95th percentiles (whisker's edges), mean (dotted line), and outliers (circles). The green line represents the monthly mean for AWARE during 2016 and the purple line the monthly mean for 2BCL5 during 2016. In order from left to right the boxes represent the months of January, March, September, October, November, then December.

Between an altitude of 0 and 1 km there is low variability between years, although September stands out with the greatest variability. This contrasts to the highest variance between 1 and 6 km, with a 20% to 40% difference between the maximum and minimum cloud occurrence. In all cases 2BCL5 sees more cloud at high altitudes and less cloud at low altitudes compared to the 2016 AWARE. That this is present across all years suggests the failure to detect cloud at certain altitudes are limitations of the instruments; satellite instruments close to the ground and ground based instruments higher in the atmosphere. Differences between 2BCL5 and AWARE can not be explained by the geophysical variability in 2BCL5.

Comparing the 2016 2BCL5 data to the 2BCL5 variability between 2006 and 2017 for each month, cloud occurrence falls within the bounds of annual variability. There is only one time the cloud occurrence for a month and altitude bin falls outside the whisker's edges (5th/95th percentiles). March 0 km to 1 km shows a higher cloud occurrence than observed during other years, which corresponds to the outlier on Figure 4.11. This can be explained due to low sampling where 2BCL5 only has measurements for a third of the month, with the

majority of the other years sampling above two-thirds of the month. Looking at the cloud as a total, only January and October fall outside the 1st and 3rd quartiles with the remaining months representing the average across all years well.

As a whole AWARE data for 2016 falls within the 2BCL5 annual variability, matching close to the median during September, October, and November. When you break this into the altitude bins there is still relatively good matching between 1 km and 6 km. Outside this range the agreement is poor. Below 1 km AWARE detects more cloud across all months. Above 6 km AWARE detects less cloud, with almost no cloud detected above 9 km.

Although 2016 2BCL5 measurements fall within the interannual variability, the way the cloud varies between months has a better match with the 2016 AWARE measurements. This is evident below 1km; 2BCL5 has a much lower cloud occurrence compared to AWARE, yet cloud occurrence still changes in the same way from month to month. Where AWARE shows an increase or decrease so does 2BCL5. During March 2BCL5 shows an outlier that falls outside the interannual variability for the other years. AWARE represents this well, also showing the highest cloud occurrence during March compared to the other months. This suggests that the 2BCL5 can still get cloud information below this level, albeit at a reduced quality compared to AWARE. It also reinforces that differences between 2BCL5 and AWARE can not be explained by the geophysical variability in 2BCL5.

4.2.5 Comparing satellite and ground based cloud occurrence ratios

2BCL5 and DARDAR cloud detections compared to AWARE

Figures 4.7 and 4.11 show that 2BCL5 underestimates cloud at low altitudes compared to AWARE, but does not quantify how much. To identify if there was a pattern between the two, the relative values for the cloud occurrence between 2BCL5 and AWARE were investigated. Cloud profiles for both AWARE and 2BCL5 for each pass over McMurdo Station during 2016 were considered separately. At each altitude the values for the cloud occurrence of each dataset were compared to get a ratio between the two.

When looking at the ratio between the satellite and ground based observations, there are times where both detect cloud and a comparison can be made. But there are also times where either AWARE or 2BCL5/DARDAR will have a cloud observation unseen by the other, which needs to be assessed. Across the 194 2BCL5/DARDAR passes over McMurdo, the frequency of these detections were investigated. Figure 4.12 shows a comparison between 2BCL5 and AWARE where either one, both, or neither dataset detects any cloud as a func-

tion of altitude. The sum of all four subplots add to 100%, as they cover all cases of cloud detection.

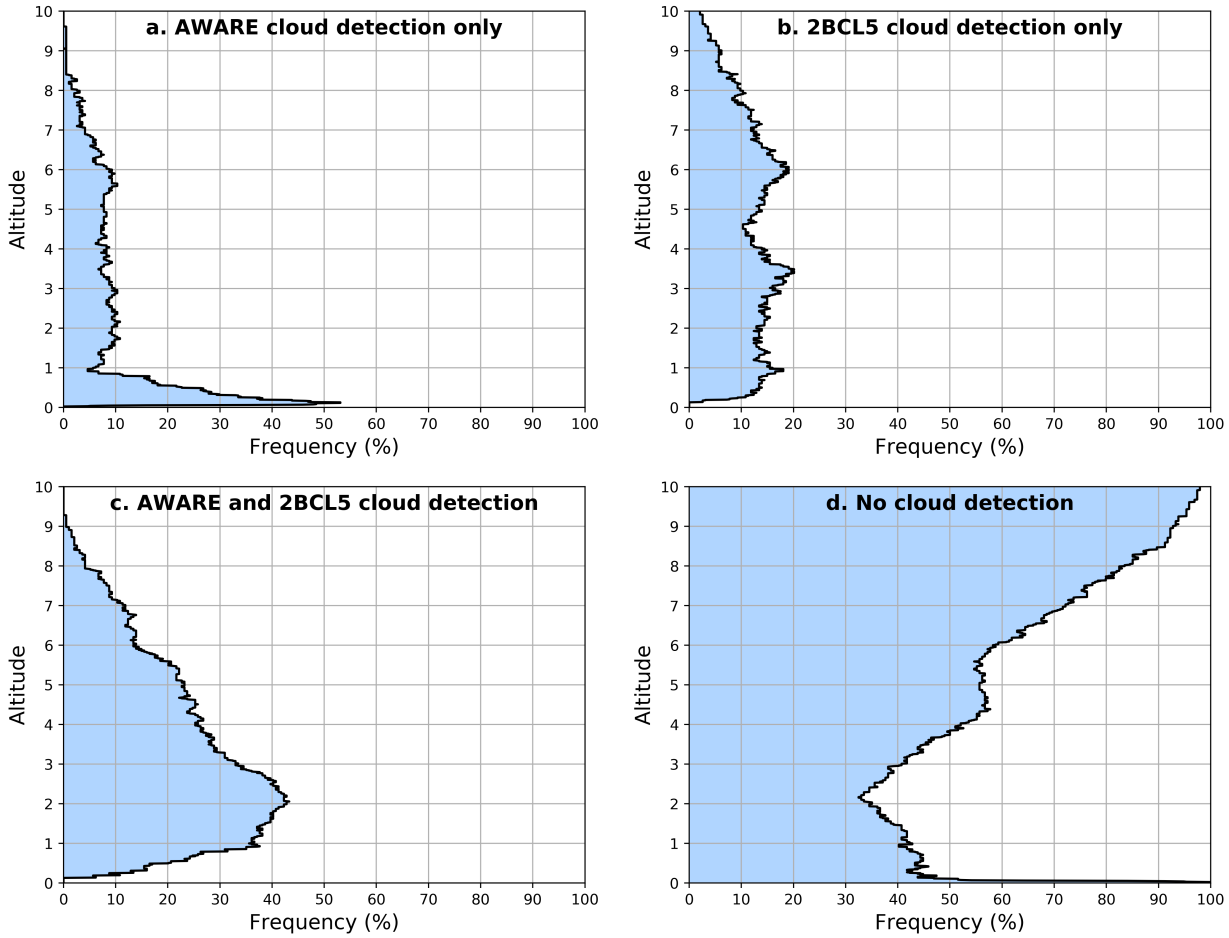

Figure 4.12: Frequency of 2BCL5 and AWARE cloud detections as a function of altitude for (a) AWARE has a cloud detection but 2BCL5 does not (b) 2BCL5 has a cloud detection but AWARE does not (c) Both AWARE and 2BCL5 have a cloud detection (d) Neither 2BCL5 or AWARE have a cloud detection.

Figure 4.12a shows that above 1 km AWARE will detect cloud that 2BCL5 does not approximately 10% of the time. However, below 1 km AWARE starts to detect greater amounts of cloud unseen by 2BCL5, up to 53%. This further highlights that the satellites are unable to see this cloud. Figure 4.12b shows that 2BCL5 detects cloud unseen by AWARE at a frequency of 10% - 20% up to an altitude of 7 km. After this the frequency falls off as AWARE observations are fewer. While 2BCL5 only cloud detections would be expected above 6 km - 7 km as the cloud occurrence for AWARE falls off (See Figure 4.5), it is surprising that 2BCL5 continues to detect cloud unseen by AWARE consistently down to the ground. This suggest either limitations in AWARE where the radar/liar instruments are not seeing the cloud, or issues with 2BCL5 where false positives in the radar/lidar signals are detected. Figure 4.12c shows that starting from an altitude of 9 km, the frequency where AWARE

and 2BCL5 both detect a cloud increases as you move toward the ground. It peaks at 42% at an altitude of 2 km then below 2 km it decreases sharply. This subplot resembles what is seen in for the cloud occurrence (Figure 4.7e-h) and suggests that the frequency of cloud detecting between 2BCL5 and AWARE is greater for increases cloud occurrence.

Figure 4.13 shows that same analysis as for Figure 4.12 but for a comparison between DARDAR and AWARE. The subplots show the frequency of where either one, both, or neither dataset detects cloud as a function of altitude.

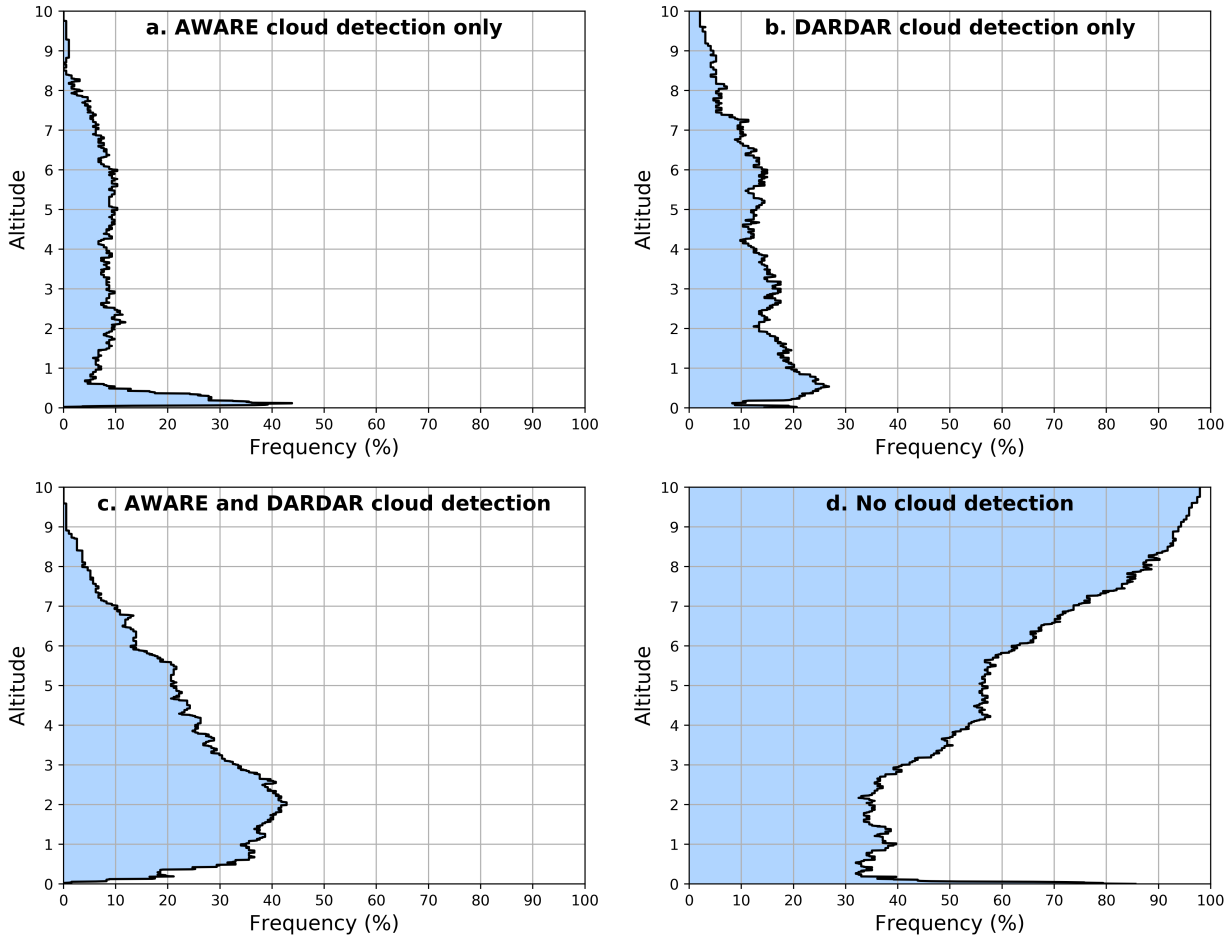

Figure 4.13: Frequency of DARDAR and AWARE cloud detections as a function of altitude for (a) AWARE has a cloud detection but DARDAR does not (b) DARDAR has a cloud detection but AWARE does not (c) Both AWARE and DARDAR have a cloud detection (d) Neither DARDAR or AWARE have a cloud detection.

Figure 4.13a shows that above 1 km AWARE will detect cloud that DARDAR does not approximately 10% of the time. However, below 0.8 km the frequency where only AWARE has a cloud detection rises to a peak of 44%. Like for 2BCL5 this highlights the satellites are unable to see cloud below 1 km. Figure 4.12b shows that between 1 km and 7 km DARDAR detects cloud unseen by AWARE at a frequency of 10% - 20%. Above 7 km the frequency

lowers to below 10% as AWARE observations become fewer. Below 1 km the frequency increases to a maximum of 25% of DARDAR passes detecting a cloud unseen by AWARE. Once again this suggest instrumental limitations in AWARE or issues with DARDAR where false positives in the radar/lidar signals are detected. Figure 4.13c displays a comparable profile to Figure 4.7a-d where both DARDAR and AWARE detect peaks in the cloud occurrence at an altitude of 2 km before decreasing.

Both 2BCL5 and DARDAR shows similar comparisons with AWARE, with some differences. In order to quantity this, Figure 4.14 shows differences between the frequency of cloud detections displayed on Figure 4.13 for DARDAR and on Figure 4.12 for 2BCL5.

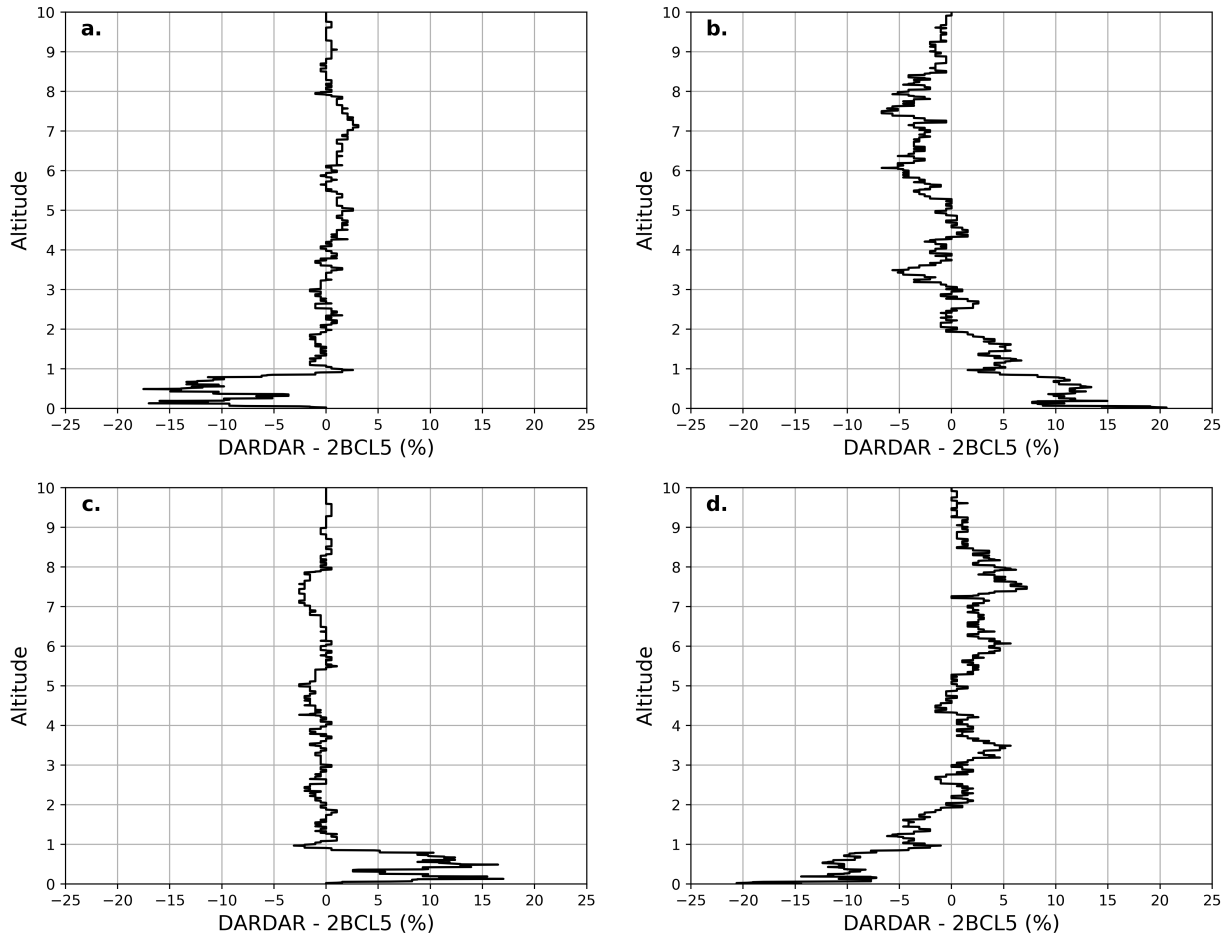

Figure 4.14: Differences between the frequency of cloud detections displayed on Figure 4.13 and on Figure 4.12 for (a) AWARE has a cloud detection but 2BCL5/DARDAR does not (b) 2BCL5/DARDAR has a cloud detection but AWARE does not (c) Both AWARE and 2BCL5/DARDAR have a cloud detection (d) Neither 2BCL5/DARDAR or AWARE have a cloud detection. A positive difference means that the DARDAR comparison shows a greater frequency than the 2BCL5 comparison.

It shows an apparent coupling between Figure 4.14a for the AWARE only cloud detections

and Figure 4.14c for where both have cloud detections. Above 1 km DARDAR and 2BCL5 show good agreements but below 1 km DARDAR there is a big difference between the two. Figure 4.14a shows that 2BCL5 shows 10% - 15% more cases where only AWARE detects a cloud, mirrored by Figure 4.14c where DARDAR shows 10% - 15% more cases where both detect cloud. This suggests that DARDAR agrees much better with AWARE than 2BCL5 below 1 km, while the two have comparable matches elsewhere.

Figure 4.14 also show a coupling between Figure 4.14b where only 2BCL5/DARDAR detects cloud, and Figure 4.14d where neither the satellite or ground based instruments have a cloud detection. Above 1 km 2BCL5 and DARDAR show small differences of up to 7%. Below 1 km the differences between the two increases to 10% - 15%. Figure 4.14b shows that DARDAR has a greater amount of detections where AWARE does not see cloud than 2BCL5. This is mirrored by Figure 4.14d where 2BCL5 shows a greater amount of detections where both 2BCL5 and AWARE do not detect any cloud. This suggests that DARDAR is detecting noise in the radar/lidar signals close to the ground as cloud and has a 10% - 15% larger false positive rate than 2BCL5.

Figure 4.14a/c show that DARDAR agrees better with AWARE below 1 km than 2BCL5, but this may be due to a greater cloud occurrence in DARDAR rather than an improved match with AWARE. In part, the ratio between the satellite and ground based measurements that both show cloud will be compared to determine whether the increased amount of DARDAR observations matches any better with AWARE than 2BCL5.

Cloud occurrence ratio of 2BCL5 and AWARE

Figure 4.15 shows the ratio of 2BCL5 to AWARE cloud occurrence as a function of altitude across the 194 passes that both 2BCL5 and DARDAR detected. Places where either 2BCL5 or AWARE do not detect cloud have been excluded. The ratio of cloud occurrence is plotted on a natural logarithmic scale to set an equal amount of 2BCL5 and AWARE cloud to a value of zero. Frequency of the ratio measurement at each altitude is also plotted using a logarithmic scale. This highlights some of the finer details overpowered by the prominent features when using a linear scale. A red line that represents the median value at each altitude is also displayed.

The median logarithmic ratio displays a period of agreement between 1.5 km and 4.5 km. Here the median value of zero means both 2BCL5 and AWARE are observing the same amount of cloud. However, there is a large spread of values, which indicates that although it may be likely for the two to observe similar cloud profiles this is not always the case. While the contour shows a 2BCL5/AWARE ratio of 0 remains the most common occurrence down

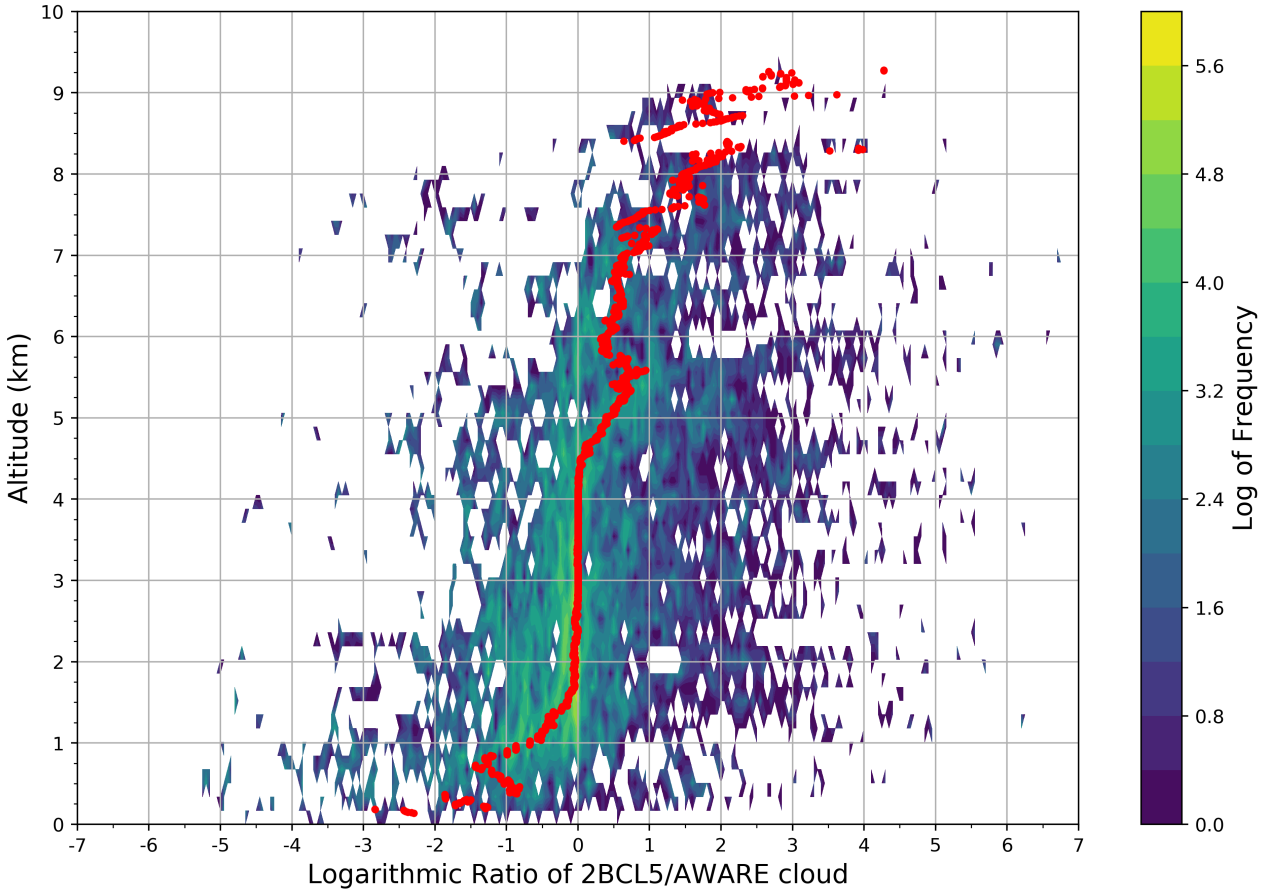

Figure 4.15: The ratio between 2BCL5 and AWARE cloud occurrence at different altitudes for overlapping daily cloud occurrence profiles during 2016. The ratio and frequency are shown on a logarithmic scale. The red line represents the median value at each altitude.

to an altitude of 1 km, below 1.5 km the median shows two starting to disagree; 2BCL5 underestimates compared to AWARE. The median logarithmic ratio decreases to -1.5 at 0.8 km, corresponding to an underestimation in 2BCL5 of 80% compared to AWARE. It then improves slightly to a median logarithmic ratio of -1, corresponding to an underestimation of 66%, before decreasing below after 0.25 km. Above 4.5 km the two also begin to disagree, but AWARE begins to underestimate compared to 2BCL5. After steadily decreasing the median logarithmic ratio stabilises and fluctuates around 0.5 to 1 up to an altitude of 7.5 km, corresponding to an underestimation in AWARE of 40% to 66%. Above this height there is little consistency as AWARE has difficulties detecting any cloud.

Cloud occurrence ratio of DARDAR and AWARE

The same comparison could also be completed between AWARE and DARDAR. Figure 4.16 shows the ratio of DARDAR to AWARE across the same 194 CloudSat/CALIPSO passes over McMurdo Station during 2016. Like before, the ratio of cloud occurrence and the frequency are plotted on a natural logarithmic scale and the red line represents the median

value at each altitude.

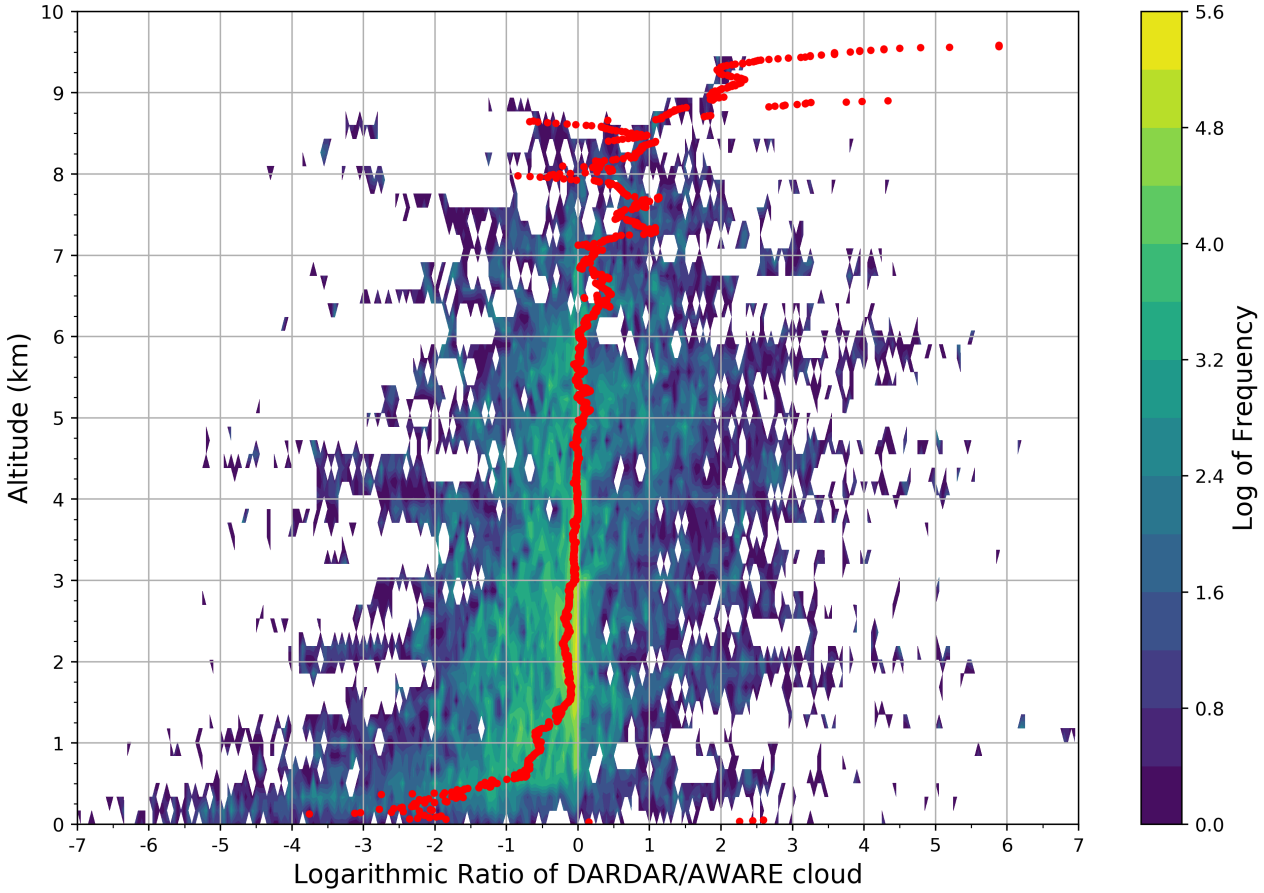

Figure 4.16: The ratio between DARDAR and AWARE cloud occurrences at different altitudes for overlapping daily cloud occurrence profiles during 2016. The ratio and frequency are shown on a logarithmic scale. The red line represents the median value at each altitude.

As in the case of the 2BCL5/AWARE comparison, there is a period of agreement between DARDAR and AWARE. It starts at 1.5 km and extends further to an altitude of 6 km although the logarithmic median values are much noisier. Like 2BCL5 there is a large spread of values, but the most common logarithmic ratio of 0 dominates down to an altitude of 0.5 km. DARDAR starts to underestimate compared to AWARE below 1.5 km. The median logarithmic ratio drops sharply to -0.5 at 500 m, corresponding to an underestimation in 2BCL5 of 40% compared to AWARE. It then steadily decreases from there down to the ground. Above 6 km the two begin to disagree with AWARE underestimating compared to DARDAR. The median logarithmic ratio fluctuates between 0 - 1 up to an altitude of 8 km, corresponding to an underestimation of 0% to 66%. At higher altitudes it begins to change rapidly as less profiles are available to determine the median.

2BCL5/AWARE and DARDAR/AWARE median logarithmic ratios

Comparing 2BCL5 and DARDAR together, profiles for the median logarithmic ratio from Figures 4.15 and 4.16 are displayed together on Figure 4.17. The 2BCL5/AWARE median is shown in blue and the DARDAR/AWARE ratio is shown in red. Both 2BCL5 and DARDAR compared to AWARE have three prominent regions; A region where the satellite likely underestimates close to the ground, a region where the ground based instruments likely underestimate at higher altitudes, and a region of agreement in the middle.

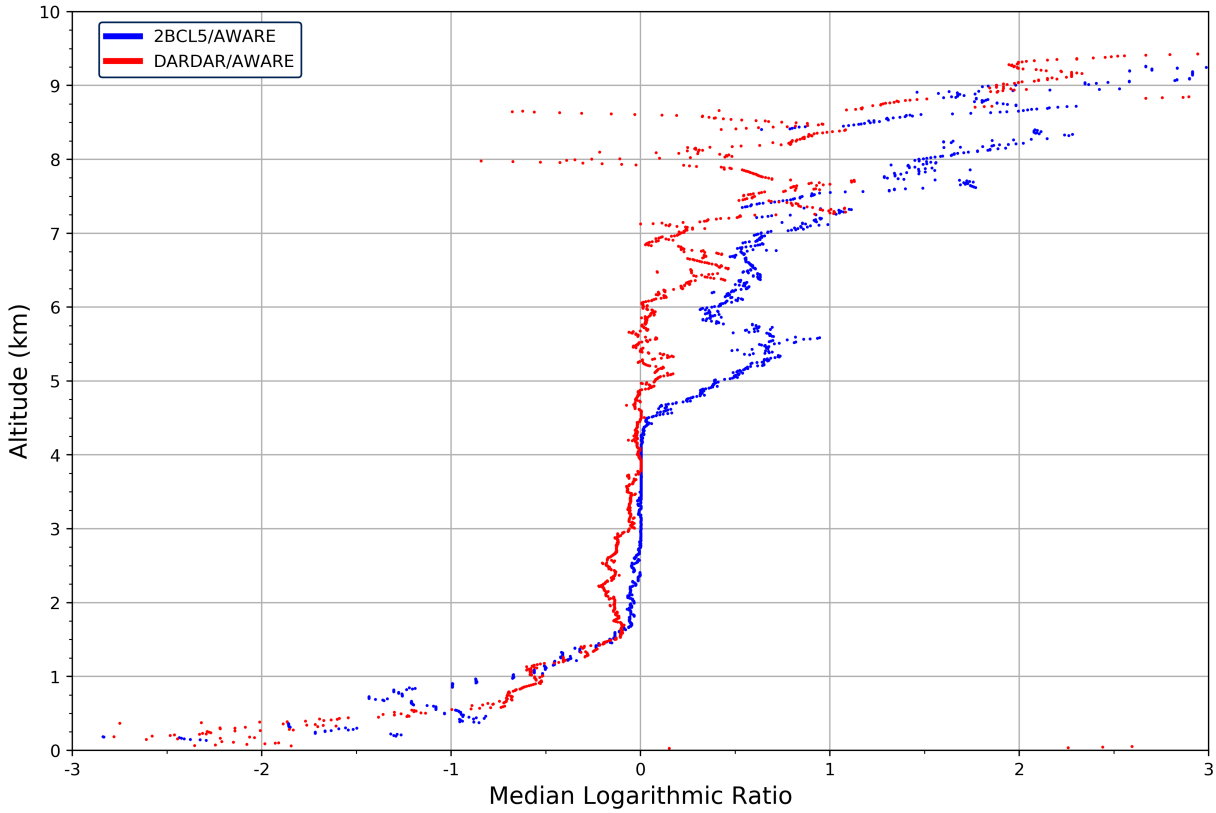

Figure 4.17: The median logarithmic ratio between 2BCL5/AWARE (blue) and DARDAR/AWARE (red) taken from Figures 4.15 and 4.16.

Below 1.5 km both 2BCL5 and DARDAR likely underestimate compared to AWARE. Closer to the ground, it would be expected that DARDAR is able to match better with AWARE than 2BCL5, because DARDAR sees more cloud below 1 km; This is not the case. Although Figure 4.16 shows a stronger amount of matching profiles to a lower altitude for DARDAR than 2BCL5, Figure 4.17 shows the place where the logarithmic median starts to deviate is the same for both DARDAR and 2BCL5. Even though DARDAR sees more cloud below 1 km than 2BCL5, it is not seeing any better than 2BCL5 compared to AWARE. Earlier in the chapter it was shown that DARDAR has a higher occurrence of detections that were seen by AWARE, as well as cloud detections only seen by DARDAR (Figure 4.14). This reinforces that DARDAR is detecting false positives in the lidar/radar signals and interpreting noise

close to the ground as cloud incorrectly.

For the matching region in the middle, 2BCL5 shows a much better match with AWARE than DARDAR does. 2BCL5/AWARE is in agreement between 1.5 km and 4.5 km and for the most part shows an equal amount of cloud. DARDAR matches best with AWARE between 1.5 km and 6 km, extending further than 2BCL5, but the match is not as good. Only in a few places does the median logarithmic ratio show equal amount of cloud between DARDAR/AWARE. It does not show comparable amounts for an altitude range greater than 0.5 km, unlike the 2BCL5/AWARE case.

Above the matching region at altitudes greater than 6 km, the median shows that both DARDAR and 2BCL5 overestimate compared to AWARE, but this is more likely to be attributed to AWARE being unable to detect the cloud accurately rather than the satellites. The reason the median logarithmic ratio is variable at high altitudes and close to the ground in both is that not all passes can be compared at all heights. If either the ground or satellite based instrument does not detect any cloud the ratio is unable to be compared, even if the other instrument does get a cloud detection. Figures 4.12 and 4.13 shows that at altitudes above 7 km the proportion of profiles that can be compared falls below 10%. This causes the underestimation of 2BCL5/AWARE and DARDAR/AWARE at high and altitudes to be worse than displayed, due to a higher proportion of incomparable profiles. Below 1 km a similar pattern is observed where the amount of profiles that can be compared drops as the satellites are unable to observe cloud detected by AWARE.

Histograms of 2BCL5/AWARE and DARDAR/AWARE

Histograms were made to sample the distributions of the logarithmic ratio at altitude ranges representative of the three regions for both 2BCL5/AWARE and DARDAR/AWARE. Figure 4.18 shows the distribution for 2BCL5/AWARE cloud occurrence at altitude ranges of (a) 7 km - 10 km (b) 3 km - 4 km and (c) 0 km - 1 km. The proportion of profiles between the satellite and ground base instruments that can be compared are annotated on each subplot. This was calculated by averaging Figure 4.12c between the appropriate altitude range.

Figure 4.18a shows between 7 km to 10 km there is a distribution that is skewed to the right, causing a tendency for a positive logarithmic ratio and underestimation of AWARE compared to 2BCL5. Figure 4.18b shows a distribution with an even spread between positive and negative logarithmic ratios but a large peak at a value of 0. Most of the time at 3 km to 4km both 2BCL5 and AWARE are detecting similar amounts of cloud. Figure 4.18c shows that under 1 km the distribution is skewed to the left, with a tendency towards negative logarithmic ratio values. This causes an underestimation of 2BCL5 compared to AWARE.

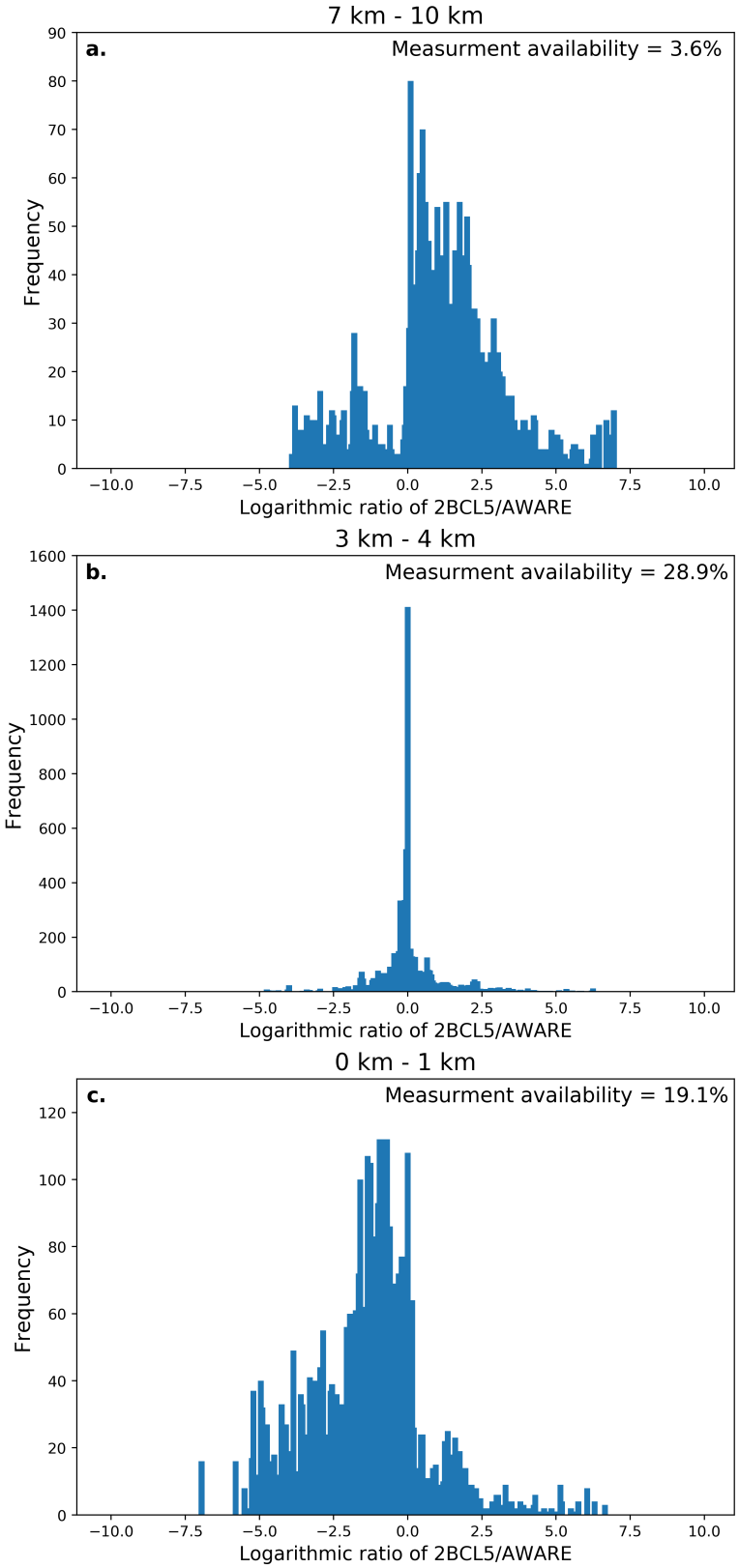

Figure 4.18: Histograms showing the distribution of the logarithmic ratio of 2BCL5/AWARE cloud occurrence for (a) 7 km to 10 km, (b) 3 km to 4 km and (c) 0 km to 1 km. The proportion of profiles that can be compared is annotated on each subplot.

The 2BCL5 histograms also show the availability of data at each altitude range. Between 3 km and 4 km shows the most data, at 28.9% . This decreases substantially below 1 km where only 19.1% of passes between AWARE and 2BCL5 are available have comparable measurements. Between 7 km to 10 km only 3.6% measurements are available, even though the altitude range is the highest. This explains the large variability in the median logarithmic ratio in Figure 4.15, as not as many profiles are available to be averaged.

Figure 4.19 shows histograms for the DARDAR/AWARE at the same altitude ranges. The proportion of profiles that can be compared is derived from Figure 4.13. Figure 4.19a shows a distribution between 7 km to 10 km that is not skewed, compared to what Figure 4.18a shows. DARDAR has a peak around a logarithmic ratio above 0 with a wide spread of values. Figure 4.19b shows a similar distribution to Figure 4.18b, with an even spread between positive and negative logarithmic ratios but with a larger spread around the large peak at a 0. Figure 4.19c shows the distribution is skewed to the left, the same as in Figure 4.18c for the 2BCL5/AWARE comparison.

For the proportion of measurements that are available to be compared Figure 4.19a shows an availability between 7 km - 10 km of only 3.0%, comparable to Figure 4.18a which shows 3.6%. Figure 4.19b shows a high availability of measurements at 28.4%, comparable to the 28.9% of 4.18b. The biggest difference comes in Figure 4.19c with 26.2% , much greater than the 19.1% seen in Figure 4.18c. This again shows that while the DARDAR/AWARE comparison is much more complete below 1 km, it does not detect the cloud any better than the 2BCL5/AWARE comparison.

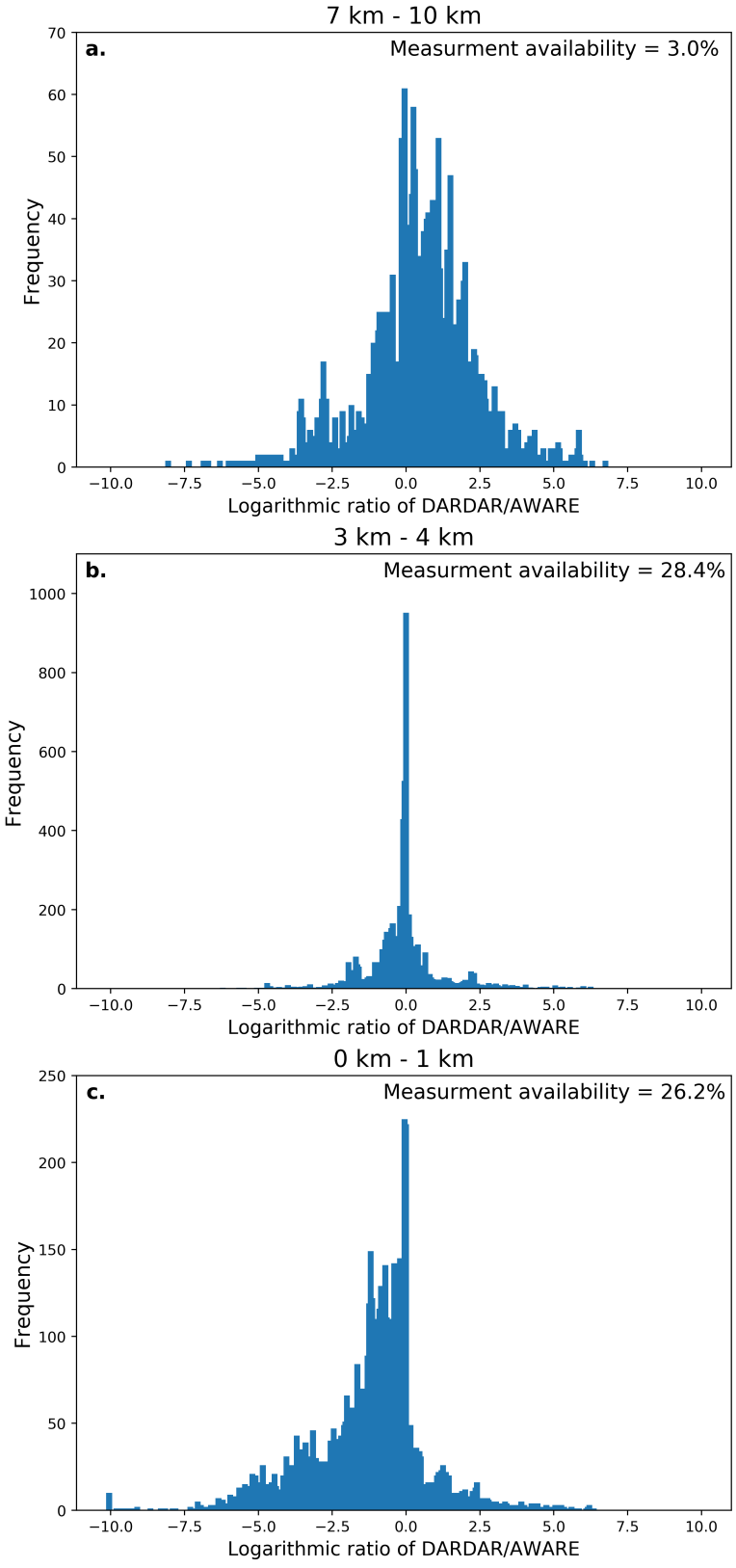

Figure 4.19: Histograms showing the distribution of the logarithmic ratio of 2BCL5/DARDAR cloud occurrence for (a) 7 km to 10 km, (b) 3 km to 4 km and (c) 0 km to 1 km. The proportion of profiles that can be compared is annotated on each subplot.

Statistical analysis of 2BCL5/AWARE and DARDAR/AWARE

The ratios of 2BCL5/AWARE and DARDAR/AWARE show differences/similarities in their distributions at different altitude ranges. In order to quantify this, statistical tests were carried out between the histograms produced in Figures 4.18 and 4.19.

A t-test was used to compares difference between the means of the 2BCL5/AWARE and DARDAR/AWARE histograms using the mean, standard deviation and number of samples in each distribution. The t-test produces a t-statistic (t) and a probability value (p). A higher t-value indicates greater differences between the means. The p-value indicates whether the means of the two distributions are likely the same. If the p-value is less than a predefined significance level (α), then the two means are different. The significance level was chosen to be 5%, or $\alpha = 0.05$. The results of the t-test are shown in Table 4.1, run by comparing the means and standard deviations of distributions representing the same altitude ranges from Figures 4.18 and 4.19.

	t-value	p-value
0 km - 1 km	2.37	0.018
3 km - 4 km	0.06	0.949
7 km - 10 km	1.29	0.197

Table 4.1: Results of the t-test test comparing the histograms generated in Figures 4.18 and 4.19. The t-value indicates differences between the means and the p-value indicates the probability that the distributions are the same.

To determine whether the means of 2BCL5/AWARE and DARDAR/AWARE are statistically similar for different altitude ranges, the p-values produced from the t-test are compared to the significance level of $\alpha = 0.05$. Table 4.1 shows that between 0 km - 1 km the means are statistically different, with a p-value of $p = 0.0018$ being less than the significance level of $\alpha = 0.05$. Between 3 km - 4 km and 7 km - 10 km, with p-values of $p = 0.949$ and $p = 0.197$ respectively, the means between 2BCL5/AWARE and DARDAR/AWARE are statistically similar.

A Kolmogorov–Smirnov (K-S) test was also used to compare whether the two distributions of 2BCL5/AWARE and DARDAR/AWARE are the same. The K-S test produces a K-S statistic (D) and a probability value (p). The D-value indicates the greatest distance between the two distributions, with a higher D-value meaning a greater distance. The p-value, as for the t-test, indicates whether the two distributions are likely the same. If the p-value is less than a predefined significance level (α), then the two distributions are different. The significance level was chosen to be 5%, or $\alpha = 0.05$. The results of the K-S test are shown in Table 4.2. The K-S test used the same input as the t-test, comparing the distributions

representing the same altitude ranges from Figures 4.18 and 4.19.

	D-value	p-value
0 km - 1 km	0.168	2.18×10^{-5}
3 km - 4 km	0.0975	0.0417
7 km - 10 km	0.0875	0.0884

Table 4.2: Results of the K-S test comparing the histograms generated in Figures 4.18 and 4.19. The D-value indicates the greatest difference between the distributions and the p-value indicates the probability that the distributions are the same.

The p-values produced from the K-S test are compared to the significance level of $\alpha = 0.05$, to determine whether the distributions of 2BCL5/AWARE and DARDAR/AWARE are statistically similar for different altitude ranges. Table 4.2 shows that between 0 km - 1 km the distributions are the statistically different, with a p value of $p = 2.18 \times 10^{-5}$ being much less than the significance level of $\alpha = 0.05$. Between 3 km - 4 km the distributions are also statistically different, as the p value of $p = 0.0417$ is still lower than the significance level. Between 7 km - 10 km the distributions between 2BCL5/AWARE and DARDAR/AWARE are statistically similar, with a p-value of $p = 0.0884$ being greater than the 0.05 significance level.

Summary and Conclusions

Investigating the ratio of cloud occurrence at different altitudes, 2BCL5 and DARDAR show different levels of correspondence with the AWARE ground based observations. Both show three prominent regions; A region which can be interpreted as the satellite observations underestimating, a region which can be interpreted as the ground based observations underestimating, and a region between the two where the satellite and ground based measurements are in agreement.

2BCL5 and AWARE agree between 1.5 km and 4.5 km while DARDAR and AWARE agree between 1.5 km and 6 km. Although DARDAR has a longer range of agreement, Figure 4.17 shows that 2BCL5 has the stronger match with AWARE. The 2BCL5/AWARE logarithmic ratio median shows a much smoother line that stays closer to an equal amount of cloud than the DARDAR/AWARE median that only shows equality between DARDAR and AWARE in a few places. Histograms displaying the distribution of the logarithmic ratio between 3 km and 4 km show that 2BCL5/AWARE has a tighter distribution compared to DARDAR/AWARE. Between 3 km - 4 km the t-test shows that the means of 2BCL5/AWARE and DARDAR/AWARE are statistically similar, wheres the K-S test shows that the distributions are statistically different. Figure 4.18b and Figure 4.19b shows that both the

2BCL5/AWARE and DARDAR/AWARE distributions between 3 km - 4 km are dominated by peaks at logarithmic ratio of 1. This offers an explanation as to why the means are statistically similar in the t-test. With the distributions however, 2BCL5/AWARE shows much less spread. 2BCL5 is overall better when compared to the AWARE dataset, where the statistical test show the differences between 2BCL5 and DARDAR in their distributions are statistically significant, if not the mean.

Below 1.5 km neither satellite dataset matches well with AWARE; Figure 4.17 shows the median logarithmic ratio falls off under an altitude of 1.5 km for both the 2BCL5/AWARE and DARDAR/AWARE comparisons. One would expect that DARDAR is able to match better with AWARE closer to the ground than 2BCL5 due to the increased amount of cloud observations below 1km in the DARDAR dataset, as seen in Figure 3.15. Instead histograms of Figure 4.18c and Figure 4.19c show that both DARDAR and 2BCL5 have distributions that are skewed to the left, although DARDAR has a greater amount of comparisons with AWARE below 1 km. Between 0 km - 1 km the t-test and K-S test show that both the means and distributions of 2BCL5/AWARE and DARDAR/AWARE are statistically different. Even though they are statistically different both underestimate compared to AWARE. DARDAR sees more cloud below 1 km than 2BCL5, but is not observing any better compared to AWARE than 2BCL5 is.

Above 7 km neither 2BCL5 or DARDAR does a good job matching with AWARE. Figure 4.17 shows the median logarithmic ratio for both DARDAR and 2BCL5 overestimates compared to AWARE, but this is more likely to be attributed to AWARE being unable to detect the cloud accurately rather than the satellites overestimating cloud. This happens because ground based lidar signal will attenuate and the radar signal has limitation detecting mid-level ice clouds. The histograms of Figure 4.18a and Figure 4.19a show that 2BCL5 has a distribution that is skewed to positive values while DARDAR has a more even distribution spread to both positive and negative values. Between 7 km - 10 km, the t-test and the K-S test show that both the means and distributions of 2BCL5/AWARE and DARDAR/AWARE are statistically similar. Both 2BCL5 and DARDAR compare poorly with AWARE in this region. That both are seeing similar distributions further highlights the limitations of AWARE at high altitudes, rather than the satellites seeing the same amount of cloud; Figure 4.8 shows that 2BCL5 observes more high level cloud than DARDAR in all cases.

When comparing with AWARE, 2BCL5 has shown itself to be a more representative dataset than DARDAR. While both 2BCL5 and DARDAR match poorly with AWARE at high and low attitudes, 2BCL5 has the better matching region between 1.5 km - 4.5 km. The K-S test shows that differences between 2BCL5/AWARE and DARDAR/AWARE during the matching region are statistically significant.

4.2.6 Comparing 2BCL5 and DARDAR cloud occurrence ratios

Cloud occurrence ratios for 2BCL5 and DARDAR can also be compared. The ratio of 2BCL5 to DARDAR cloud occurrence across the coincident CloudSat/CALIPSO passes is displayed on Figure 4.20. As for the comparison with AWARE, the ratio of cloud occurrence and the frequency are plotted on a natural logarithmic scale and the red line that represents the median value at each altitude.

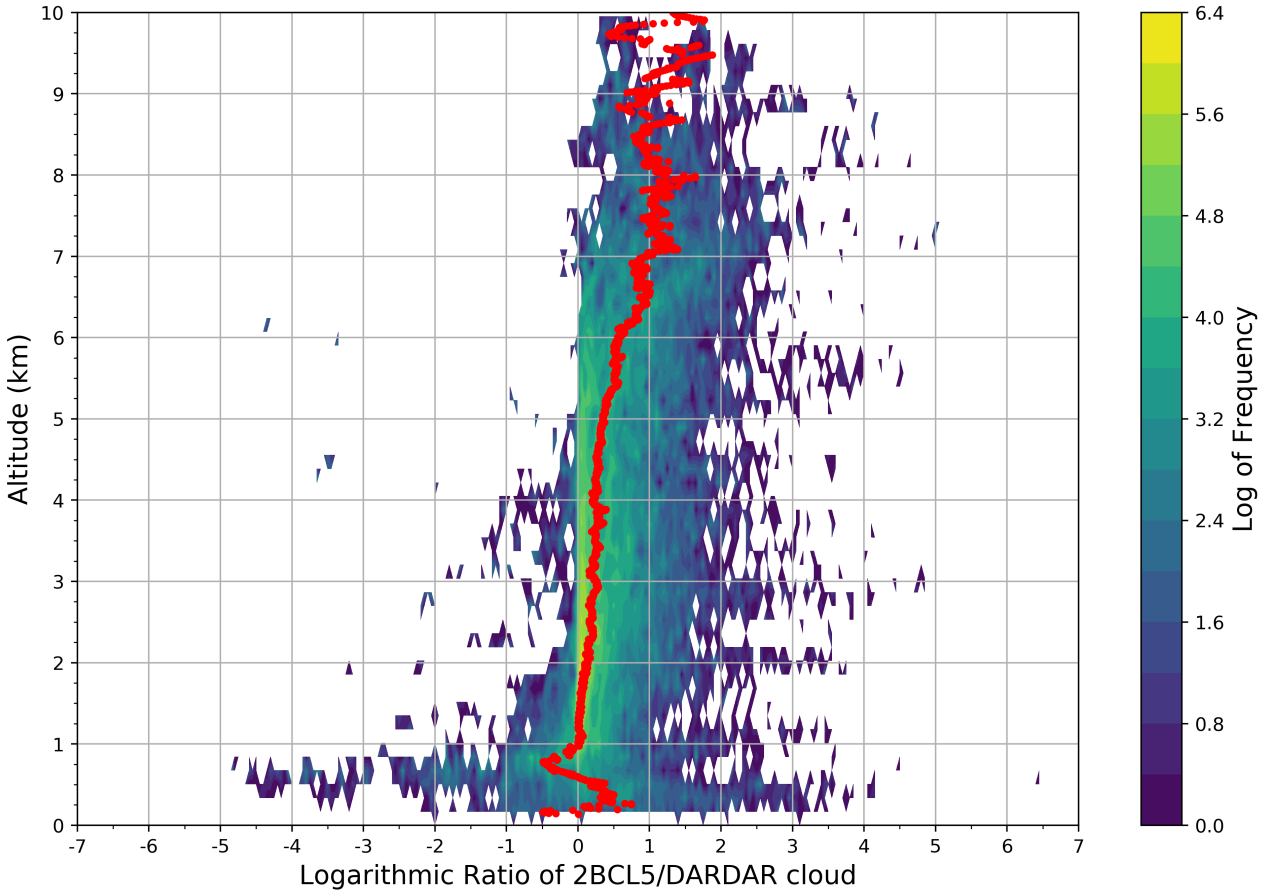

Figure 4.20: The ratio between 2BCL5 and DARDAR cloud occurrences at different altitudes for overlapping daily cloud occurrence profiles during 2016. The ratio and frequency are shown on a logarithmic scale. The red line represents the median value at each altitude.

DARDAR consistently underestimates compared to 2BCL5 above 1 km, with the underestimation increasing to 66% at 7 km. The spread of the logarithmic ratio shows only a few instances above 1 km where DARDAR detects more cloud compared to 2BCL5. Below 1 km the distribution broadens with both 2BCL5 and DARDAR showing more cloud at different altitudes. You would expect DARDAR to show greater levels of cloud below 1km compared to 2BCL5 as it detects more cloud at these altitudes (See Figure 3.15). This shows that the

extra cloud DARDAR sees is not detected by 2BCL5, and further suggests that DARDAR has a greater level of false cloud detections.

4.2.7 Comparing liquid phase cloud occurrence ratios

Something that could not be determined when comparing 2BCL5 to DARDAR was how well each was determining cloud phase. 2BCL5 shows a spread of ice, mixed and liquid phase cloud while DARDAR mostly classifies cloud as ice or liquid phase with little mixed phase cloud. As discussed earlier in the chapter, comparisons with AWARE are difficult due to a large part of the AWARE cloud being classified as an "unknown" phase. Only liquid phase cloud could be compared and did not show a consistent match between the satellite and ground based measurements, as seen in Figure 4.7. This was confirmed by producing contour plots showing ratio of 2BCL5 to AWARE cloud occurrence as a function of altitude as produced for the total cloud. Figure 4.21 shows the liquid cloud comparison for 2BCL5 and Figure 4.22 shows the same for DARDAR. There is no consistent match between the liquid phase cloud observed by AWARE and 2BCL5/DARDAR.

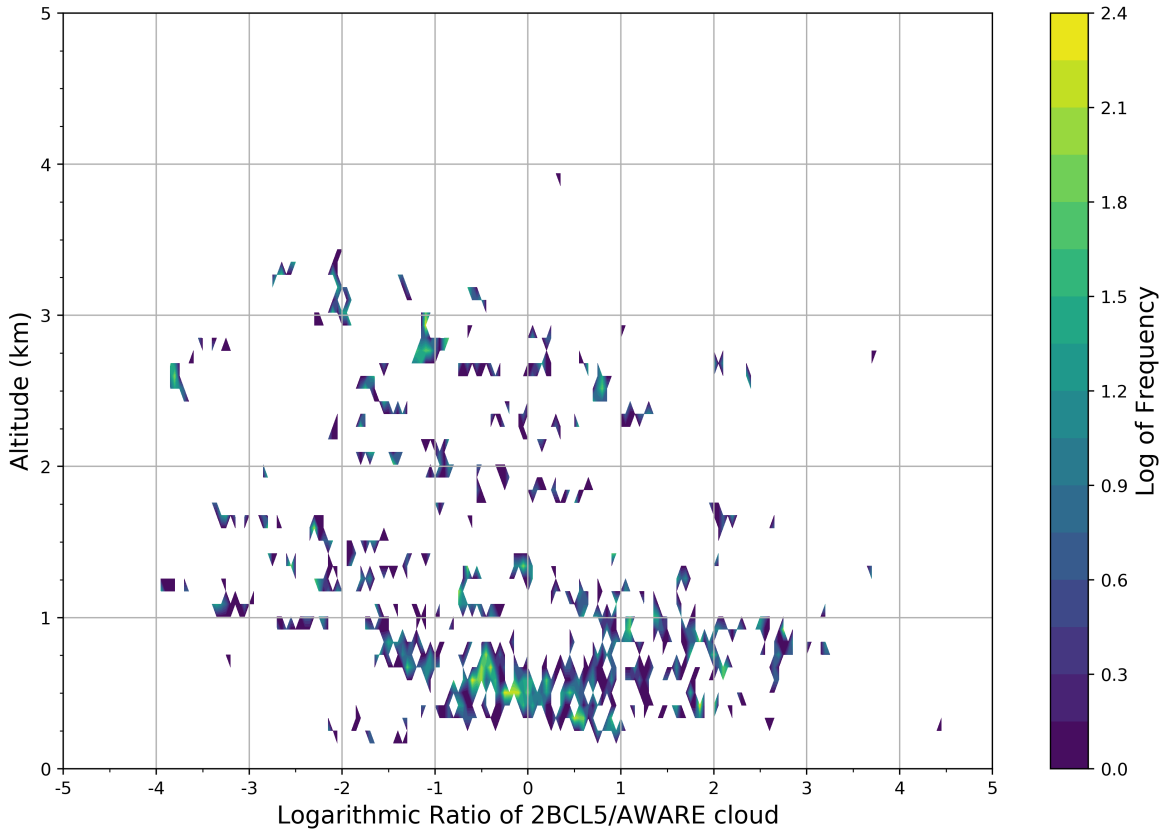

Figure 4.21: The ratio between 2BCL5 and AWARE liquid cloud occurrences at different altitudes for overlapping daily cloud occurrence profiles during 2016. The ratio and frequency are shown on a logarithmic scale.

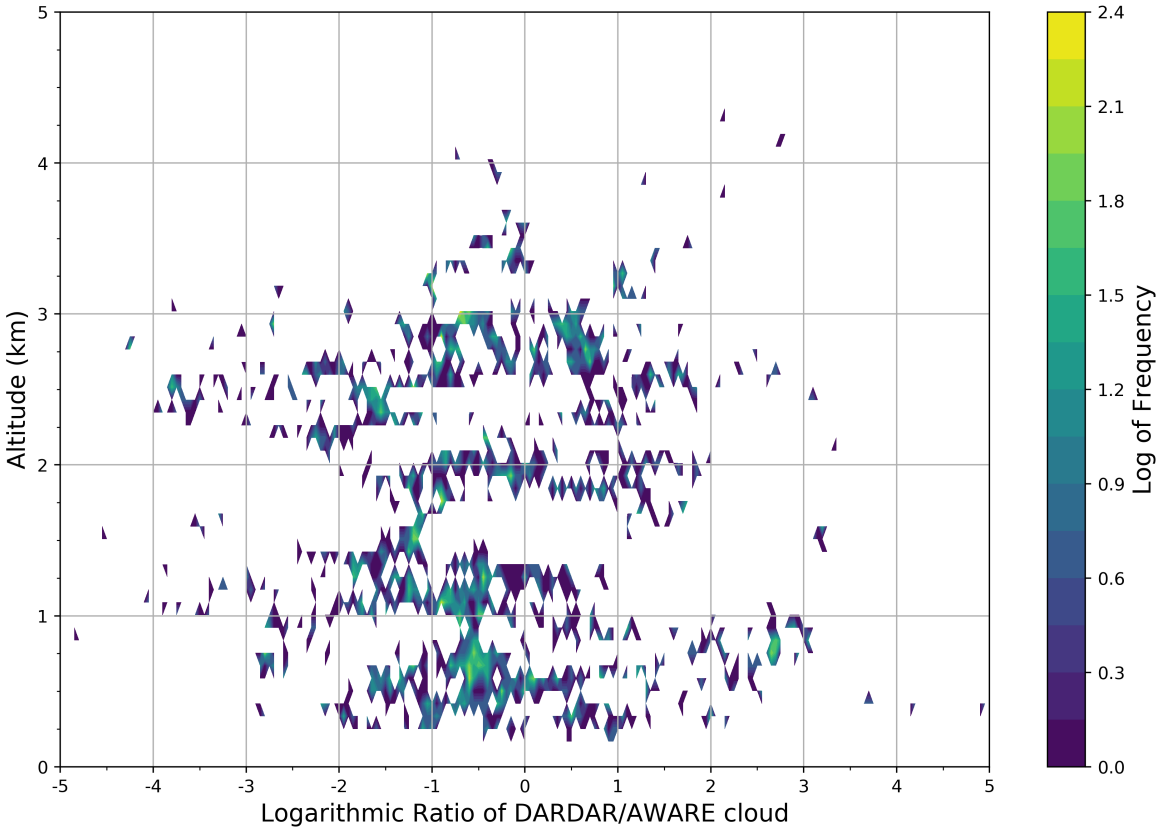

Figure 4.22: The ratio between DARDAR and AWARE liquid cloud occurrences at different altitudes for overlapping daily cloud occurrence profiles during 2016. The ratio and frequency are shown on a logarithmic scale.

Chapter 5

Discussion

5.1 Comparing results with previous observational studies

It was found that both 2BCL5 and DARDAR compared with AWARE underestimate cloud occurrence close to the ground. The satellite and ground based comparisons then have a region of agreement before 2BCL5 and DARDAR begin to observe more cloud compared to AWARE. Overall results from Chapter 4 show that 2BCL5 does a better job at matching with AWARE than DARDAR does. The obtained results from this study can be compared with the results from similar studies comparing satellite and ground based observations of cloud.

Protat et al. (2014) compared the differences in the frequency of occurrence and radiative effect of clouds between satellite and ground based measurement over Darwin, Australia. They used the 2B-GEOPROF-lidar satellite observations as well as millimeter wavelength cloud radar and the micropulse lidar measurements from the Atmospheric Radiation Measurement (ARM) site in Darwin. They found that the satellite observations under-report hydrometeor occurrence below altitudes of 2 km. This was not quantified in their study, which was more concerned with the underestimation of high level cirrus clouds by ground based observations.

Blanchard et al. (2014) used lidar and radar measurements from the ground and space to combine and assess their detection efficiency over the Eureka site in the Arctic. Ground based observations were taken by a millimeter wavelength cloud radar and high resolution spectral lidar. Satellite observations were compared using DARDAR, as well as CloudSat 2B-GEOPROF and CALIPSO cloud and aerosol layer measurements that did not combine the radar/lidar together. Comparing 267 passes over Eureka between 2006 to 2010 they found that CloudSat and DARDAR matched well with the Eureka measurements between 2 km and 6 km. CALIPSO lidar measurements only matched well between 5 km and 6 km. Below 2 km all satellite datasets underestimated compared to Eureka, with DARDAR performing the best. Above 6 km DARDAR and CALIPSO overestimated compared to Eureka, while CloudSat underestimated. DARDAR matched well with CloudSat between 3 km and 5 km then well with CALIPSO above 5 km.

Mioche et al. (2015) looked into the variability of mixed phase clouds over the Svalbard region in the Arctic. As a part of their study they compared DARDAR cloud occurrence measurements to those obtained at Ny-Alesund using a micropulse lidar. They used an older

version of DARDAR, v1.1.4. They found the DARDAR detects more cloud above 5 km, the two agree between 5 km and 2 km, and DARDAR overestimates below 2 km compared to the ground based measurements; This disagrees with findings in this study.

Y. Liu et al. (2017) investigated the cloud vertical distribution from using surface and space observations of radar and lidar over two sites (Eureka and Barrow) in the Arctic. Ground based measurements were taken using a Ka band radar and micropulse lidar/high resolution spectral lidar similar to that used in the AWARE campaign. Satellite observation came from the CloudSat and CALIPSO 2B-GEOPROF-LIDAR product. This is similar to 2BCL5, although they were using an older version than what is currently available so results are not directly comparable to what has been undertaken here. By looking at the differences in the monthly means of cloud occurrence between 2006 and 2010, they found that cloud occurrence from space-based observations showed 25–40% fewer clouds below 0.5 km, comparable cloud occurrences between 1 and 2 km, and larger cloud occurrences above 2 km than from surface-based observations.

Alexander and Protat. (2018) used lidar based measurements at Cape Grim (41° S) compared with DARDAR satellite data. They found that DARDAR underestimated cloud below 1.5 km by a factor of three. They used DARDAR v2.2.1, which is more comparable to DARDAR v2.11 used in this study that the others. However, due to a lack of a cloud radar at Cape Grim they filtered their dataset to exclude thick clouds that attenuated the lidar. This included only low level single cloud layers where both the ground based lidar and DARDAR cloud mask could detect both the cloud top and cloud base. While this gave the greatest chance that both the surface lidar and DARDAR could fully determine the clouds unattenuated, their result likely underestimates the correction needed when accounting for thicker multi-layer clouds.

Previous studies mostly show and underestimation of cloud by satellites compared to the ground based measurements at low altitudes. Studies disagree on what point this underestimation starts, but this level will change depending on region, where the thickness and heights of the cloud will vary. The observed threshold of 1.5 km matches well overall with previous work. Only one study (Mioche et al., 2015) finds that the satellite overestimates below 2 km compared to the ground based measurements. They authors associate this overestimate with different cloud determination algorithms and a dataset with a short duration.

Two studies quantified the underestimation of low level cloud by satellite observations. Alexander and Protat. (2018) found underestimation of a factor of three while Y. Liu et al. (2017) found underestimation of 25–40%. These studies disagree with what was found here, where both 2BCL5 and DARDAR continue to underestimate close to the ground, with the satellite seeing less than 20% of the cloud reported by AWARE. Reasons for the disagree-

ment are possibly due to the methods used in each study. Alexander and Protat. (2018) only included low level single cloud layers where both the ground based lidar and DARDAR mask could detect the cloud top and cloud base. Their detections will not have full attenuation of the lidar. Y. Liu et al. (2017) looked at the monthly means across four years of satellite and ground based data. This is less direct than what has been undertaken in this thesis, which looks at the specific passes over McMurdo. Methodology carried out in this study is superior as it provides a more direct comparison between then satellite and ground based observations.

Blanchard et al. (2014) carried out the most comparable study to what has been completed here, analysing more than one set of satellite observations with ground based measurements. They used DARDAR in their comparison, but instead of using a secondary joint CloudSat/CALIPSO product like 2BCL5 they considered CloudSat/CALIPSO observations separately. This gave three datasets, the radar/lidar combined product of DARDAR, the radar observations of CloudSat, and the lidar observations of CALIPSO. While their analysis of the satellite and ground cloud occurrences agrees with the results presented here, they also have a comparison between the satellite datasets. Below 1 km they find that DARDAR and CALIPSO match well, while CloudSat falls off faster due to ground clutter. Between 1 km and 6 km DARDAR and CloudSat match well although CloudSat shows a greater peak in cloud occurrence. Above 6 km DARDAR and CALIPSO match well and CloudSat underestimates. Overall DARDAR matches well with either CloudSat/CALIPSO at all heights, which suggests DARDAR would agree well with 2BCL5. This does not match the results found here, where DARDAR shows more cloud at low altitudes, but shows less cloud elsewhere. A key difference in the datasets used is that an older version of DARDAR v1.1.4 was used in their study. It has been seen that the second version of DARDAR shows more cloud close to the ground and less cloud elsewhere over the polar regions (Delanoë & Hogan 2010). The difference in the DARDAR versions could explain the differences between this study and Blanchard et al. (2014), as well as the changing conditions between McMurdo Station and Eureka such as temperature, cloud coverage and geography.

5.2 Relating to research aims of the Deep South clouds and aerosols project

Work carried out in this thesis was motivated by ongoing work in the clouds and aerosols project of the Deep South National Science Challenge. One of the project's goals is to quantify the proportions of liquid, ice and mixed phase cloud above the Southern Ocean in an effort to improve parameterizations of cloud phase in the NZESM. Initially the aim of this thesis was to collect and compare satellite and ground based cloud observations to develop a representation of the vertical structure of clouds and cloud phase over the Southern

Ocean. This has not been achieved adequately for comparison with model output because the datasets show large relative biases. However, we have been able to determine which satellite datasets might be preferable for analysis with model data. In order to develop a representative picture of cloud and cloud phase, the satellite and ground based observations need to be joined together. The cloud occurrences for 2BCL5 and AWARE show promise for a blended product where cloud occurrences from the two are combined together. However, the cloud and aerosols part of Deep South is analysing clouds specifically, which 2BCL5 and AWARE do not clearly resolve. 2BCL5/AWARE do not distinguish between cloud and precipitation, which might also limit their suitability. This suggests that more low-level cloud observations will be important to constraining model runs. Even if the cloud occurrences for all cloud could be joined, significant differences in the way cloud phase is determined between the two. AWARE does not classify mixed phase cloud. While 2BCL5/DARDAR do classify mixed phase cloud, they differ in the amount and distribution. Because of these differences the cloud occurrences for the separate phases could not be matched together well enough for sensible comparisons with model data. Raw radar/lidar measurements from both ground and space based instruments might need to be processed together using consistent algorithms to be able to accurately compare between the phases, which would be both time consuming and computationally expensive. A better path might be to examine output from the models using instrument simulators and comparing raw returns from the observations. However, this would require significant work as the corresponding simulation of scatter between different types of particles (such as ice crystals and water droplets) would contain significant uncertainties.

5.3 2BCL5 cloud layer statistics

One aspect this thesis touches on, but does not address, is the underlying assumption that one of the reasons satellites have difficulties observing low level cloud due to lidar attenuation by thick cloud layers. Figure 5.1 shows the median logarithmic ratio between 2BCL5/AWARE for single and multiple cloud layers passes over McMurdo. This comparison could not be carried out for DARDAR easily, as DARDAR does not produce cloud layer information. While DARDAR is expected to have a different match with AWARE both have the same assumption about lidar attenuation and both 2BCL5 and DARDAR see reduced cloud occurrences below 1.5 km. It therefore seems reasonable to assume that the result for the 2BCL5/AWARE comparison will be similar to the DARDAR/AWARE comparison. Figure 5.1 shows evidence that passes with single cloud layers have better agreement with AWARE that multiple cloud layers. This backs up the underlying assumption that attenuation of the lidar by multiple cloud layers is reducing the quality of comparison with AWARE. However, below 1.5 km both single and multiple cloud show poor matching with AWARE. It shows that even in cases where only a single cloud layer is observed, the low level satellites based observations still struggles to match well with AWARE. This is a similar result to Alexander

and Protat. (2018), where they exclude multiple cloud layers from their analysis and still found an underestimate of the satellite observations compared to the ground based observations. Reasons for this include that single layer cloud may still partially attenuate the lidar signal and the the radar signal will still be effected by ground clutter below 1.5 km (Marchand et al., 2008; Tanelli et al., 2008). In order to get a full picture of the vertical distribution of cloud, a combination of ground and satellite based measurements are needed as the satellites are fundamentally unable to observe clearly down to the ground.

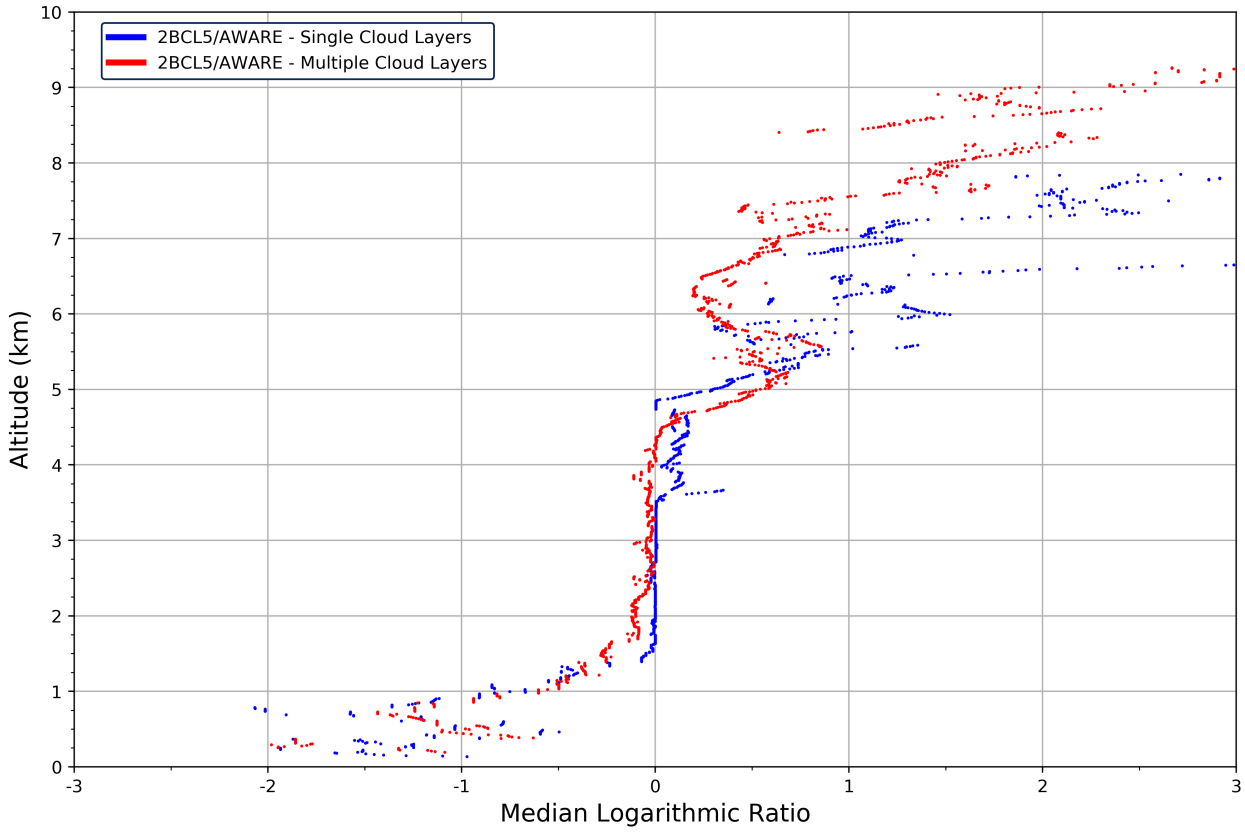

Figure 5.1: The median logarithmic ratio for 2BCL5/AWARE across single and multiple cloud layers during passes over McMurdo.

Chapter 6

Conclusion

Clouds play an important role in the climate. They cool the climate by reflecting incoming solar radiation back into space. Clouds also absorb outgoing infrared radiation and re-radiate it back towards the surface, trapping heat and causing the climate to warm. In order to predict future climate it is important that climate models accurately represent clouds. Currently climate models poorly represent cloud, which has been attributed to factors that include simulating too little cloud cover and under-representing the amount of supercooled liquid water in clouds. This leads to biases in the cloud radiative effect, which in turn causes a positive shortwave radiation bias over the Southern Ocean in particular, where too much sunlight is hitting the surface of the ocean. One of the results of the poor representation of clouds and their feedback processes in the models are biases in the cloud radiative effect. This causes a positive bias over the Southern Ocean in particular, where too much sunlight is hitting the surface of the ocean. This thesis was undertaken with the aim of collecting and comparing satellite and ground based observations of cloud to develop a representation of the vertical structure of clouds and their phase over the Southern Ocean.

A comparison is undertaken between the 2BCL5 (Sassen et al., 2008) and DARDAR (Delanoë & Hogan, 2010) satellite datasets, derived using CloudSat/CALIPSO observations. Cloud observations are binned into five degree latitude regions and cloud occurrence, cloud fraction and cloud phase measurement area derived for each region. These are used to derive the global distribution of cloud as a function of latitude, altitude and cloud phase for both DARDAR and 2BCL5. The two display differences in the amount of cloud and its partitioning between the ice, mixed and liquid cloud phases. 2BCL5 detects more clouds than DARDAR, except below 1 km where DARDAR shows a greater amount of cloud. 2BCL5 always detects more mixed phase cloud; DARDAR classifies these clouds as either ice or liquid depending on geographical position. Ice and liquid cloud are well represented with respect to constraints placed by the 0 °C and -38 °C isotherms, but mixed phase cloud is poorly determined by both DARDAR and 2BCL5. DARDAR mixed phase cloud falls within the isotherms well, but misses coverage over the tropics. 2BCL5 shows mixed phase cloud at all latitudes, but 2BCL5 mixed phase cloud falls outside the isotherm ranges where both ice and liquid phase cloud should not coexist. Due to differences in their cloud determination 2BCL5 will generalise a whole cloud as mixed phase cloud if it detects both ice and supercooled liquid water while DARDAR will classify the parts of cloud that are ice, liquid, and mixed phase separately. While this offers an explanation to the differences it does not give a clear picture of whether either one is better. Using external datasets to validate whether 2BCL5 of DARDAR is better proves difficult, as they tend to use observational products related to 2BCL5/DARDAR that bias comparisons. The difference in cloud occurrence be-

tween 2BCL5 and DARDAR is shown to be greatest over the Southern Ocean, while the cloud fraction observations are in agreement. This gave motivation for the use of a ground based dataset to validate the low level cloud detections of 2BCL5 and DARDAR.

To further assess whether 2BCL5 or DARDAR were more representative of cloud, ground based observations taken over McMurdo Station during the 2016 AWARE campaign are used (Silber et al., 2018). Satellite data is restricted to observations falling within a 5 degree box centered on McMurdo, and AWARE observations are restricted to a three hour window centred around a satellite overpasses. Satellite data is also constrained to passes that are observed by both 2BCL5 and DARDAR. This means that individual passes are likely to be comparing similar cloud structures.

Cloud occurrence profiles show that AWARE underestimates cloud occurrence compared to 2BCL5/DARDAR above 6 km - 7 km. Below 1 km DARDAR and 2BCL5 underestimates compared to AWARE. Neither 2BCL5 or DARDAR do a consistent job detecting the liquid phase cloud reported by AWARE, and the other phases can not be compared easily due to differences in phase processing. Investigating the interannual variability between 2BCL5 and comparing it to AWARE finds that differences between 2BCL5 and AWARE cannot be explained by the the geophysical variability in 2BCL5.

To quantify the differences between the 2BCL5/DARDAR and AWARE, the ratio between the satellite and ground based observations are determined for each pass over McMurdo Station at different altitudes. Comparisons between 2BCL5/AWARE and DARDAR/AWARE show three prominent regions; A region where the satellite underestimates close to the ground, a region where the ground based measurements underestimate at higher altitudes, and a region of agreement in the middle. Between 3 km - 4 km 2BCL5 matches better with AWARE than DARDAR does, appearing to be the more representative dataset. The 2BCL5/AWARE median logarithmic ratio median shows a smoother, tighter line that stays close to an equal amount of cloud between the two. The DARDAR/AWARE median only shows equality between DARDAR and AWARE in a few places, and has a much larger spread during the matching region. Below 1.5 km neither satellite dataset matches better with AWARE, even though DARDAR sees more cloud below 1 km than 2BCL5. DARDAR seeing more cloud at low altitudes is likely be attributed to a greater amount of false positives where DARDAR is classifying noise in the lidar/radar signal incorrectly as cloud. Above 7 km neither 2BCL5 or DARDAR does a good job matching with AWARE, which likely highlights the limitations of AWARE at high altitudes rather than the satellites seeing the same amount of cloud. Overall 2BCL5 has shown itself to be a better match with AWARE than DARDAR. While both 2BCL5 and DARDAR match poorly with AWARE at high (> 7 km) and low (< 1.5 km) attitudes, 2BCL5 has the better matching range in the middle (1.5 km - 4.5 km). Statistical tests are completed to evaluate whether the means and distributions of

2BCL5/AWARE and DARDAR/AWARE are different. The t-test indicated that between 3 km - 4km the means are statistically similar and the K-S test shows that differences between 2BCL5/AWARE and DARDAR/AWARE are statistically significant.

The obtained results from this study are found to be in agreement with similar studies comparing satellite and ground based observations of cloud, showing three prominent regions. Most studies show an underestimation of the satellites observations compared to the ground based measurements, followed by a period of agreement, then an underestimation of the ground based observations. While the studies report different altitudes at which these three regions occur, they all used different methodologies and are carried out over different ground sites with varying geographic and atmospheric conditions.

There is future work that can be produced comparing satellite and ground based measurements of cloud over the Southern Ocean. For the AWARE analysis as presented in this thesis, the next step would be a blended product joining the cloud occurrences from both AWARE and 2BCL5, as 2BCL5 is found to be the more representative dataset. Other work includes incorporating more ground based sites in and around the Southern Ocean into this analysis. As AWARE is only one ground based dataset it might not be representative of the Southern Ocean as a whole. Further comparisons between new ground based observations and 2BCL5/DARDAR would be used to verify whether 2BCL5 is the better dataset and represents cloud better. In the discussion it was shown 2BCL5 passes over McMurdo Station with single cloud layers compared better with AWARE than passes with multiple cloud layers (Figure 5.1). Future work could include expanding on these initial findings to assess the differences between single and multiple cloud layers for the DARDAR/AWARE analysis, and a comparison could be drawn between the two. One of the areas of research that could not be properly investigated during this study was the comparison of cloud phase, due to the differing algorithms between 2BCL5, DARDAR and AWARE that process the observations. What could be produced in the future is the creation of a new phase classification scheme between the satellite and ground based datasets that strives for consistency between the two.

Appendices

Appendix A

Quality of 2BCL5 observations

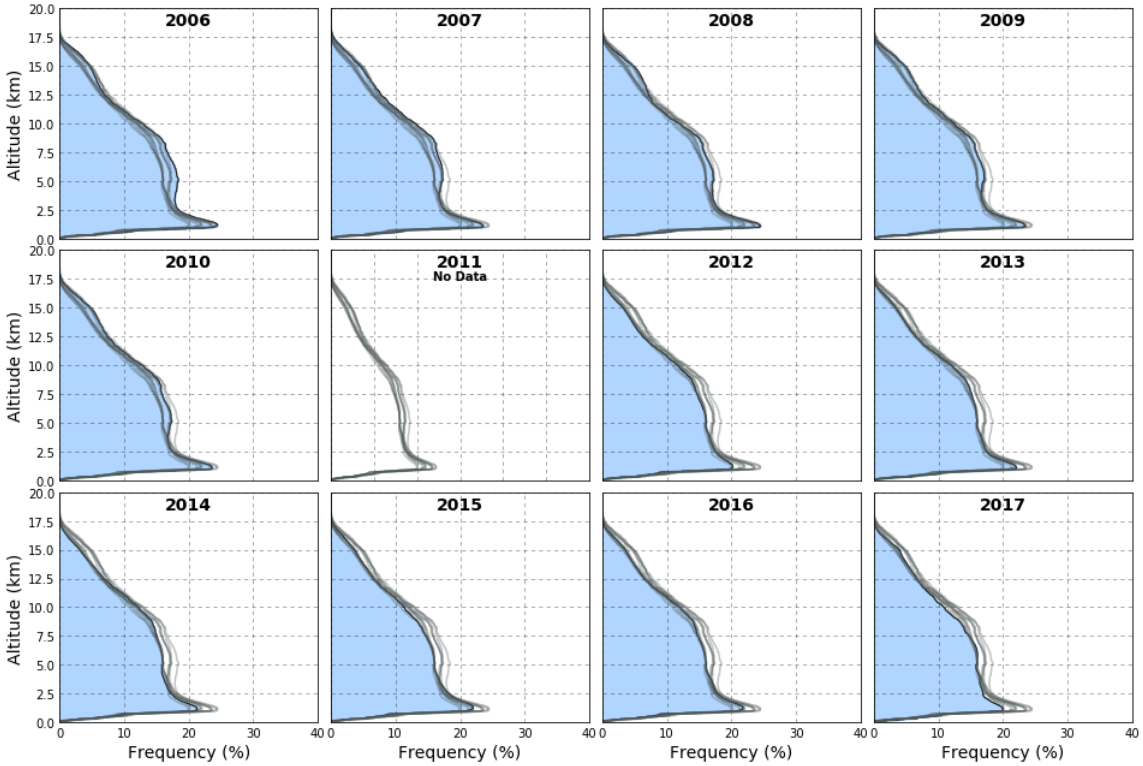

Figure A.1: Geophysical variability of 2BCL5 cloud occurrence between 2006 and 2017 for the month of June. The target year is indicated by the filled blue curve with the grey lines representing the profiles from the other sub-figures.

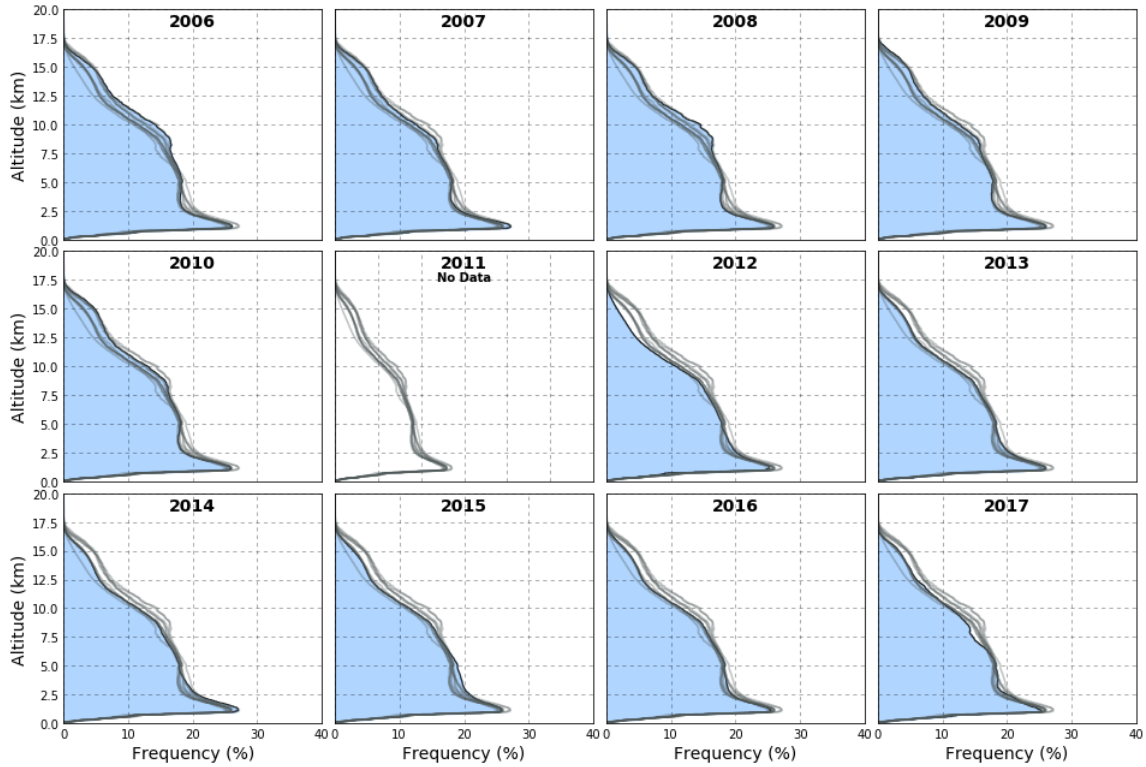

Figure A.2: Geophysical variability of 2BCL5 cloud occurrence between 2006 and 2017 for the month of September. The target year is indicated by the filled blue curve with the grey lines representing the profiles from the other sub-figures.

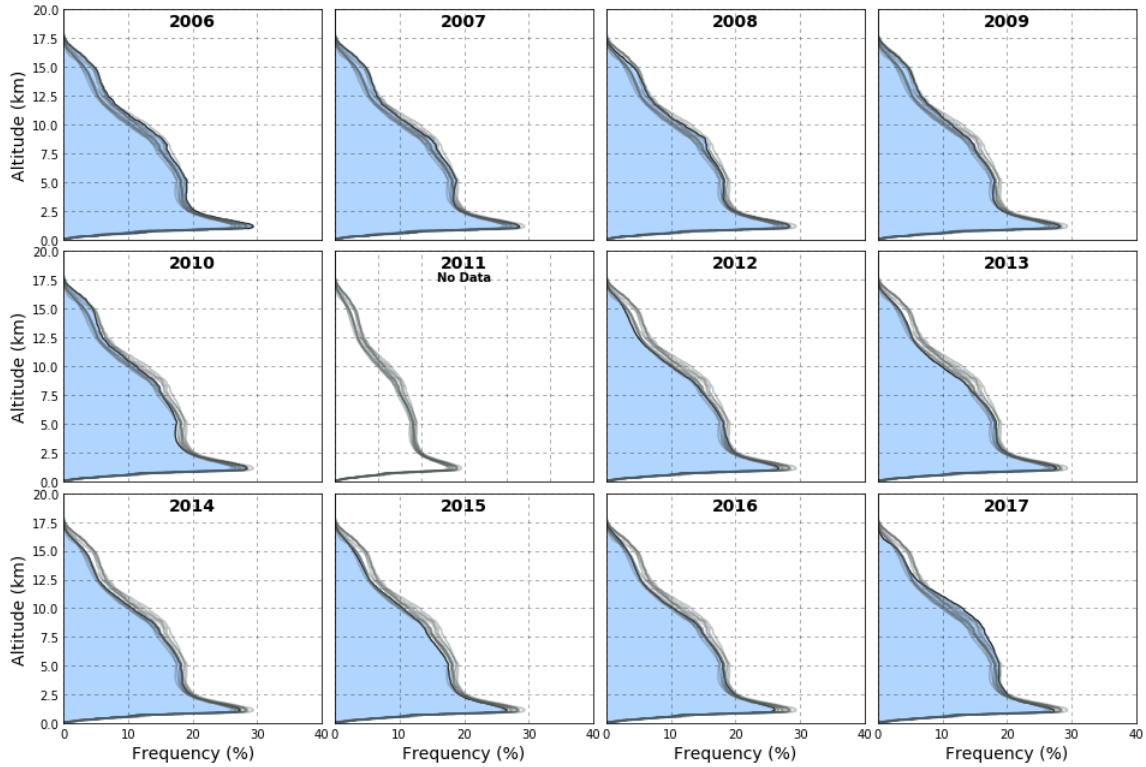

Figure A.3: Geophysical variability of 2BCL5 cloud occurrence between 2006 and 2017 for the month of October. The target year is indicated by the filled blue curve with the grey lines representing the profiles from the other sub-figures.

Appendix B

Seasonal and latitudinal variations of 2BCL5 cloud occurrence

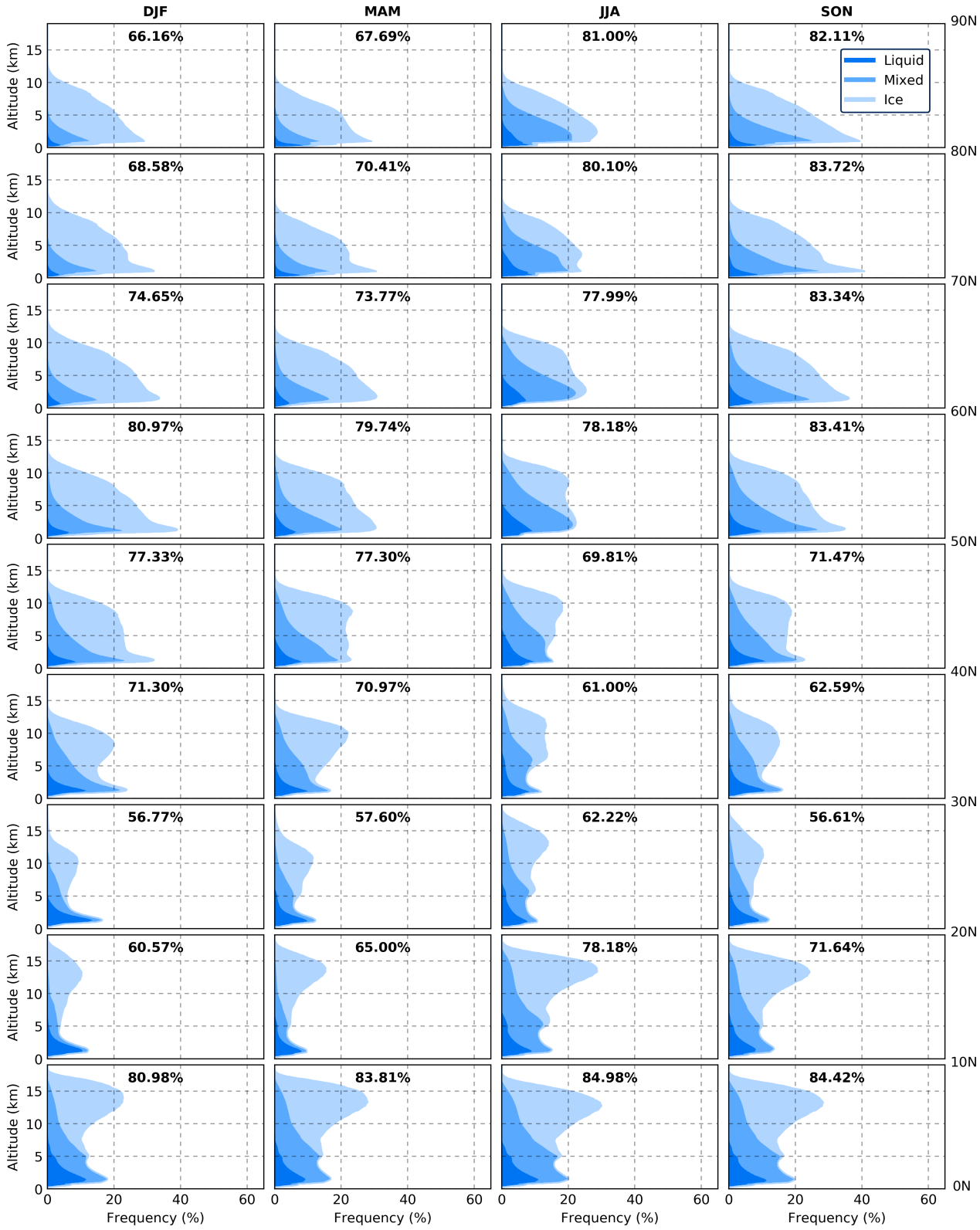

Figure B.1: Profiles of cloud occurrence for different cloud phase derived form 2BCL5 data over different latitudes and seasons for the Northern Hemisphere. The cloud occurrences for liquid, mixed and ice phase cloud are given by the filled blue lines, as indicated by the legend. The cloud fraction is annotated at the top of each sub-figure.

Figure B.2: Profiles of cloud occurrence for different cloud phase derived form 2BCL5 data over different latitudes and seasons for the Southern Hemisphere. The cloud occurrences for liquid, mixed and ice phase cloud are given by the filled blue lines, as indicated by the legend. The cloud fraction is annotated at the top of each sub-figure.

Appendix C

2BCL5 latitudinal cloud occurrence during 2016

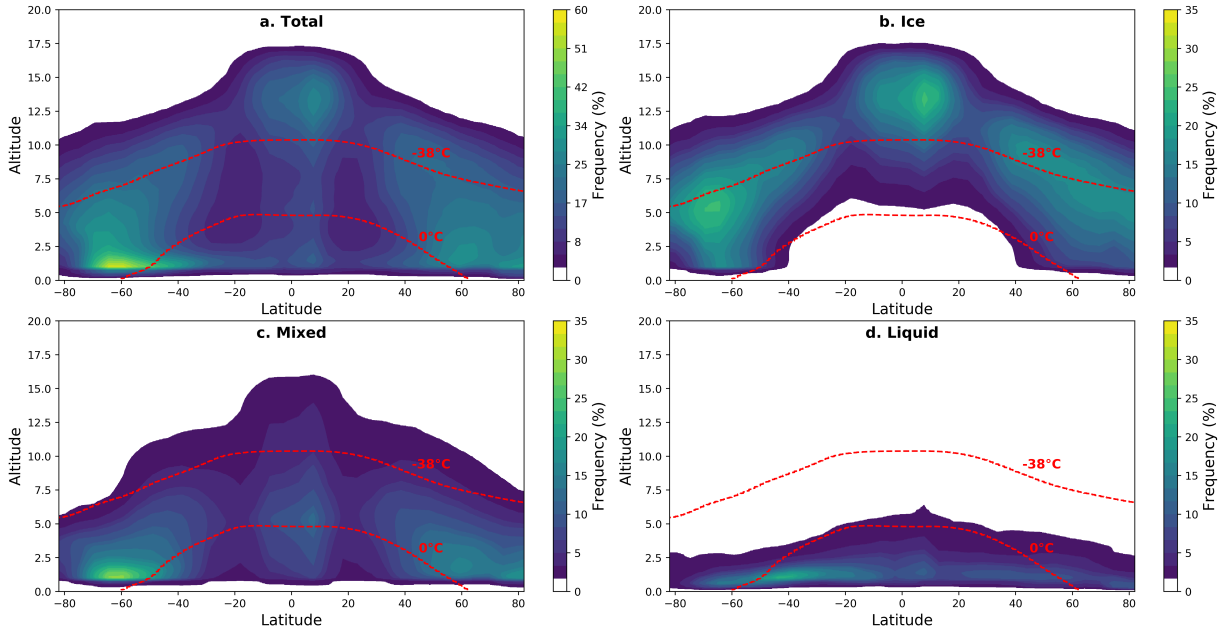

Figure C.1: Latitudinal distribution of cloud occurrence as a function of altitude for the total cloud (a.) as well as the ice (b.), mixed (c.) and liquid (d.) phase clouds for 2BCL5 observations during 2016. The red dashed lines indicate isotherms of constant temperature.

Appendix D

AWARE cloud occurrence

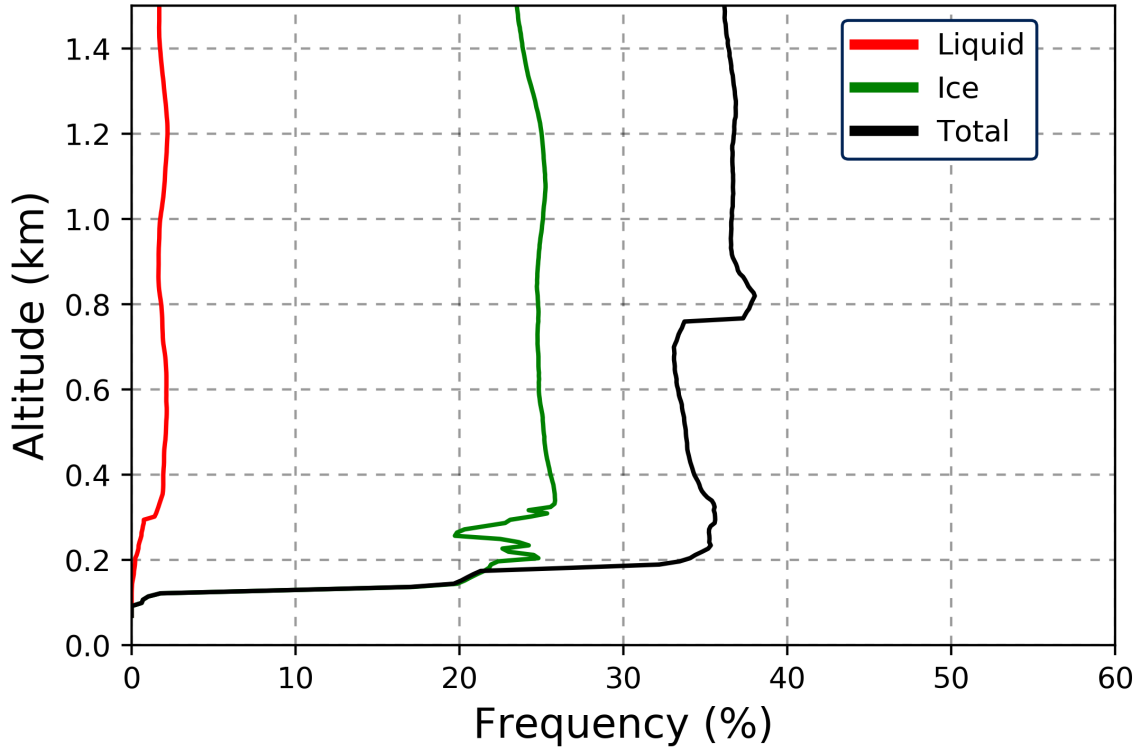

Figure D.1: Cloud occurrence for 2016 AWARE data as in Figure 4.6, but for all AWARE observations unfiltered by the 2BCL5/DARDAR passes over McMurdo. Cloud occurrence has been restricted to altitudes below 1.5 km

Appendix E

2BCL5, DARDAR and AWARE cloud occurrences

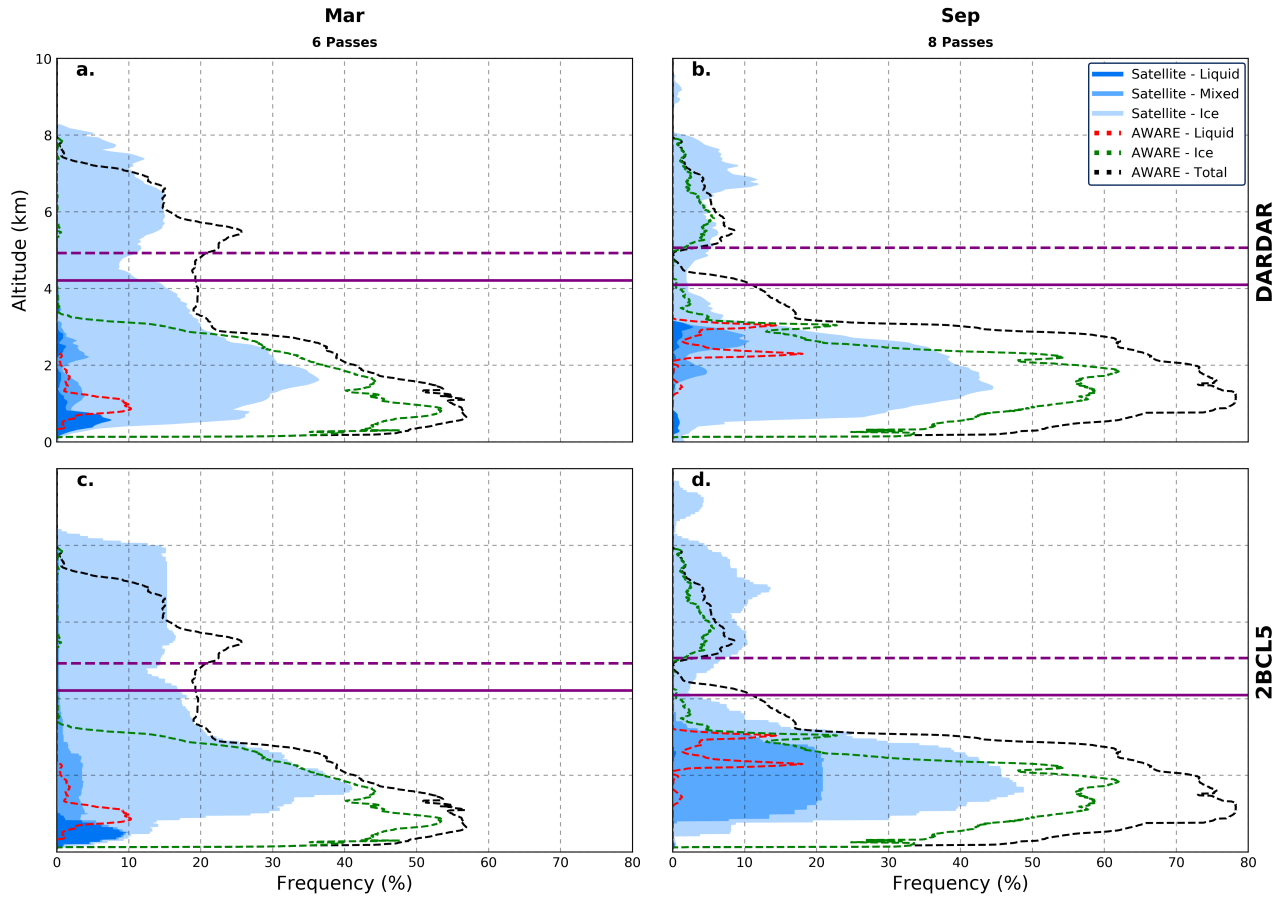

Figure E.1: Mean vertical profiles of cloud occurrence for different cloud phases derived from observations over McMurdo Station during March and September 2016. The dashed lines represent the AWARE cloud occurrence and the filled curves represent DARDAR (a - d) and 2BCL5 (e - h) cloud occurrences. Each month as well as the number of passes are annotated at the top of the figure. The purple lines represents the mean (solid) and maximum (dashed) altitudes of the -38 °C isotherm, the edge of the homogeneous freezing regime.

Appendix F

2BCL5 interannual variability

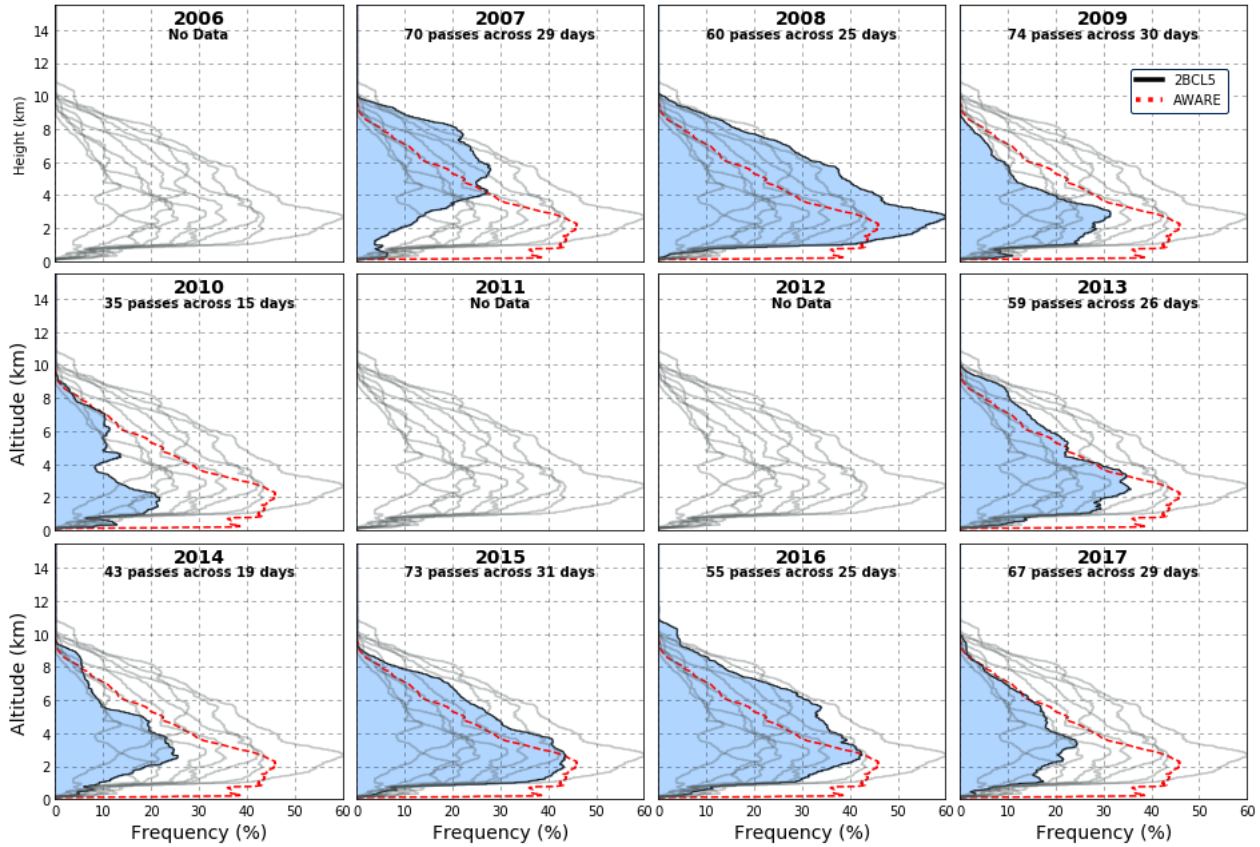

Figure F.1: Geophysical variability of the 2BCL5 cloud occurrence over McMurdo Station, between 2006 and 2017 for the month of January.

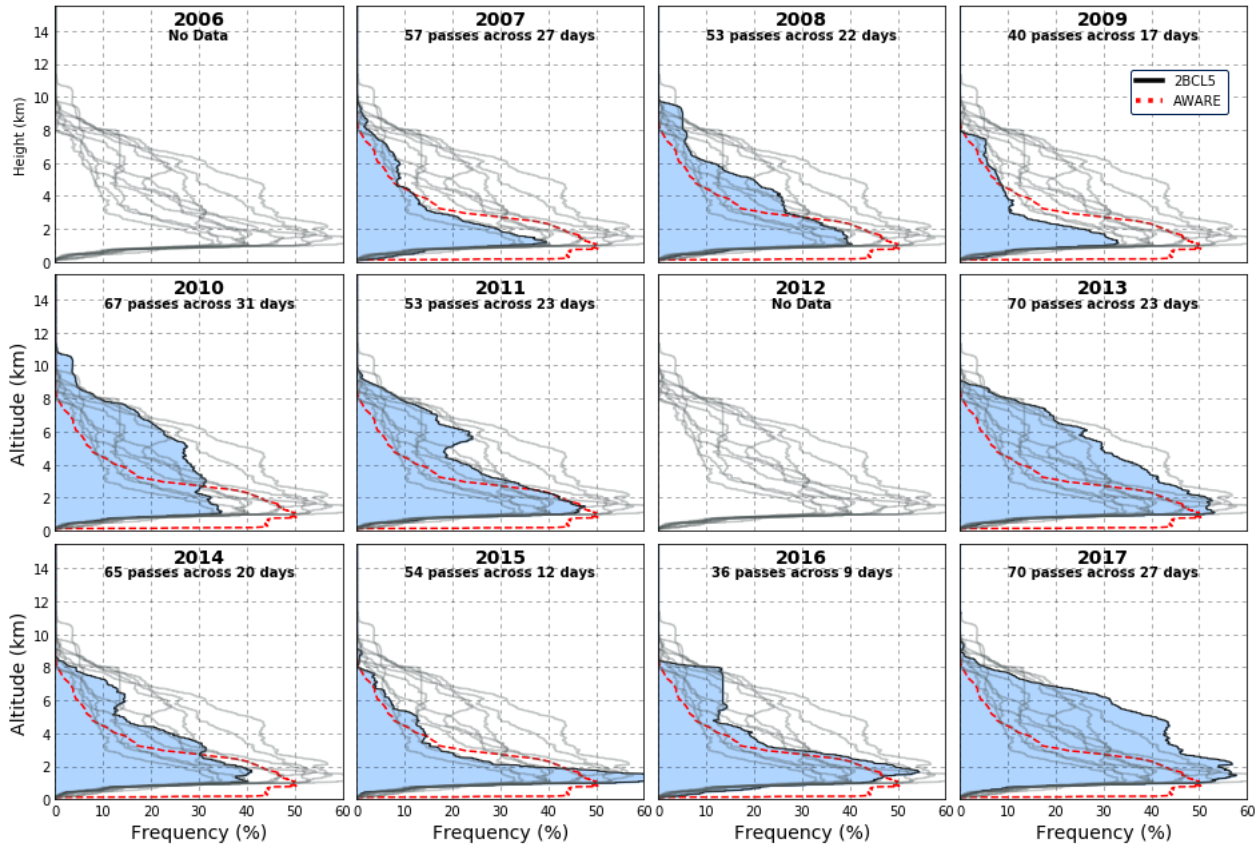

Figure F.2: Geophysical variability of the 2BCL5 cloud occurrence over McMurdo Station between 2006 and 2017 for the month of March.

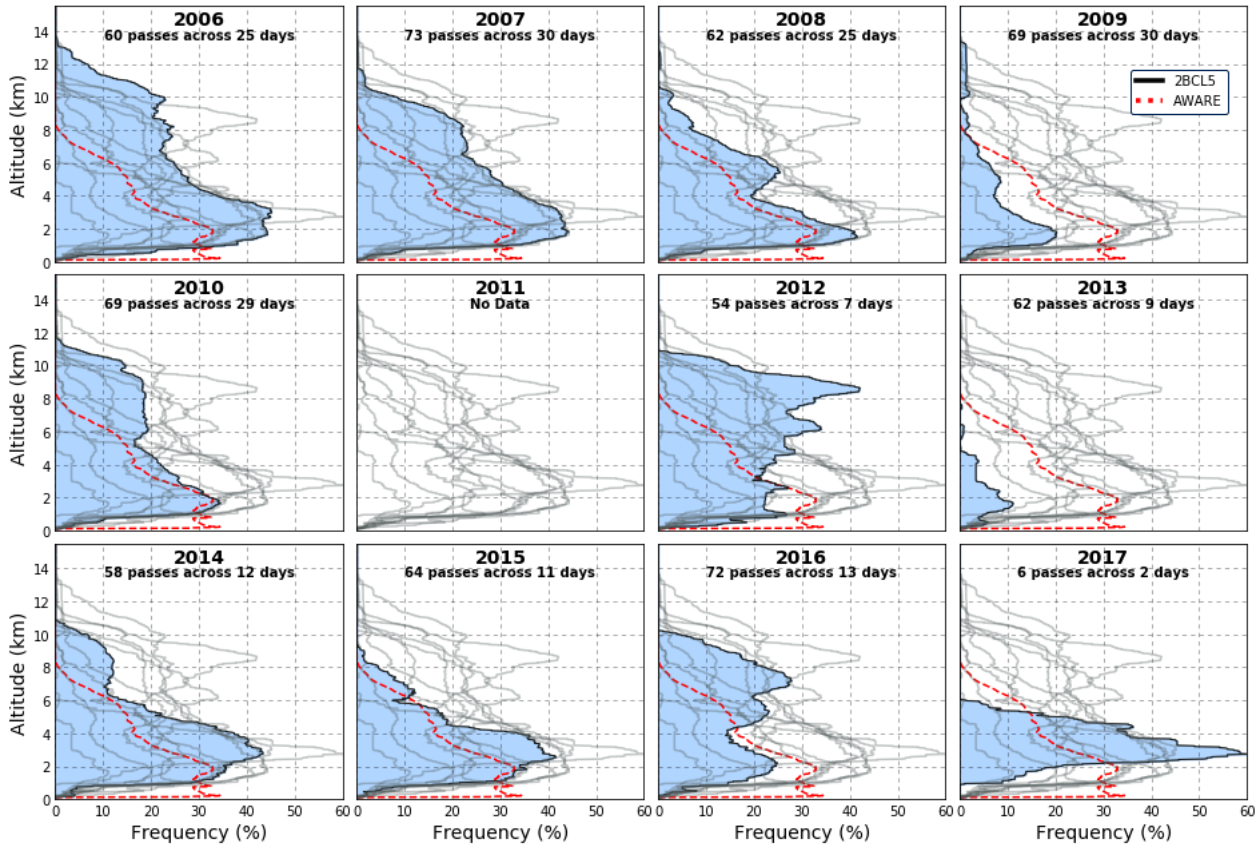

Figure F.3: Geophysical variability of the 2BCL5 cloud occurrence over McMurdo Station between 2006 and 2017 for the month of September.

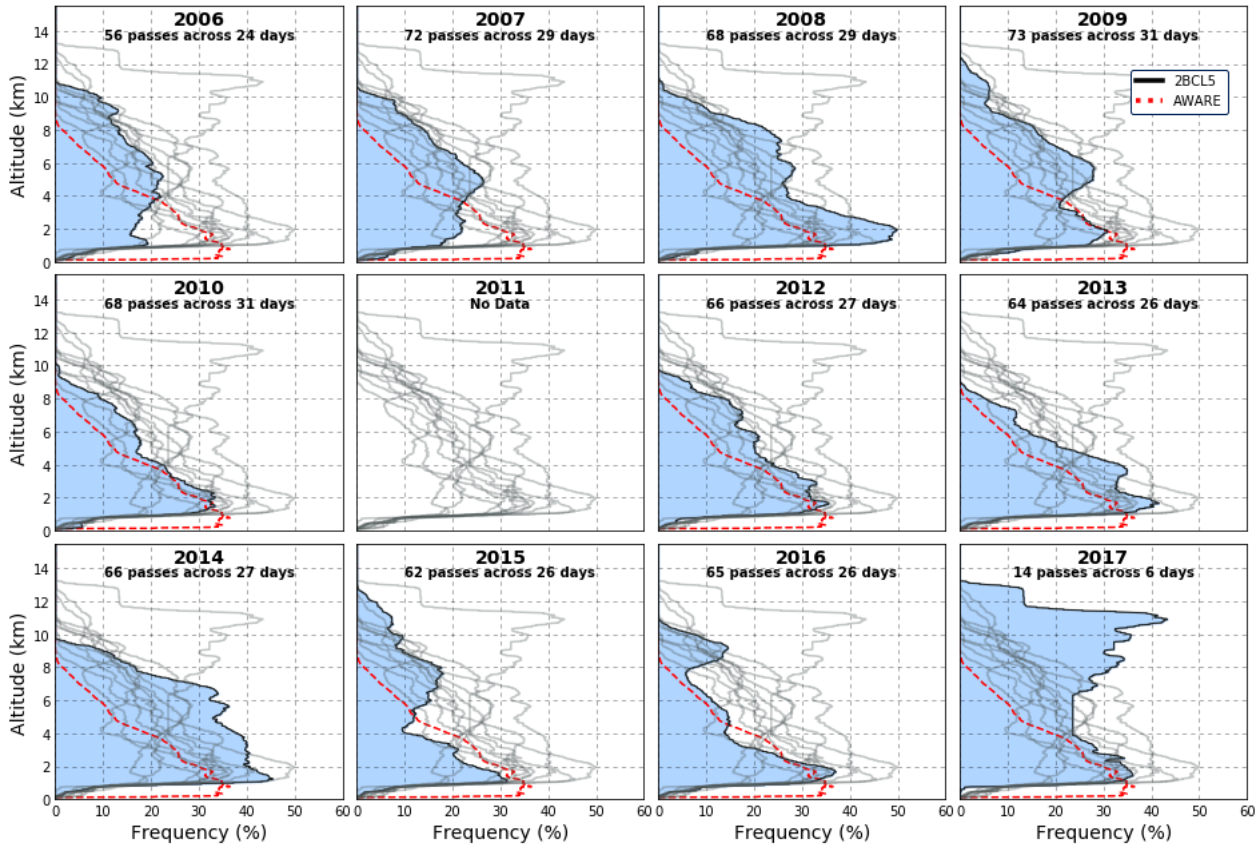

Figure F.4: Geophysical variability of the 2BCL5 cloud occurrence over McMurdo Station between 2006 and 2017 for the month of October.

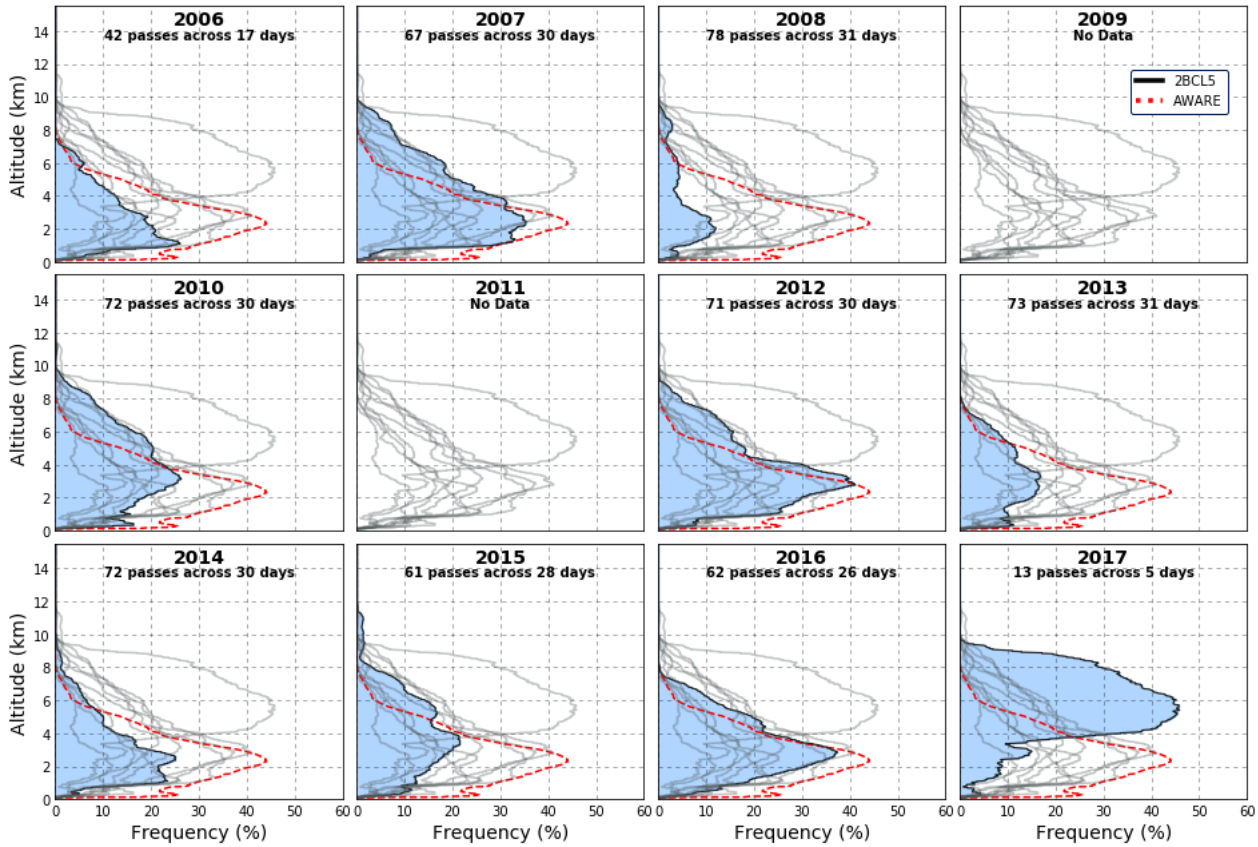

Figure F.5: Geophysical variability of the 2BCL5 cloud occurrence over McMurdo Station between 2006 and 2017 for the month of December.

References

Alexander, S. P., & Protat., A. (2018). Cloud properties observed from the surface and by satellite at the northern edge of the southern ocean. *Journal of Geophysical Research: Atmospheres*, *123*(1), 443-456. doi: 10.1002/2017jd026552

Alexandrov, M., Cairns, B., van Diedenhoven, B., Ackerman, A., Wasilewski, A., McGill, M., ... Arnold, G. T. (2016). Polarized view of supercooled liquid water clouds. *Remote Sensing of Environment*, *181*, 96-110. doi: 10.1016/j.rse.2016.04.002

Andrews, T., Gregory, J. M., Webb, M. J., & Taylor, K. E. (2012). Forcing, feedbacks and climate sensitivity in cmip5 coupled atmosphere-ocean climate models. *Geophysical Research Letters*, *39*(9). doi: 10.1029/2012gl051607

Barry, R. G., & Carleton, M., A. (2001). *Synoptic and dynamic climatology.* Routledge.

Bender, F. A., Ramanathan, V., & Tselioudis, G. (2011). Changes in extratropical storm track cloudiness 1983–2008: Observational support for a poleward shift. *Climate Dynamics*, *38*(9-10), 2037-2053. doi: 10.1007/s00382-011-1065-6

Bigg, G. R., Jickells, T. D., Liss, P. S., & Osborn, T. J. (2003). The role of the oceans in climate. *International Journal of Climatology*, *23*(10), 1127-1159. doi: 10.1002/joc.926

Blanchard, Y., Pelon, J., Eloranta, E. W., Moran, K. P., Delanoë, J., & Sèze, G. (2014). A synergistic analysis of cloud cover and vertical distribution from a-train and ground-based sensors over the high arctic station eureka from 2006 to 2010. *Journal of Applied Meteorology and Climatology*, *53*(11), 2553-2570. doi: 10.1175/jamc-d-14-0021.1

Bodas-Salcedo, A., Hill, P., Furtato, K., Williams, K., Field, P., Manners, J., & Hyder, P. (2016). Large contribution of supercooled liquid clouds to the solar radiation budget of the southern ocean. *Journal of Climate*, *29*(11), 4213-4228. doi: 10.1175/jcli-d-15-0564.1

Bodas-Salcedo, A., Webb, M. J., Bony, S., Chepfer, H., Dufresne, J., Klein, S. A., ... John, V. O. (2011). Cosp: Satellite simulation software for model assessment. *Bulletin of the American Meteorological Society*, *92*(8), 1023-1043. doi: 10.1175/2011bams2856.1

Bodas-Salcedo, A., Williams, K., Field, P., & Lock, A. (2012). The surface downwelling solar radiation surplus over the southern ocean in the met office model: The role of midlatitude cyclone clouds. *Journal of Climate*, *25*, 7467–7486. doi: 10.1175/jcli-d-11-00702.1

Bodas-Salcedo, A., Williams, K. D., Ringer, M. A., Beau, I., Cole, J. N. S., Dufresne, J. L., ... Yokohata, T. (2014). Origins of the solar radiation biases over the southern ocean in cfmip2 models. *Journal of Climate*, *27*, 41-56. doi: 10.1175/JCLI-D-13-00169.1

Bony, S., B., S., D., F., C., J., M., K., R., P., ... M., W. (2015). Clouds, circulation and climate sensitivity. *Nature Geoscience*, *8*(4), 261-268. doi: 10.1038/ngeo2398

Boucher, O., Randall, D., Artaxo, P., Bretherton, C., Feingold, G., Forster, P., ... X., Z. (2013). Clouds and aerosols", in: Climate change 2013: the physical science basis. contribution of working group i to the fifth assessment report of the intergovernmental panel on climate change. *Cambridge University Press, Cambridge, United Kingdom and New York, NY, USA.*.

Bretherton, C. S. (2015). Insights into low-latitude cloud feedbacks from high-resolution models. *Philosophical Transactions of the Royal Society A: Mathematical, Physical and Engineering Sciences*, *373*(2054). doi: 10.1098/rsta.2014.0415

C3S. (2017). *Era5: Fifth generation of ecmwf atmospheric reanalyses of the global climate.* Retrieved from `https://cds.climate.copernicus.eu/cdsapp#!/home`

Ceccaldi, M., Delanoë, J., Hogan, R. J., Pounder, N. L., Protat, A., & Pelon, J. (2013). From cloudsat-calipso to earthcare: Evolution of the dardar cloud classification and its comparison to airborne radar-lidar observations. *Journal of Geophysical Research: Atmospheres*, *118*(14), 7962-7981. doi: 10.1002/jgrd.50579

Ceppi, P., Hwang, Y.-T., Frierson, D. M., & Hartmann, D. L. (2012). Southern hemisphere jet latitude biases in cmip5 models linked to shortwave cloud forcing. *Geophysical Research Letters*, *39*(19). doi: 10.1029/2012GL053115

Cess, R. D. (1990). General circulation model intercomparisons for understanding climate. long-term monitoring of the earth's radiation budget. *Journal of Geophysical Research - Atmospheres*, *95*(D10), 16601-16615. doi: 10.1117/12.21359

Chen, G., & Held, I. M. (2007). Phase speed spectra and the recent poleward shift of southern hemisphere surface westerlies. *Geophysical Research Letters*, *34*(21). doi: 10.1029/2007gl031200

Chepfer, H., Brogniez, H., & Noel, V. (2019). Diurnal variations of cloud and relative humidity profiles across the tropics. *Scientific Reports*, *9*(1). doi: 10.1038/s41598-019-52437-6

Chubb, T. H., Jensen, J. B., Siems, S. T., & Manton, M. J. (2013). In situ observations of supercooled liquid clouds over the southern ocean during the hiaper pole-to-pole observation campaigns. *Geophysical Research Letters*, *40*(19), 5280-5285. doi: 10.1002/grl.50986

Coggins, J., A., M., & Jolly, B. (2014). Synoptic climatology of the ross ice shelf and ross sea region of antarctica: k-means clustering and validation. *nternational Journal of Climatology*, *34*(7), 2330-2348. doi: 10.1002/joc.3842

Cook, K. (2013). *Climate dynamics.* Princeton University.

Dai, A., Giorgi, F., & Trenberth, K. E. (1999). Observed and model-simulated diurnal cycles of precipitation over the contiguous united states. *Journal of Geophysical Research: Atmospheres*, *104*(D6), 6377-6402. doi: 10.1029/98jd02720

Delanoë, J., & Hogan, R. J. (2010). Combined cloudsat-calipso-modis retrievals of the properties of ice clouds. *Journal of Geophysical Research*, *115*. doi: 10.1029/2009jd012346

Dessler, A. E., & Wong, S. (2009). Estimates of the water vapor climate feedback during el niño–southern oscillation. *Journal of Climate*, *22*(23), 6404-6412. doi: 10.1175/2009jcli3052.1

Donohoe, A., & Battisti, D. (2013). The seasonal cycle of atmospheric heating and temperature. *Journal of Climate*, *26*(14), 4962-4980. doi: 10.1175/JCLI-D-12-00713.1

Eastman, R., Warren, S. G., & Hahn, C. J. (2011). Variations in cloud cover and cloud types over the ocean from surface observations, 1954–2008. *Journal of Climate*, *24*(22), 5914-5934. doi: 10.1175/2011jcli3972.1

ECMWF. (2019). *Era5: data documentation.* Retrieved from `https://confluence.ecmwf.int/display/CKB/ERA5%3A+data+documentation`

Fallmann, J., Lewis, H., Castillo, J. M., Arnold, A., & Ramsdale, S. (2017). Impact of sea surface temperature on stratiform cloud formation over the north sea. *Geophysical Research Letters.*, *44*(9), 4296-4303. doi: 10.1002/2017gl073105

Fedorov, V. (2008). Ocean-atmosphere coupling, in the oxford companion to global change. *Oxford University Press, Oxford.*, 369-374.

Flato, G., Marotzke, J., Abiodun, B., Braconnot, P., Chou, C. W., S., Cox, P., ... Rummukainen, M. (2013). "evaluation of climate models", in: Climate change 2013: The physical science basis. contribution of working group i to the fifth assessment report of the intergovernmental panel on climate change. *Cambridge University Press*, 741-866.

Gettelman, A., & Sherwood, S. C. (2016). Processes responsible for cloud feedback. *Current Climate Change Reports*, *2*(4), 179-189. doi: 10.1007/s40641-016-0052-8

Grise, K. M., & Polvani, L. M. (2016). Is climate sensitivity related to dynamical sensitivity? *Journal of Geophysical Research: Atmospheres*, *121*(10), 5159-5176. doi: 10.1002/2015jd024687

Gruber, N., Landschützer, P., & Lovenduski, N. S. (2019). The variable southern ocean carbon sink. *Annual Review of Marine Science*, *11*(1), 159-186. doi: 10.1146/annurev-marine-121916-063407

Haynes, J. M., Jakob, C., Rossow, W. B., Tselioudis, G., & Brown, J. (2011). Major

characteristics of southern ocean cloud regimes and their effects on the energy budget. *Journal of Climate*, *24*(19), 5061-5080. doi: 10.1175/2011jcli4052.1

Heavens, N. G., Ward, D. S., & Natalie, M. M. (2013). Studying and projecting climate change with earth system models. *Nature Education Knowledge*, *4*(5).

Hersbach, H., & Dee, D. (2016). *Era5 reanalysis is in production, ecmwf newsletter* (Vol. 147). Retrieved from `https://www.ecmwf.int/en/newsletter/147/news/era5-reanalysis-production`

Hoffmann, L., Günther, G., Li, D., Stein, O., Wu, X., Griessbach, S., ... Wright, J. S. (2019). From era-interim to era5: the considerable impact of ecmwf's next-generation reanalysis on lagrangian transport simulations. *Atmospheric Chemistry and Physics*, *19*, 3097-3124. doi: doi.org/10.5194/acp-19-3097-2019.

Hogan, R., Behera, M. D., O'connor, E. J., & Illingworth, A. J. (2004). Estimate of the global distribution of stratiform supercooled liquid water clouds using the lite lidar. *Geophysical Research Letters*, *31*(5). doi: 10.1029/2003gl018977

Hogan, R., Illingworth, A. J., O'connor, E. J., & Poiares-Baptista, J. P. (2003). Characteristics of mixed-phase clouds. ii: A climatology from ground-based lidar. *Quarterly Journal of the Royal Meteorological Society*, *129*(592), 2117-2134. doi: 10.1256/qj.01.209

Holton, J. R. (2004). *An introduction to dynamic meteorology, 4th edition.* Academic Press.

Hu, Y., Winker, D., Vaughan, M., Lin, B., Omar, A., Trepte, C., & Flittner, D. (2009). Calipso/caliop cloud phase discrimination algorithm. *Journal of Atmospheric and Oceanic Technology*, *26*(11), 2293-2309. doi: 10.1175/2009jtecha1280.1

Hwang, Y., & Frierson, D. (2013). Link between the double-intertropical convergence zone problem and cloud biases over the southern ocean. *Proceedings of the National Academy of Sciences*, *110*(13), 4935-4940. doi: 10.1073/pnas.1213302110

Hyder, P., Edwards, J., Allan, R., Hewitt, H., Bracegirdle, T., Gregory, J., ... Belcher, E. (2018). Critical southern ocean climate model biases traced to atmospheric model cloud errors. *Nature Communications*, *9*(1), 3625. doi: 10.1038/s41467-018-05634-2

Ingram, W. (2012). Some implications of a new approach to the water vapour feedback. *limate Dynamics*, *40*(3-4), 925-933. doi: 10.1007/s00382-012-1456-3

IPCC, . (2001). Climate change 2001: The scientific basis. contribution of working group i to the third assessment report of the intergovernmental panel on climate change [houghton, j.t., y. ding, d.j. griggs, m. noguer, p.j. van der linden, x. dai, k. maskell, and c.a. johnson (eds.)]. *Cambridge University Press, Cambridge, United Kingdom and New York, NY, USA.*.

Jolly, B., Kuma, P., Mcdonald, A., & Parsons, S. (2018). An analysis of the cloud environ-

ment over the ross sea and ross ice shelf using cloudsat/calipso satellite observations: The importance of synoptic forcing. *Atmospheric Chemistry and Physics*, *18*(13), 9723-9739. doi: 10.5194/acp-18-9723-2018

Kay, J., Hillman, B., Klein, S., Zhang, Y., Medeiros, B., Pincus, R., ... T., A. (2012). Exposing global cloud biases in the community atmosphere model (cam) using satellite observations and their corresponding instrument simulators. *Journal of Climate*, *25*(15), 5190-5207. doi: 10.1175/jcli-d-11-00469.1

Kay, J., Wall, C., Yettella, V., Medeiros, B., Hannay, C., Caldwell, P., & Bitz, C. (2016). Global climate impacts of fixing the southern ocean shortwave radiation bias in the community earth system model (cesm). *Journal of Climate*, *29*(12), 4617-4636. doi: 10.1175/jcli-d-15-0358.1

Kiehl, J., & Trenberth, K. (1997). Earth's annual global mean energy budget. *Bulletin of the American Meteorological Society*, *78*, 197-208. doi: 10.1175/1520-0477(1997)078⟨0197:EAGMEB⟩2.0.CO;2

Klekociuk, A. R., French, W. J., Alexander, S. P., Kuma, P., & Mcdonald, A. J. (2019). The state of the atmosphere in the 2016 southern kerguelen axis campaign region. deep sea research part ii: Topical studies in oceanography. *Elsevier*. doi: 10.1016/j.dsr2.2019.02.001

Korolev, A., McFarquhar, G., Field, P. R., Franklin, C., Lawson, P., Wang, Z., ... Wendisch, M. (2017). Mixed-phase clouds: Progress and challenges. *Meteorological Monographs*, *58*. doi: 10.1175/amsmonographs-d-17-0001.1

Kuma, P., McDonald, A., Morgenstern, O., Alexander, S., Cassano, J., Garrett, A., ... Williams, J. (2019). Evaluation of southern ocean cloud in the hadgem3 general circulation model and merra-2 reanalysis using ship-based observations. *In review, Atmospheric Chemistry and Physics Discussions*. doi: 10.5194/acp-2019-201

Lamb, D., & Verlinde, J. (2011). *Physics and chemistry of clouds.* New York: Cambridge University Press.

Leahy, S. M., Kingsford, M. J., & Steinberg, C. R. (2013). Do clouds save the great barrier reef? satellite imagery elucidates the cloud-sst relationship at the local scale. *PLoS ONE*, *8*(7). doi: 10.1371/journal.pone.0070400

Listowski, C., Delanoë, J., Kirchgaessner, A., Lachlan-Cope, T., & King, J. (2018). Antarctic clouds, supercooled liquid water and mixed-phase investigated with dardar: Geographical and seasonal variations. *In review, Atmospheric Chemistry and Physics Discussions*. doi: 10.1371/journal.pone.0070400

Liu, Y., Shupe, M. D., Wang, Z., & Mace, G. (2017). Cloud vertical distribution from combined surface and space radar–lidar observations at two arctic atmospheric ob-

servatories. *Atmospheric Chemistry and Physics*, *17*(9), 5973-5989. doi: 10.5194/acp-17-5973-2017

Liu, Z. (2009). The calipso lidar cloud and aerosol discrimination: Version 2 algorithm and initial assessment of performance. *Journal of Atmospheric and Oceanic Technology*, *26*(7), 1198-1213. doi: 10.1175/2009jtecha1229.1

Lubin, D., Bromwich, D. H., Russell, L. M., Verlinde, J., & Vogelmann, A. M. (2015). Arm west antarctic radiation experiment (aware) science plan. *U.S. DOE, Office of Science, Office of Biological and Environmental Research.*

Mace, G., Zhang, Q., Vaughan, M., Marchand, R., Stephens, G., Trepte, C., & Winker, D. (2009). A description of hydrometeor layer occurrence statistics derived from the first year of merged cloudsat and calipso data. *Journal of Geophysical Research*, *114*. doi: 10.1029/2007jd009755

Marchand, R., Mace, G., Ackerman, T., & G., S. (2008). Hydrometeor detection using cloudsat—an earth-orbiting 94-ghz cloud radar. *Journal of Atmospheric and Oceanic Technology*, *25*, 519-533. doi: 10.1175/2007JTECHA1006.1

Marshall, J., & Plumb, R. A. (2008). *Atmosphere, ocean and climate dynamics: An introductory text.* Elsevier.

Mason, S., Fletcher, J. K., Haynes, J. M., Franklin, C., Protat, A., & Jakob, C. (2015). A hybrid cloud regime methodology used to evaluate southern ocean cloud and shortwave radiation errors. *Journal of Climate*, *28*, 6001-6018. doi: 10.1175/JCLI-D-14-00846.1

Matus, A. V., & L'ecuyer, T. S. (2017). The role of cloud phase in earth's radiation budget. *Journal of Geophysical Research: Atmospheres*, *122*(5), 2559-2578. doi: 10.1002/2016jd025951

McCoy, D., Hartmann, D., & Grosvenor, D. (2014). Observed southern ocean cloud properties and shortwave reflection. part i: Calculation of sw flux from observed cloud properties. *Journal of Climate*, *27*(23), 8836-8857. doi: 10.1175/jcli-d-14-00287.1

McCoy, D., Hartmann, D. L., Zelinka, M. D., Ceppi, P., & Grosvenor, D. P. (2015). "mixed-phase cloud physics and southern ocean cloud feedback in climate models. *Journal of Geophysical Research: Atmospheres*, *120*(18), 9539-9554. doi: 10.1002/2015jd023603

McGuffie, K., & Henderson-Sellers, A. (2014). *Climate modelling primer.* Wiley.

MetOffice. (2019). *Hadgem3 family: Met office climate prediction model.* Retrieved from `https://www.metoffice.gov.uk/research/approach/modelling-systems/unified-model/climate-models/hadgem3`

Mioche, G., Jourdan, O., Ceccaldi, M., & Delanoë, J. (2015). Variability of mixed-phase clouds in the arctic with a focus on the svalbard region: A study based on spaceborne

active remote sensing. *Atmospheric Chemistry and Physics*, *15*(5), 2445-2461. doi: 10.5194/acp-15-2445-2015

Morrison, A. E., Siems, S. T., & Manton, M. J. (2011). A three-year climatology of cloud-top phase over the southern ocean and north pacific. *Journal of Climate*, *24*(9), 2405-2418. doi: 10.1175/2010jcli3842.1

Myhre, G., Myhre, C. E., Samset, B. H., & Storelvmo, T. (2013a). Aerosols and their relation to global climate and climate sensitivity. *Nature Education Knowledge*, *4*(5).

Myhre, G., Shindell, D., Bréon, F., Collins, W., Fuglestvedt, J., Huang, J., ... Zhang, H. (2013b). Anthropogenic and natural radiative forcing", in: Climate change 2013: The physical science basis. contribution of working group i to the fifth assessment report of the intergovernmental panel on climate change. *Cambridge University Press*, 659-740.

Mülmenstädt, J., Sourdeval, O., Delanoë, J., & Quaas, J. (2015). Frequency of occurrence of rain from liquid-, mixed-, and ice-phase clouds derived from a-train satellite retrievals. *Geophysical Research Letters*, *42*(15), 6502-6509. doi: 10.1002/2015gl064604

NASA. (2013). *Earth's vital signs.* Retrieved from `https://www.nasa.gov/multimedia/imagegallery/image_feature_2495.html`

Nayak, M. (2012). Cloudsat anomaly recovery and operational lessons learned. *SpaceOps 2012 Conference*. doi: 10.2514/6.2012-1295798.

Noel, V., Chepfer, H., Chiriaco, M., & Yorks, J. (2018). The diurnal cycle of cloud profiles over land and ocean between 51 °s and 51 °n, seen by the cats spaceborne lidar from the international space station. *Atmospheric Chemistry and Physics*, *18*(13), 9457-9473. doi: 10.5194/acp-18-9457-2018

Norris, J. R., Allen, R. J., Evan, A. T., Zelinka, M. D., O'Dell, C. W., & Klein, S. A. (2016). Evidence for climate change in the satellite cloud record. *Nature*, *536*(7614), 72-75. doi: 10.1038/nature18273

Pidwirny, M. (2006). *Global heat balance: Introduction to heat fluxes". fundamentals of physical geography, 2nd edition.* Retrieved from `http://www.physicalgeography.net/fundamentals/7j.html`

Protat, A., Young, S. A., Mcfarlane, S. A., L'Ecuyer, T., Mace, G. G., Comstock, J. M., ... Delanoë, J. (2014). Reconciling ground-based and space-based estimates of the frequency of occurrence and radiative effect of clouds around darwin, australia. *Journal of Applied Meteorology and Climatology*, *53*(2), 456-478. doi: 10.1175/jamc-d-13-072.1

Qu, X., Hall, A., Klein, S. A., & Deangelis, A. M. (2015). Positive tropical marine low-cloud cover feedback inferred from cloud-controlling factors. *Geophysical Research Letters*, *42*(18), 7767-7775. doi: 10.1002/2015gl065627

Quante, M. (2004). The role of clouds in the climate system. *Journal De Physique IV (Proceedings)*, *121*, 61-86. doi: doi:10.1051/jp4:2004121003

Rosenfeld, D., & Woodley, W. L. (2000). Deep convective clouds with sustained supercooled liquid water down to -37.5 °c. *Nature*, *405*(6785), 440-442. doi: 10.1038/35013030

Sassen, K. (1991). The polarization lidar technique for cloud research: A review and current assessment. *Bulletin of the American Meteorological Society*, *72*(12), 1848-1866. doi: 10.1175/1520-0477(1991)0722.0.co;2

Sassen, K., & Khvorostyanov, V. (1998). Radar probing of cirrus and contrails: Insights from 2d model simulations. *Geophysical Research Letters*, *25*(7), 975-978. doi: 10.1029/98gl00731

Sassen, K., Wang, Z., & Liu, D. (2008). Global distribution of cirrus clouds from cloudsat/cloud-aerosol lidar and infrared pathfinder satellite observations (calipso) measurements. *Journal of Geophysical Research*, *113*. doi: doi:10.1029/2008jd009972

Schneider, T., Teixeira, J., Bretherton, C. S., Brient, F., Pressel, K. G., Schär, C., & Siebesma, A. P. (2017). Climate goals and computing the future of clouds. *Nature Climate Change*, *7*(1), 3-5. doi: doi:10.1038/nclimate3190

Schuddeboom, A., McDonald, A. J., Morgenstern, O., Harvey, M., & Parsons, S. (2018). Regional regime-based evaluation of present-day general circulation model cloud simulations using self-organizing maps. *Journal of Geophysical Research: Atmospheres*, *123*(8), 4259-4272. doi: 10.1002/2017jd028196

Schuddeboom, A., Varma, V., McDonald, A. J., Morgenstern, O., Harvey, M., Parsons, S., ... Furtado, K. (2019). Cluster-based evaluation of model compensating errors: A case study of cloud radiative effect in the southern ocean. *Geophysical Research Letters*, *46*(6), 3446-3453. doi: 10.1029/2018gl081686

Scott, R., & Lubin, D. (2014). Mixed-phase cloud radiative properties over ross island, antarctica: The influence of various synoptic-scale atmospheric circulation regimes. *Journal of Geophysical Research: Atmospheres*, *119*(11), 6702-6723. doi: doi:10.1002/2013jd021132

Shang, H., Letu, H., Nakajima, T. Y., Wang, Z., Ma, R., Wang, T., ... Shi, J. (2018). Diurnal cycle and seasonal variation of cloud cover over the tibetan plateau as determined from himawari-8 new-generation geostationary satellite data. *Scientific Reports*, *8*(1). doi: 10.1038/s41598-018-19431-w

Silber, I., Verlinde, J., Eloranta, E. W., & Cadeddu, M. (2018). Antarctic cloud macrophysical, thermodynamic phase, and atmospheric inversion coupling properties at mcmurdo station: I. principal data processing and climatology. *Journal of Geophysical Research: Atmospheres*, *123*(11), 6099-6121. doi: 10.1029/2018jd028279

Smith, R. (1986). *Cloud forms.* NZ Meteorological Service.

Soden, B. (2000). The diurnal cycle of convection, clouds, and water vapor in the tropical upper troposphere. *Geophysical Research Letters*, *27*(15), 2173-2176. doi: 10.1029/2000gl011436

Stephens, G., Vane, D., Boain, R., Mace, G., Sassen, ., K, Wang, Z., ... Mitrescu, C. (2002). The cloudsat mission and the a-train: A new dimension of space-based observations of clouds and precipitation. *Bulletin of the American Meteorological Society*, *83*(12), 1771-1790. doi: 10.1175/bams-83-12-1771

Stephens, G., Vane, D. G., Tanelli, S., Im, E., Durden, S., Rokey, M., ... Marchand, R. (2008). Cloudsat mission: Performance and early science after the first year of operation. *Journal of Geophysical Research: Atmospheres*, *113*. doi: 10.1029/2008jd009982

Stubenrauch, C. J., Chédin, A., Rädel, G., Scott, N. A., & Serrar, S. (2006). Cloud properties and their seasonal and diurnal variability from tovs path-b. *Journal of Climate*, *19*(21), 5531-5553. doi: 10.1175/jcli3929.1

Tanelli, S., Durden, S. L., Im, E., Pak, K. S., Reinke, D. G., Partain, P., ... Marchand, R. T. (2008). Cloudsat's cloud profiling radar after two years in orbit: Performance, calibration, and processing. *IEEE Transactions on Geoscience and Remote Sensing*, *46*(11), 3560-3573. doi: 10.1109/tgrs.2008.2002030

Trenberth, K. E., & Fasullo, J. T. (2010). Simulation of present-day and twenty-first-century energy budgets of the southern oceans. *Journal of Climate*, *23*(2), 440-454. doi: 10.1175/2009jcli3152.1

Trenberth, K. E., & Smith, L. (2008). Atmospheric energy budgets in the japanese reanalysis: Evaluation and variability. *Journal of the Meteorological Society of Japan*, *86*(5), 579-592. doi: doi:10.2151/jmsj.86.579

Trenberth, K. E., & Stepaniak, D. P. (2006). The flow of energy through the earth's climate system. *Quarterly Journal of the Royal Meteorological Society*, *130*(603), 2677-2701. doi: doi:10.1256/qj.04.83

Vallis, G. K. (2006). *Atmospheric and oceanic fluid dynamics: fundamentals and large-scale circulation.* Cambridge University Press.

Vergara-Temprado, J., Miltenberger, A., Furtado, K., Grosvenor, D., Shipway, B., Hill, A., ... Carslaw, K. (2018). Strong control of southern ocean cloud reflectivity by ice-nucleating particles. *Proceedings of the National Academy of Sciences*, *115*(11), 2687-2692. doi: 10.1073/pnas.1721627115

Vial, D. J. . B. S., J. (2013). On the interpretation of inter-model spread in cmip5 climate sensitivity estimates. *Climate Dynamics*, *41*(11-12), 3339-3362. doi: 10.1007/s00382

-013-1725-9

Visconti, G. (2016). *Springer*. Fundamentals of Physics and Chemistry of the Atmospheres.

Viterbo, P. (2002). The role of the land surface in the climate system. *European Centre for Medium-Range Weather Forecasts*, https://www.ecmwf.int/node/16961.

Wang, Z. (2019). *Cloudsat 2b-cldclass-lidar product process description and interface control document.* Retrieved from `http://www.cloudsat.cira.colostate.edu/sites/default/files/products/files/2B-CLDCLASS-LIDAR_PDICD.P1_R05.rev0_.pdf`

Wielicki, B. A., Harrison, E. F., Cess, R. D., King, M. D., & Randall, D. A. (1995). Mission to planet earth: Role of clouds and radiation in climate. *Bulletin of the American Meteorological Society*, *76*(11), 2125-2153. doi: 10.1175/1520-0477(1995)0762.0.co;2

Williams, J., Morgenstern, O., Varma, V., Behrens, E., Hayek, W., Oliver, H., ... Frame, D. (2016). Development of the new zealand earth system model: Nzesm. *Weather and Climate*, *36*. doi: 10.2307/26779386

Winker, D., Hunt, W. H., & McGill, M. J. (2007). Initial performance assessment of caliop. *Geophysical Research Letters*, *34*(19). doi: 10.1029/2007gl030135

Winker, D., Vaughan, M., Omar, A., Hu, Y., & Powell, K. (2009). Overview of the calipso mission and caliop data processing algorithms. *Journal of Atmospheric and Oceanic Technology*, *26*(11), 2310-2323. doi: 10.1175/2009jtecha1281.1

Witze, A. (2016). Antarctic clouds studied for first time in five decades. *Nature*, *529*(7584), 12. doi: 10.1038/529012a

Wood, R. (2012). Stratocumulus clouds. *Monthly Weather Review*, *140*(8), 2373-2423. doi: 10.1175/mwr-d-11-00121.1

Yang, G., & Slingo, J. (2001). The diurnal cycle in the tropics. *Monthly Weather Review*, *129*(4), 784-801. doi: 10.1175/1520-0493(2001)1292.0.co;2

Zhang, D., Wang, Z., & Liu, D. (2010). A global view of midlevel liquid-layer topped stratiform cloud distribution and phase partition from calipso and cloudsat measurements. *Journal of Geophysical Research*, *115*. doi: 10.1029/2009jd012143

Zhang, Y., & Klein, S. A. (2010). Mechanisms affecting the transition from shallow to deep convection over land: Inferences from observations of the diurnal cycle collected at the arm southern great plains site. *Journal of the Atmospheric Sciences*, *67*(9), 2943-2959. doi: 10.1175/2010jas3366.1

Zhao, W., Marchand, R., & Fu, Q. (2017). The diurnal cycle of clouds and precipitation at the arm sgp site: Cloud radar observations and simulations from the multiscale modeling framework. *Journal of Geophysical Research: Atmospheres*, *122*(14), 7519-

7536. doi: 10.1002/2016jd026353